Acid ceramidase of macrophages traps herpes simplex virus in multivesicular bodies and protects from severe disease

Lang, Judith ; Bohn, Patrick ; Bhat, Hilal ; Jastrow, Holger ; Walkenfort, Bernd ; Cansiz, Feyza ; Fink, Julian ; Bauer, Michael ; Olszewski, Dominik ; Greber, Urs F ; et al

Abstract: Macrophages have important protective functions during infection with herpes simplex virus type 1 (HSV-1). However, molecular mechanisms that restrict viral propagation and protect from severe disease are unclear. Here we show that macrophages take up HSV-1 via endocytosis and transport the virions into multivesicular bodies (MVBs). In MVBs, acid ceramidase (aCDase) converts ceramide into sphingosine and increases the formation of sphingosine-rich intraluminal vesicles (ILVs). Once HSV-1 particles reach MVBs, sphingosine-rich ILVs bind to HSV-1 particles, which restricts fusion with the limiting endosomal membrane and prevents cellular infection. Lack of aCDase in macrophage cultures or in Asah1−/− mice results in replication of HSV-1 and Asah1−/− mice die soon after systemic or intravaginal inoculation. The treatment of macrophages with sphingosine enhancing compounds blocks HSV-1 propagation, suggesting a therapeutic potential of this pathway. In conclusion, aCDase loads ILVs with sphingosine, which prevents HSV-1 capsids from penetrating into the cytosol.

DOI: https://doi.org/10.1038/s41467-020-15072-8

Acid ceramidase of macrophages traps herpes simplex virus in multivesicular bodies and protects from severe disease

Judith Lang[1], Patrick Bohn[1], Hilal Bhat[1], Holger Jastrow[2,3], Bernd Walkenfort[3], Feyza Cansiz[1], Julian Fink[4], Michael Bauer[5], Dominik Olszewski[5], Ana Ramos-Nascimento[6], Vikas Duhan[1], Sarah-Kim Friedrich[1], Katrin Anne Becker[7], Adalbert Krawczyk[8,9], Michael J. Edwards[10], Andreas Burchert[11], Magdalena Huber[12], Justa Friebus-Kardash[1], Joachim R. Göthert[13], Cornelia Hardt[1], Hans Christian Probst[14], Fabian Schumacher[7,15], Karl Köhrer[16], Burkhard Kleuser[15], Eduard B. Babiychuk[17], Beate Sodeik[6], Jürgen Seibel[4], Urs F. Greber[5], Philipp A. Lang[18*], Erich Gulbins[7,10*] and Karl S. Lang[1*#]

[1]Institute of Immunology, University of Duisburg-Essen, Hufelandstr. 55, D-45147 Essen, Germany
[2]Institute of Anatomy, University of Duisburg-Essen, Hufelandstr. 55, D-45147 Essen, Germany
[3]Imaging Center Essen, University of Duisburg-Essen, Hufelandstr. 55, D-45147 Essen, Germany
[4]Institute of Organic Chemistry, Julius-Maximilians University of Würzburg, Am Hubland, D-97074 Würzburg, Germany
[5]Department of Molecular Life Sciences, University of Zurich, Winterthurerstr. 190, CH-8057 Zurich, Switzerland
[6]Institute of Virology, Hannover Medical School, Carl-Neuberg-Str. 1, D-30625 Hannover, Germany
[7]Institute of Molecular Biology, University of Duisburg-Essen, Hufelandstr. 55, D-45147 Essen, Germany
[8]Institute of Virology, University of Duisburg-Essen, Hufelandstr. 55, D-45147 Essen, Germany
[9]Department of Infectious Diseases, University Hospital of Essen, University of Duisburg-Essen, D-45147 Essen, Germany
[10]Department of Surgery, University of Cincinnati, Cincinnati, Ohio, USA
[11]Department of Hematology, Oncology and Immunology, University Hospital Marburg, Marburg, Germany
[12]Institute of Medical Microbiology and Hospital Hygiene, Philipps-University Marburg, Hans-Meerwein Str. 2, D-35032 Marburg, Germany
[13]Department of Hematology, West German Cancer Center, University Hospital of Essen, University of Duisburg-Essen, D-45147 Essen, Germany
[14]Institute of Immunology, University Medical Center Mainz, Langenbeckstr. 1, D-55131 Mainz, Germany
[15]Institute of Nutritional Science, University of Potsdam, Arthur-Scheunert Allee 114-116, D-14558 Nuthetal, Germany
[16] Biological and Medical Research Center (BMFZ), Heinrich-Heine-University, Universitätsstr. 1, D-40225 Düsseldorf, Germany
[17]Institute of Anatomy, University of Bern, Baltzerstr. 4, CH-3012 Bern, Switzerland
[18]Institute of Molecular Medicine II, Heinrich-Heine-University, Universitätsstr. 1, D-40225 Düsseldorf, Germany

[*]These senior-authors contributed equally to this work

[#]Correspondence: karlsebastian.lang@uk-essen.de

Summary:

Macrophages have key protective functions during infection with herpes simplex virus type 1 (HSV-1). However, molecular mechanisms, which restrict viral propagation and protect from severe disease remain to be identified. Here we found that macrophages take up HSV-1 via endocytosis and transport the virions into multivesicular bodies (MVBs). In MVBs acid ceramidase (aCDase) converted ceramide into sphingosine and increased the formation of sphingosine-rich intraluminal vesicles (ILVs). Once HSV-1 particles passed MVBs, sphingosine-rich ILVs bound to HSV-1 particles, which restricted fusion with the limiting endosomal membrane and prevented cellular infection. Lack of aCDase in macrophage cultures or in *Asah1*$^{-/-}$ mice led to overwhelming replication of HSV-1 and *Asah1*$^{-/-}$ mice died quickly after systemic or intravaginal inoculation. The treatment of macrophages with sphingosine enhancing compounds blocked HSV-1 propagation, suggesting a therapeutic potential of this pathway. In conclusion, we demonstrate that aCDase loads ILVs with sphingosine, which prevents HSV-1 capsids from penetrating into the cytosol.

Introduction

Macrophages are one of the most important components of the innate immune system. With their strong phagocytic capacity they engulf pathogens early after their invasion and inactivate them by proteolysis[1]. Especially during virus infection, macrophages are the key effector cells of innate immunity. Mice lacking macrophages are highly susceptible to mouse hepatitis virus, lymphocytic choriomeningitis virus and vesicular stomatitis virus and show overwhelming viral propagation[2-4]. The contribution of macrophages to control of systemic infection was linked to their capacity to take up infectious particles and limit their propagation in a type I interferon (IFN-I) dependent manner[4], which leads to upregulation of the antiviral genes Mx, OAS, RNase L and Protein kinase R[4]. While these antiviral mechanisms act hours after infection, macrophages exhibit in addition robust antiviral suppression already minutes after virus inoculation[4-6], suggesting the presence of preexisting IFN-I-independent antiviral mechanisms.

Herpes simplex virus type 1 (HSV-1) is an enveloped DNA virus, which can replicate in several different cell types[7]. After binding to a target cell, HSV-1 either fuses directly with the plasma membrane or is taken up into endosomes of the cell[8,9]. Within these endosomes fusion of the outer limiting membrane with HSV-1 membrane leads to infection of the cells in a pH dependent manner[10,11]. Upon penetration, the HSV-1 capsid traffics on microtubules to the nucleus[12,13], uncoats its DNA genome at the nuclear pore complex[14-16], and delivers the genome to the nucleus for replication and assembly of capsids[17,18]. Newly formed capsids bud through the nuclear envelope[19] and exit the infected cell through the secretory pathway or by cell lysis[20,21]. In an HSV-1 infection model, macrophages do play an essential role[22,23]. This is linked to the high IFN-I sensitivity of HSV-1, which limits the replication of HSV-1 DNA and the production of newly formed capsids[24,25]. Interestingly even in the absence of IFN-I replication of HSV-1 is restricted in macrophages, a phenomenon that could be explained by limited uptake of HSV-1 into macrophages or an aggravated or limited infection of the macrophage after HSV-1 has entered the endosome. Whether indeed macrophage-specific mechanisms regulate HSV-1 infection remains unknown.

Mulitvesicular bodies (MVBs) are complex membrane rich organelles of the cytoplasm, which contain high amounts of vesicles. These so called intraluminal vesicles (ILVs) are formed by invagination and budding from the outer limiting membranes (OLMs) into the MVB lumen and play a crucial role in sorting, degrading, and recycling of proteins[26,27]. Sphingolipids are enriched in MVBs and are involved in the MVB biogenesis and the regulation of their functions[28]. Thereby sphingolipids

modulate diverse cellular processes, including proliferation, differentiation, apoptosis, signal transduction, and membrane trafficking[29-31]. Modulation of biophysical membrane properties such as fluidity, polarity, vesicle formation, and deformation is one major factor of the regulatory capacity of sphingolipids[32-34]. One key enzyme in sphingolipid metabolism in MVBs is the acid ceramidase (aCDase)[35-37]. It catalyzes the degradation of ceramide into sphingosine and free fatty acid, which modulates the shape and the charge of membranes. Whether this process can modulate HSV-1 entry remains unknown.

Here we analyze whether the acid ceramidase (aCDase) dependent modulation of membrane properties can affect HSV-1 entry after uptake into macrophages. In a model of HSV-1 infection in bone marrow derived murine macrophages (BMDMs) we found that strong activity of aCDase blocked the fusion of the HSV-1 membrane with the outer limiting membrane of MVBs. Antiviral activity of aCDase was independent of IFN-I, but aCDase expression was dependent on IRF8 during macrophage development. In vivo, expression of aCDase in macrophages limited early steps of HSV-1 propagation and protected mice from severe outcome of infection.

Results

Macrophages control herpes simplex virus type 1 (HSV-1) infection

To prove the importance of macrophages during HSV-1 control *in vivo,* we infected C57BL/6 mice intravenously with HSV-1 and then analyzed the distribution of virus in the liver by histology. Naïve mice and HSV-1 infected macrophage-depleted mice served as controls. One hour after infection most of the virus inoculum co-localized with F4/80$^+$ macrophages within the liver (Fig. 1a), suggesting that macrophages are equipped to take up HSV-1 quickly after systemic administration. Naïve mice did not show HSV-1 staining (Fig. 1a) and macrophage-depleted mice showed no F4/80$^+$ cells in spleen and liver and no co-localization (Supplementary Fig. 1)[4]. To obtain insights on the functional role of macrophages we treated C57BL/6 mice with clodronate-liposomes to deplete macrophages. Control mice were treated with control-liposomes and all mice were infected with HSV-1. In the presence of macrophages, HSV-1 replication was nearly undetectable 24 hours after infection (Fig. 1b&c). In strong contrast, HSV-1 showed overwhelming replication in the absence of macrophages (Fig. 1b&c). Enhanced replication of HSV-1 correlated with production of infectious HSV-1 in liver and spleen of macrophages-deficient mice (Fig. 1d). In line with overwhelming virus

propagation, macrophage deficient mice developed liver cell damage and died quickly after infection (Fig. 1e&f). To analyze the importance of macrophages during a natural infection route we infected mice intravaginal with HSV-1 and analyzed local replication of HSV-1 and outcome of the infection. HSV-1 replication and production of infectious particles was comparable between control and macrophage-depleted mice (Fig. 1g&h). However macrophage-depleted mice died after intravaginal infection while control mice were protected (Fig. 1i). This suggested that macrophages in the vagina do not limit early local HSV-1 replication, however contributed to the systemic control of HSV-1. In conclusion we found that macrophages do play an essential role to protect from systemic HSV-1 propagation.

Virus trapping in multivesicular bodies correlates with expression of acid ceramidase

As elucidated in Fig. 1, macrophages are of high importance to limit HSV-1 propagation during systemic infection. Following this, we aimed to investigate antiviral mechanisms that are specific to macrophages. To get insights into the macrophage-specific antiviral mechanism we generated bone marrow derived macrophages (BMDMs) and compared their antiviral activity to isolated alveolar fibroblasts. HSV-1 propagated strongly in fibroblasts and infectious HSV-1 was released into the supernatant (Fig. 2a&b). In contrast to fibroblasts, HSV-1 showed limited propagation in macrophages and infectious particles were hardly measurable in the supernatants (Fig. 2a&b). Even higher infection doses up to MOI 1 did not result in productive infection in cultured macrophages (Fig. 2b). Treatment with interferon-α4 (IFN-α4) reduced the infectious particles (Fig. 2b), however the striking difference in virus production between fibroblasts and macrophages remained. These results suggest that administration of IFN-I cannot induce the strong antiviral capacities of macrophages in fibroblasts. While there are multiple differences between macrophages and fibroblasts, we hypothesized that macrophages have specific antiviral protection mechanisms independent of the presence of type I interferon (IFN-I).

To explore potential antiviral mechanisms we performed microarray analysis to compare cellular pathways between macrophages and fibroblasts. The strongest difference between fibroblasts and macrophages was the high expression of endosomal, lysosomal and vesicular transport pathways in macrophages (Fig. 2c). From these data, we considered it likely that in macrophages the vesicular trafficking of HSV-1 might be extraordinary, and therefore restricts a productive infection. To directly

visualize HSV-1 entry in macrophages and fibroblasts, we performed electron microscopy of macrophages and fibroblasts, which were infected with HSV-1 (MOI 250) for 30 minutes. We chose 30 minutes, as this is the time that HSV-1 requires to enter cells and first incoming capsids to reach the nuclear envelope of fibroblasts or epithelial cells[15,38,39]. Indeed, 30 minutes after infection we could detect first viral capsids at the nuclear envelope of fibroblasts, but no newly produced viral capsids (Supplementary Fig. 2). Therefore we concluded that 30 minutes is an ideal time point to analyze the early internalization and intracellular distribution of HSV-1 within the cell. As expected, we found in macrophage and fibroblast cell cultures HSV-1 virions close to the plasma membrane (Fig. 2d). In macrophages, about 30% of all particles were found in endosomes and significantly more particles, about 50% of all particles, were found in multivesicular bodies (Fig. 2d&e). We could hardly detect viral capsids in the cytosol of macrophages (Fig. 2d&e). In fibroblasts, HSV-1 was detectable in vesicular compartments like early endosomes, late endosomes, MVBs and/or lysosomes (Fig. 2d). In addition electron microscopy revealed cytosolic capsids after 30 minutes of infection (Fig. 2d), indicating fusion of the viral envelopes with host membrane and successful capsid delivery into the cytosol. From these results we concluded that after HSV-1 is internalized by macrophages, it passes early and late endosomes, accumulates in MVBs but cannot deliver its capsid through the outer limiting membrane to the cytosol. This phenomenon might be responsible for limited productive infection in macrophages.

To determine why HSV-1 cannot release its capsid through the outer limiting MVB membrane, we analyzed our microarray data for differences in membrane-modulating proteins. Strikingly we found overexpression of phospholipase C subtypes, acid sphingomyelinase (Asm, *Smpd3*) and acid ceramidase (aCDase, *Asah1*) in macrophages (Fig. 2f) in comparison to fibroblasts. Differential expression of these proteins was independent of IFN-I (Fig. 2f). Using real-time polymerase chain reaction (RT-PCR) and Western blot analysis we confirmed the high expression of *Asah1* mRNA and cleaved aCDase protein in macrophages compared to fibroblasts (Fig. 2g&h). From these experiments we concluded that macrophages accumulate HSV-1 in MVBs without being productively infected. This strong antiviral activity of macrophages correlated with aCDase expression.

aCDase protects macrophages from HSV-1 infection and prevents severe outcome of disease

Since we identified that aCDase is a membrane modulating molecule that is highly upregulated in macrophages, we next analyzed the antiviral activity of aCDase. WT macrophages showed limited propagation of HSV-1 (Fig. 3a). In strong contrast macrophages which lack aCDase (*Asah1*$^{-/-}$) showed strong propagation of HSV-1 (Fig. 3a&b). Next we tested the role of aCDase *in vivo*. We infected WT and *Asah1*$^{-/-}$ mice with HSV-1. In *Asah1*$^{-/-}$ mice, HSV-1 showed overwhelming propagation after 12 hours to 3 days (Fig. 3c&d) and infectious particles were produced in spleen and liver of *Asah1*$^{-/-}$, but not control mice (Fig. 3e). Next we aimed to determine the importance of *Asah1* in relation to the known anti-HSV-1 effectors type I interferon (IFN-I)[40] and SAMHD1[41]. Therefore we infected mice, which show limited production of IFN-I (*MyD88*$^{-/-}$ *x Trif*$^{-/-}$ *x Cardif*$^{-/-}$ mice), limited response to IFN-I (*Ifnar*$^{-/-}$ mice) and mice, which lack SAMHD1 (*Samhd1*$^{-/-}$ mice) with HSV-1. Similarly to *Asah1*$^{-/-}$ mice, *Ifnar*$^{-/-}$ mice, *MyD88*$^{-/-}$ *x Trif*$^{-/-}$ *x Cardif*$^{-/-}$ mice and *Samhd1*$^{-/-}$ mice showed highly elevated HSV-1 DNA when compared to control mice (Supplementary Fig. 3). In *Ifnar*$^{-/-}$ mice and *MyD88*$^{-/-}$ *x Trif*$^{-/-}$ *x Cardif*$^{-/-}$ mice, but not in *Samhd1*$^{-/-}$ mice, we detected infectious HSV-1 particles in liver and spleen after HSV-1 infection, which was comparable to HSV-1 production in *Asah1*$^{-/-}$ mice (Fig. 3f). From these data we considered aCDase to be an important antiviral effector mechanism.

To determine the macrophage-specific role of aCDase we generated bone marrow chimeras, where *Asah1*$^{-/-}$ bone marrow was transplanted into macrophage-depleted WT mice. In these mice macrophages repopulate from *Asah1*$^{-/-}$ bone marrow. Chimeric mice with aCDase-deficient macrophages showed enhanced HSV-1 copies when compared to control mice (Fig. 3g), suggesting that indeed aCDase in macrophages contributed to control of HSV-1. To determine the overall importance of aCDase during systemic and local infection we infected Tamoxifen treated Cre-ER *Asah1*$^{fl/fl}$ (inducible aCDase deficient mice) with HSV-1. aCDase deficient Cre-ER *Asah1*$^{fl/fl}$ mice died quickly after systemic and local intravaginal infection (Fig. 3h&i). Therefore we concluded that aCDase is an important effector mechanism against HSV-1, which acts partially in macrophages.

Sphingosine protects against HSV-1 infection

After analyzing aCDase deficiency, we investigated effects of increasing sphingolipid content during HSV-1 infection. From literature it is known that aCDase is usually active in lysosomes and MVBs[35-37,42,43]. To see whether there is a direct interaction of aCDase with HSV-1 we infected

macrophages with HSV-1 and stained for aCDase and HSV-1 after 30 minutes. HSV-1 and aCDase were in close approximation, however we did not see a direct co-localization of aCDase with HSV-1 (Fig. 4a). This suggests that aCDase is not directly modulating HSV-1, but might modulate cellular components such as MVBs which could affect HSV-1 infection. Functionally, aCDase converts ceramide into sphingosine (Fig. 4b) and we considered that enhancement of sphingosine in MVBs was the reason for viral protection in WT macrophages against HSV-1. Indeed, addition of CDase 30 minutes before infection limits HSV-1 propagation, which suggests that the enzymatic function is most relevant for the antiviral activity (Fig. 4c-e).To reveal the role of sphingosine in HSV-1 infection, we treated macrophages with sphingosine (Sph), sphingomyelinase (SMase), and sphingosine kinase inhibitor (SKI-II), which are all involved in sphingolipid pathway and could enhance sphingosine levels[44]. Sphingosine treatment, which strongly elevated total sphingosine levels of primary macrophages and the Raw264.7 macrophage cell line (Supplementary Fig. 4), suppressed propagation of HSV-1 (Fig. 4d-g). Treatment with ceramidase, sphingomyelinase, and sphingosine kinase inhibitor resulted in smaller increases of cellular sphingosine levels, most likely because these proteins only affect local levels of sphingosine (Supplementary Fig. 4). From these data we concluded that enhanced amount of sphingosine was most likely the reason for antiviral activity in the presence of aCDase. To determine whether sphingosine acted cell type specific, we tested the antiviral activity of sphingosine in different cell types including human monocytes (THP-1), human cervix carcinoma cells (HeLa) and monkey kidney cells (Vero). To note, HSV-1 infects Vero cells via fusion at the plasma membrane while Hela cells are infected after HSV-1 is endocytosed[11,45]. We found that sphingosine and/or SKI-II acted antiviral in undifferentiated THP-1 and Hela cells (Fig. 4f&g). However we found limited antiviral activity of sphingosine in Vero cells (Fig. 4h), suggesting that the cell type and/or the route of infection might limit the antiviral activity of sphingosine. Taken together we concluded, that sphingosine, which is produced by aCDase in MVBs is antivirally active in macrophages.

Sphingosine-rich intraluminal vesicles trap HSV-1

Next we aimed to determine the mechanism, how aCDase and sphingosine limit HSV-1 infection in macrophages. To this end, we incubated cells for 30 minutes with an HSV-1, carrying a fluorescently labeled tegument (HSV-1-VP16-GFP), and stained with an antibody for viral capsids

(VP5[46]), which recognizes the uncoated capsid after virus membrane fusion. In this experimental setup capsid is only visible after dissociation of the tegument[12]. We mainly observed HSV-1-VP16-GFP puncta, in WT macrophages (Fig. 5a&b), indicating that the HSV-1 capsids were not released from the envelope. In strong contrast, in aCDase lacking (*Asah1*$^{-/-}$*)* macrophages we detected almost exclusively exposed capsids without tegument (Fig. 5a&b), suggesting that the capsids were released from the envelope and the tegument due to virus infection. To get more insights into the reason for limited infection in WT macrophages, we performed electron microscopy experiments in WT and *Asah1*$^{-/-}$ macrophages. WT and *Asah1*$^{-/-}$ macrophages showed similar amounts of HSV-1 particles which were attached to the plasma membrane (Fig. 5c&d). In line similar amounts of HSV-1 particles were detected in WT and *Asah1*$^{-/-}$ macrophages in endosomes and MVB (Fig. 5c&d). In WT macrophages HSV-1 particles were located in close proximity to the ILVs, and in some cases appeared to fuse with ILVs (Fig. 5c&d). This correlated with trapping of HSV-1 in ILVs (Fig. 5c&d). In contrast, in *Asah1*$^{-/-}$ macrophages, the HSV-1 envelopes were more frequently associated with the outer limiting membranes (OLMs) of the MVBs (Fig. 5c&d), so that membrane fusion here led to a productive release of capsids into the cytosol and infection of the cell. Therefore, we concluded that aCDase-derived sphingosine promotes binding of HSV-1 envelope to ILVs membrane, which results in trapping of the virus.

To prove that indeed sphingosine on ILVs interacted with HSV-1 we loaded WT macrophages with *ω*-azido-sphingosine, which can be visualized by a click reaction[47]. Three hours after sphingosine loading, we infected cells with HSV-1 and co-stained cells with the ILV marker CD9. Indeed, sphingosine accumulated in ILVs (Fig. 5e). As expected HSV-1 co-stained with these sphingosine-rich ILVs (Fig. 5e). To determine that indeed sphingosine is responsible for interaction between HSV-1 and ILVs, we generated liposomes and loaded them either with ceramide or sphingosine. Liposomes were then incubated with HSV-1 and binding of virions was analyzed after 10 minutes by flow cytometry. Control and ceramide-liposomes did not bind HSV-1 (Fig. 5f&g). In contrast sphingosine-liposomes bound HSV-1 (Fig. 5f&g). Concluding, we found that the antiviral effects of aCDase are mediated via fusion of viral envelop to sphingosine containing ILVs of MVBs.

aCDase expression depends on interferon regulatory factor 8, but not on type I interferon

Our data show that the *Asah1* gene encoding aCDase is a crucial factor involved in antiviral

protection against HSV-1. Next, we aimed to define, how aCDase expression is induced. We aimed to analyze whether *Asah1* is also induced by IFN-I. *Asah1* expression was hardly influenced by IFN-I, nor did *Asah1* influence the induction of IFN-I or interferon induced genes (Fig. 6a&b). Therefore we concluded that *Asah1* is not specifically upregulated during infection, but shows already basal activity in macrophages before infection. To get insights how *Asah1* expression is upregulated in macrophages we considered that interferon regulatory factor 8 (IRF8) might play a role in this process. IRF8 is a factor, which induces natural resistance in macrophages during their development[48,49]. Furthermore, it was shown that IRF8 regulates the expression of aCDase during the induction of apoptosis in cancer cells[50]. RT-PCR analysis of myeloid pre-cursor cells in the bone marrow revealed IRF8-dependent upregulation of *Asah1* (Supplementary Fig. 5). To determine the role of IRF8 in regulating *Asah1* in mature macrophages, we analyzed *Asah1* expression in the spleen, an organ showing high numbers of macrophages. RT-PCR and Western blot analysis revealed limited levels of *Asah1* mRNA and aCDase precursor protein in spleens of *Irf8*$^{-/-}$ mice when compared to WT spleens (Fig. 6c&d). In line, *Irf8*$^{-/-}$ mice showed elevated levels of HSV-1 DNA as well as increased production of viral particles after infection with HSV-1 (Fig. 6e&f). We concluded that *Asah1* is not induced during infection or by IFN-I, however IRF8 regulates *Asah1* expression during development of macrophages.

Discussion

Macrophages are one of the most important effector cells of the innate immune system[5,51,52]. During infection with viruses such as vesicular stomatitis virus (VSV), lymphocytic choriomeningitis virus (LCMV), adenovirus or mouse hepatitis virus, macrophages play a major protective role in limiting infection and preventing severe disease[2-4,53-55]. In particular, tissue resident macrophages such as Kupffer cells in the liver clear a range of systemic virus infections[4,53]. Molecular mechanisms explaining this strong antiviral activity are presently unknown. Here we found that macrophages are essential for the control of HSV-1. We linked the strong antiviral activity of macrophages to the expression of aCDase. aCDase produced sphingosine-rich ILVs in MVBs. Once HSV-1 is taken up into MVBs, ILVs bind to HSV-1 particles and thereby trap them in MVBs and prevent infection of the cell. Expression of aCDase was not regulated by IFN-I, but was induced in macrophages in response to IRF8 signaling.

It remains to be explored whether the restriction mechanism of sphingosine-rich ILVs is specific for HSV-1 or whether also other viruses are sensitive to sphingosine-rich ILVs. Indeed, infection of *Asah1*$^{-/-}$ mice with LCMV or VSV resulted also in death of mice (data not shown). While the reason for this phenotype remains to be studied, it underlines the importance of aCDase during virus infection. Interestingly, VSV, the flaviviruses Japanese encephalitis virus (JEV) and yellow fever virus (YFV) fuse with ILVs in MVBs [56,57]. Le Blanc et al. and Nour et al. considered the release of viral capsids into ILVs a relevant step in virus life cycle, and suggested that back-fusion of ILVs, harboring capsids, with the OLMs of MVBs leads to productive infection. In macrophages, our data show that although back-fusion might occur, fusion of viral membrane with ILV membrane is rather a cellular mechanism to limit infection of the cell. Further experiments are required to determine whether other enveloped viruses and non-enveloped viruses are also restricted by sphingosine in MVBs.

Viruses frequently have an acidic isoelectric point at low pH[58], implying that these viruses are negatively charged at physiological pH. The isoelectric point of HSV-1 is around 4.9[59]. In contrast, sphingosine is net positively charged at neutral or acidic pH, as occurring in MVBs. We suggest that sphingosine gives ILVs a positive charge, which facilitates the interaction with negatively charged HSV-1. Indeed it was shown that sphingosine containing vesicles interact with negatively charged membranes at the plasma membrane or in late endosomes and accelerates fusion of these membranes[60,61]. More biophysical work is needed to better understand the interaction of HSV-1 with sphingosine.

We compared the *in vivo* phenotype of *Asah1*$^{-/-}$ mice to mice, which show limited production of IFN-I (*MyD88*$^{-/-}$ *x Trif*$^{-/-}$ *x Cardif*$^{-/-}$ mice), limited response to IFN-I (*Ifnar*$^{-/-}$ mice) and mice, which lack SAMHD1 (*Samhd1*$^{-/-}$ mice) during HSV-1 infection. SAMHD1 was previously reported to be of importance for HSV-1 control in myeloid cells[41,62]. Viral replication in *Asah1*$^{-/-}$ was comparable or even enhanced to that in *Samhd1*$^{-/-}$, *MyD88*$^{-/-}$ *x Trif*$^{-/-}$ *x Cardif*$^{-/-}$ mice and *Ifnar*$^{-/-}$ mice. From these data we concluded that *Asah1* is one important innate effector mechanism. While SAMHD1 and IFN signaling counteract mainly viral replication and production of infectious particles, we think that aCDase protects macrophages from infection with HSV-1 immediately after the virus is taken up.

From our electron microscopy analysis it seems that HSV-1 fuses with ILVs. We consider that trapped viral particles are unable to leave MVBs and are targeted to lysosomes for degradation. This pathway of degradation might also facilitate antigen-presentation and immune activation, as high numbers of tetraspanins and MHC-II molecules are contained within ILVs[26,63]. More experiments are

required to identify the relationship of aCDase, sphingosine and antigen-presentation on MHC-II. In our study we focused mainly on the role of sphingosine and aCDase in macrophages. In addition, aCDase is expressed in several other tissues, especially in lung, colon and stomach as well as spleen[64] (Supplementary Fig. 6). Cells in these organs are involved in building a barrier, which protects against invading viruses. We consider it likely that in addition to macrophages, potentially also other cell types express aCDase in MVBs and are thereby protected against invading viruses.

From our data we would suggest enhanced virus infections in patients with Farber disease, which are deficient in activity of aCDase[65]. While such associations were not determined yet, patients with Farber disease have a limited life span and die early after birth[65]. Akin to other innate or adaptive deficiencies, a limited lifespan of the patients may obscure a link between innate or adaptive deficiencies to infectious agents [66]. Whether other mutations, which affect the activity of aCDase, are widespread in the population and whether such mutations influence the susceptibility to viral infections will be subject to future studies.

In conclusion, we found that macrophages are essential to survive an infection with HSV-1. Mechanistically, macrophages took up HSV-1 and accumulated it in MVBs. aCDase in macrophages enriched ILVs with sphingosine. Once HSV-1 entered MVBs sphingosine-rich ILVs trapped HSV-1 and prevented productive infection of the cells.

Methods:

Mice: For acid ceramidase 1 (*Asah1*) deficient heterozygous mice, the exon-intron organization of the gene was established on the basis of the *Asah1* cDNA sequence. A targeting vector was constructed, including *Asah1* genomic sequences on the C57BL/6 genetic background, a long homology region of 5.8 kb and a short homology region of 1.7 kb. It also included two loxP sites flanking *Asah1* exon 1, a neomycin gene flanked by flipase recognition target sites for positive selection of homologous recombination, and a diphtheria toxin, a negative-selection marker to detect insertions and nonhomologous recombinant embryonic stem cell clones. This targeting vector was inserted into C57BL/6 embryonic stem cells by homologous recombination. Offspring were crossed with CreER mice (Gt[ROSA]26Sor$^{tm9[cre/ESR1]Arte}$) mice, which were developed by Taconic Artemis Pharmaceuticals (Köln, Germany) and provided by Jens Fischer (University of Düsseldorf, Germany). In some experiments we used mice in which acid ceramidase deficiency could be induced (Cre × *Asah1*$^{fl/fl}$).

CreER x *Asah1*$^{fl/fl}$ offspring express a Cre recombinase under the tamoxifen promoter and the *Asah1* gene with two LoxP sites flanking exon 1. Administering tamoxifen thus led to the expression of Cre recombinase and loss of function mutation by deletion of exon 1 in the *Asah1* gene. In this model, knock out of *Asah1* occurs right before infection. Potential developmental defects due to long term knock out of *Asah1* are excluded in this model.

Asah1$^{fl/fl}$ x EIIa-Cre mice carry a Cre transgene under the control of the adenovirus EIIa promoter that targets expression of Cre recombinase to the early mouse embryo, and are used for germ line deletion of *Asah1* gene, referred to as *Asah1*$^{-/-}$ mice. *Asah1*$^{-/-}$ mice were on C57BL/6J background. Sibling animals with the genotype *Asah1*$^{+/+}$ were used as control animals. We bred *Irf8*$^{-/-}$ and *Samhd1*$^{-/-}$ mice on C57BL/6J background. *Samhd1*$^{-/-}$ mice were originally developed by Prof. Jan Rehwinkel (MRC Human Immunology Unit, MRC Weatherall Institute of Molecular Medicine, University of Oxford, Oxford, England)[67] and used with permission.

All animals were housed in single ventilated cages. Animal experiments were authorized by the Landesamt für Natur, Umwelt und Verbraucherschutz (LANUV) Nordrhein-Westfalen and in accordance with the German law for animal protection and/or according to institutional guidelines at the Ontario Cancer Institute of the University Health Network.

Cell lines, bone marrow macrophages: Raw264.7 cells were purchased from the American Type Culture Collection (ATCC, Manassas, VA, USA). THP-1 cells were purchased from the German Collection of Microorganisms and Cell Cultures (DSMZ, Braunschweig, Germany). Vero cells were provided by the Ontario Cancer Institute (Toronto, ON, Canada). For the generation of macrophages, bone marrow was isolated from mice and cultured for 9 days with macrophage colony-stimulating factor (M-CSF). Cells were plated on new cell culture plates and the experiment was started the next day. For generation of primary fibroblasts, lungs were isolated from mice and digested using DNase/Liberase. Fibroblasts were harvested after 6 days of culture and experiment was started the subsequent day.

Viruses: We used HSV-1(17+)Lox-CheVP26 in which monomeric Cherry has been fused to the N-terminus of the small capsid protein VP26[68] from Prof. Beate Sodeik (Institute of Virology, Hannover, Germany), HSV-1F (kindly provided by Prof. Hartmut Hengel, Institute of Virology, Freiburg, Germany) and HSV-VP16-GFP[69] (kindly provided by Dr. Yohei Yamauchi, University of Bristol, United Kingdom).

Reagents: D-erythro-sphingosine (C18, 860490) and D-Galactosyl-β1-1'-N-Nervonoyl-D-erythro-sphingosine (C24:1, β-D-Galactosyl Ceramide, 110759), were obtained from Avanti Polar Lipids

(Alabaster, AL, USA). Glycoceramidase (E9030-100MUN), sphingomyelinase (S8633-25UN), Cy3-linked DBCO (777366-1mg) and DAPI (D9542) were purchased from Millipore Sigma (Darmstadt, Germany). Murine recombinant Asah2 (3558-AH) was purchased from R&D Systems (Minneapolis, MN, USA). The sphingosine kinase inhibitor SKI-II (CAS # 312636-16-1; Cat # 2097) was obtained from Tocris Bioscience (Bristol, United Kingdom) and tamoxifen (CAS # 10540-29-1, Cat # T5648-5G) and cornoil (CAS # 8001-30-7, Cat # C8267-500ML) from Millipore Sigma. Clodronate and control liposomes were purchased from Liposoma (CP-005-005, Amsterdam, Netherlands). Clickable *ω*-azido-sphingosine (JF 169, ((2*S*,3*R*,*E*)-2-amino-18-azidooctadec-4-ene-1,3-diol)) was synthesized by Julian Fink, Institute of Organic Chemistry, Julius-Maximilians University of Würzburg, Germany.

Tamoxifen treatment: Tamoxifen was dissolved in corn oil. Eight, six, and four days before an experiment, Cre^- × $Asah1^{fl/fl}$ control animals and Cre^+ × $Asah1^{fl/fl}$ animals were treated with 4 mg tamoxifen (in 100 µL corn oil) intraperitoneally.

Depletion of macrophages: For macrophage-depleted mouse experiments, mice were treated with clodronate liposomes to deplete tissue resident macrophages. After 3 days, mice were ready to be used in experiments.

Survival experiments: To analyze the effect of macrophage/ sphingosine deficiency on the course of infection, we performed survival experiments. For this purpose, animals were infected with a dose that was sublethal for WT animals. Animals were checked daily, killed with corresponding termination criteria, and counted as dead. Termination criteria were body weight, general condition, spontaneous behavior and clinical findings.

Bone marrow chimera mice: For bone marrow chimera experiments, 10-12 weeks old female C57BL / 6J mice were irradiated with 9.5 Gy. On the following day, bone marrow from donor mice was isolated under sterile conditions and i.v. administered. On day 10 after irradiation, mice were treated with clodronate liposomes to deplete tissue resident macrophages. After 50 days of reconstitution mice were ready to be used in experiments.

Infection of cells and animals: For *in vitro* infection with warm binding, the virus was added to the cell cultures. After incubation for one hour, the supernatant was washed away and new medium added. The supernatant was collected at various times after infection. For *in vitro* infections with cold binding, cell cultures were preincubated on ice for 20 minutes at 4°C; the virus was added under these conditions and incubated for one hour. The supernatant was removed, new medium was added, and the cell cultures were stored at 37°C until analysis. This process is known as synchronized infection.

For intravenous infection, 100µL of the virus was injected into the tail vein. For intravaginal infection, 20µL of the virus was pipetted into the vagina of anesthetized mice. The opening was briefly closed with skin glue to reduce variability of inoculation time and volume.

Immunofluorescence microscopy: Immunofluorescence was used to detect viruses in cells and organs. For *in vitro* experiments, cells were seeded in 24-well plates, each containing a coverslip. After 24 hours, the cells were correspondingly infected, fixed after incubation, and labeled with antibodies. Organs of infected animals were shock-frozen, and 8 µm thick sections were recovered on a microscope slide. The sections were fixed, and virus was visualized with virus-specific antibodies. The following primary antibodies were used: anti-HSV-1 capsid (SY4563[39], anti-capsid), anti-HSV-1 capsid (hu2c[70], anti-glycoprotein gB) or anti-HSV-1 VP5 (NC-1[46], anti-capsid). Alternatively, virus directly labeled with a dye (e.g., Cy3; carboxylfluorescein succinimidyl ester [CFSE]) was used. Zeiss ELYRA PS.1 SIM/PAL-M/STORM/TIRF and LSM710 (ZEISS, Oberkochen, Germany), was used to acquire images.

Immunofluorescence microscopy of sphingosine: Immunofluorescence was used to detect sphingosine in cells. Cells were seeded in 24-well plates, each containing a coverslip. After 24 hours, the cells were correspondingly treated, fixed after incubation, and labeled with antibodies. As primary antibody monoclonal anti-sphingosine antibody (clone NHSPH, ALF-274042010, Alfresa Pharma Corporation, Osaka, Japan) and as secondary antibody Cy3-coupled anti-IgM F(ab)2 fragments (Jackson ImmunoResearch, Ely, United Kingdom) were used. Samples were examined with a Leica TCS-SP5 confocal microscope equipped with a 100× lens, and images were analyzed with Leica LCS software version 2.61 (Leica Microsystems, Mannheim, Germany). Fluorescence intensity was determined in 100 randomly selected cells/sample (total of 300 cells). We determined the fluorescence of the cell periphery.

Detection of herpes simplex virus in cell supernatant and organs by tissue culture infection dose 50 ($TCID_{50}$) assay: Vero cells were seeded onto a 96-well plate and let grow to confluence overnight. To determine the viral titer, cell culture supernatant was titrated and transferred to the 96-well plate. After 7 days of incubation, the plaque positive wells were counted, and the number of infectious particles per ml of supernatant or organ was determined.

Detection of herpes simplex virus in organs by quantitative real-time polymerase chain reaction (qRT-PCR): DNA was isolated from organs using the innuPREP Virus DNA Kit (Order #: 845-KS-4600050, Analytik Jena, Jena, Germany). RealStar® HSV PCR Kit 1.0 CE (Order #: 061013,

Altona Diagnostics, Hamburg, Germany) was used to quantify the amount of HSV-1 genomes per organ. A LightCycler 480 Instrument (Roche Life Science, Basel, Switzerland) was used for detection.

Capsid uncoating assay of herpes simplex virus: Cells were incubated with HSV-1 expressing GFP at the tegument protein VP16 (HSV-1-VP16-GFP[69]). After 30min of incubation, cells were fixed and stained for HSV capsid with anti-VP5 (NC-1[46]) and DAPI. Images were acquired on Leica SP8 microscope (Wetzlar, Germany) and analyzed using CellProfiler by segmentation and counting of single VP16-GFP or VP5 puncta.

Production of sphingosine-containing liposomes for fluorescence-activated cell sorting analysis: Liposomes were prepared by sonication as previously described[71]. Phosphatidylcholine (PC), cholesterol (Ch), sphingomyelin (SM), ceramide (Cer) and D-sphingosine (Sph) were from Millipore Sigma. The lipid composition of the liposomes was as follows: control-liposomes (PC: Ch: SM 33.3:33.3:33.3 mol/%), ceramide-rich liposomes (PC: Ch: SM: Cer 33:33:24:10 mol/%) and sphingosine-rich liposomes (PC: Ch: SM: Sph 33:33:24:10 mol/%).

Isolation of total RNA, reverse transcription and quantitative real-time reverse transcription polymerase chain reaction: Total RNA was isolated from cells using Trizol. Complementary DNA synthesis was performed with the QuantiTect Reverse Transcription Kit *(*Qiagen, Hilden, Germany).

For quantitative real-time polymerase chain reaction (qRT-PCR) either Fast SYBR Green Master Mix (Applied Biosystems, Darmstadt, Germany) or TaqMan Fast Universal PCR Master Mix (ThermoFisher Scientific) was used on the 7500 Fast Real-Time PCR System (Applied Biosystems)**.** For analysis, the expression levels of all target genes were normalized against glyceraldehyde 3-phosphate dehydrogenase (Gapdh; ΔCt). Relative gene expression values were calculated with the ΔΔCt method. Following primers were used: *Gapdh* (Mm99999915_g1, ThermoFisher Scientific), *Gapdh* (QT01658692, Qiagen), *Asah1* (Mm00480021_m1, ThermoFisher Scientific) IRF7 (Mm00516788_m1, ThermoFisher Scientific), Isg15 (QT00322749, Qiagen), RnaseL (QT01066086, Qiagen), Tetherin/Bst2 (QT01066184 ,Qiagen), IFNα4 (QT01774353, Qiagen), IFNα5 (QT00327656, Qiagen), IFNβ1 (QT00249662, Qiagen), Mx-1 (QT01064231, Qiagen), Oas1 (QT01056048, Qiagen) and PKR (QT00162715, Qiagen).

Click chemistry[47]: Clickable *ω*-azido-sphingosine ((2*S*,3*R*,*E*)-2-amino-18-azidooctadec-4-ene-1,3-diol) was synthesized as described (Solger F *et al.*, unpublished). Cells were seeded and grown to confluence. After pre-incubation with clickable azido-sphingosine, infection was performed as

described. Click reaction was visualized by using Cy3-linked DBCO and other markers were stained according to protocol.

Microarray: Total RNA preparations were checked for RNA integrity with an Agilent 2100 Bioanalyzer. All samples in this study exhibited high-quality RNA Integrity Numbers (RIN 9.8-10). Synthesis of cDNA and subsequent fluorescence labelling of cRNA were performed according to the manufacturer's protocols (One-Color Microarray-Based Gene Expression Analysis/Low Input Quick Amp Labeling; Agilent Technologies, Waldbronn, Germany). Briefly, 100 ng of total RNA was converted to cDNA, followed by in vitro transcription and incorporation of Cy3-CTP into nascent cRNA. After fragmentation, labelled cRNA was hybridized to AgilentSurePrint G3 Mouse GE 8×60k microarrays for 17 hours at 65°C and scanned as described in the manufacturer's protocol. Signal intensities on 20-bit TIFF images were calculated by Feature Extraction software (FE, Vers. 10.7.1.1; Agilent Technologies). Data analyses were conducted with GeneSpring GX software (Vers. 10.5; Agilent Technologies). Probe signal intensities were quantile-normalized across all samples for reduction of inter-array variability. Input data preprocessing was concluded by baseline transformation to the median of all samples.

To ensure innate immune activation macrophages and fibroblasts were infected with LCMV and treated with IFN-α4. To analyze the microarray data a gene set enrichment analysis with GSEA (Broad Institute, v3.0[72,73]) using the Gene Ontology Cellular Components (CC) gene set database (c5.cc.v6.2[74,75], accessed on 15.07.19) was performed using default settings. Results were further subjected to network analysis using the Enrichment Map plugin v3.2.0[76] in Cytoscape v3.7.1[77] with the following settings: FDR q-value cutoff 0.05, p-value cutoff 1, Metric: Jaccard+Overlap Combined (50/50) with cutoff 0.375. Clusters were identified by the AutoAnnotate plugin v1.3[78] and labeled manually for visualization. For visualization gene sets upregulated in LCMV-infected and interferon-treated macrophages or fibroblasts were sorted to the left or right side of the diagram respectively. Several membrane modulating proteins from the families of sphingolipids (including gangliosides), cholesterol and phosphatidylcholine were considered for simplified comparison of macrophages and fibroblasts (see Supplementary Table 2).

Flow cytometry: Liposomes were incubated with fluorescent virus. Samples were diluted, and liposomes could be detected because of size and granularity. Mean fluorescence intensity was determined using LSR Fortessa. Data was analyzed using the software FlowJo (FlowJo LLC).

FACS Sorting: Bone marrow was isolated from tibia and femur of mice and erythrocytes were lysed. To sort pre-progenitor cells staining for linage markers anti-CD3e (Cat # 45-0031-80, eBioscience), anti-GR1 (Cat # 108428, BioLegend), anti-Mac-1 (Cat # 101228, BioLegend), anti-CD4 (Cat # 101228, BioLegend), anti-CD8a (Cat # 100734, BioLegend), anti-TCRb (Cat # 109228, BioLegend), anti-NK1.1 (Cat # 45-5941-82, eBioscience), anti-B220 (Cat # 103236, BioLegend) and anti-CD19 (Cat # 115534, BioLegend) was performed. Additionally anti-CD16/32 (Cat # 101305, BioLegend), anti-CD41 (Cat # 133906, BioLegend), anti-Sca-1 (Cat # 108114, BioLegend), anti-c-kit (Cat # 47-1171-82, Invitrogen), anti-CD105 (Cat # 120412, BioLegend) and anti-CD150 (Cat # 115910, BioLegend) were stained to further classify cells. To sort immature granulocytes, mature granulocytes and monocytes anti-Ly6G (Cat # 17-5931-82, Invitrogen), anti-CD11b (Cat # 25-0112-82, eBioscience) and anti-CD115 (Cat # 11-1031-85, eBioscience) were used. Gating strategy was performed as shown in Supplementary Fig 6.

Western blot for aCDase protein expression: Frozen mouse spleen or cultured primary mouse cells were lysed in radioimmunoprecipitation buffer containing 1x HALT Protease Inhibitor Cocktail and 50 mM EDTA (Thermo Fisher, Cat. No. 78430) using 100 µl lysis buffer per 10 mg organ or 30 µl lysis buffer per 10^6 cells respectively. Spleens were homogenized using a homogenizer (Qiagen Tissue Lyser II, Cat. No. 85300) for 2 min at 20 Hz. Lysates were then centrifuged for 20 min at 20,000 x g at 4 °C, keeping the supernatants. Protein concentration was measured using detergent compatible (DC) Protein Assay (Bio-Rad, Cat. No. 5000112), standardized to 4 µg/µl and prepared for SDS-PAGE by addition of 4x Laemmli sample buffer (Bio-Rad, Cat. No. 1610747), incubation at 95 °C for 5 min followed by cool-down on ice. 30 µg per organ or 10 µg per cell lysate was loaded per lane into a precast TGX AnyKD Stain-free gel (Bio-Rad, Cat. No. 4568126), using Bio-Rad AllBlue protein standard (Cat. No. 1610373) and ran for 45 min at 140 V in Tris/glycine/SDS running buffer (Bio-Rad, Cat. No. 1610732). Transfer was performed using the Trans-Blot Turbo system (Bio-Rad, Cat. No. 1704150) with Mini PVDF Transfer Packs (Bio-Rad, Cat. No. 1704156). Membranes were blocked in Pierce StartingBlock (TBS) Blocking Buffer (Thermo Fisher, Cat. No. 37542) for 2 h and primary antibody was incubated shaking at 4 °C for 2 days: 1:500 for anti-aCDase rabbit polyclonal (Proteintech, Cat. No. 11274-1-AP) for spleens, or 1:500 anti-aCDase rabbit polyclonal (ProSci, Cat. No. 4741) for cell lysates, and 1:1000 for anti-GAPDH mouse (Meridian Life Science, Cat. No. H86504M) diluted in blocking buffer. Membranes were washed three times with Tris-buffered saline-0.1 % Tween 20 (TBS-T) and incubated with secondary antibody at 1:5000 (from GE Life Sciences,

anti-Rabbit IgG, HRP-linked, Cat. No. NA934 or anti-mouse IgG, HRP linked, Cat No. NA931) diluted in 25 % blocking buffer in TBS-T shaking at room temperature for 2 h. After washing twice in TBS-T and twice in TBS membranes were incubated with Pierce ECL (Thermo Fisher, Cat. No. 32106) for 5 min and imaged on a Bio-Rad ChemiDoc MP (Cat. No. 1708280) with ImageLab version 6.0.1 (Bio-Rad). For making figures Inkscape (0.92) was used.

Histology: Histological analysis of liver and spleen tissues was performed with monoclonal fluorescence labeled antibodies against HSV-1-capsid (SY4563) anti-HSV-1 (hu2c[70], anti-gB), anti-Asah1 (4741, ProSci, San Diego, CA, USA), anti-CD9 (124809, Biolegend, San Diego, CA, USA) and anti-sphingosine (clone NHSPH, ALF-274042010, Alfresa Pharma Corporation, Osaka, Japan). Nuclei were stained using Hoechst 33342 (Cat # B2261-100MG, Sigma). Zeiss ELYRA PS.1 SIM/PAL-M/STORM/TIRF and LSM710, Leica SP8 gSTED and FLIM, Leica TCS-SP5, or Keyence BZ-9000 (Keyence, Osaka, Japan) were used to acquire images. Quantification of histology was done using standard procedures in Fiji software version 1.52e (Image J, NIH, Bethesda, MD, USA) or Cell Profiler[79]. In Fiji we used the raw images, applied a mean filter of two/ten to exclude noise. We took the total signal area and the intensity per area after an empirically fixed threshold for further evaluation.

Mass spectrometry analysis: 10^6 cells were subjected to lipid extraction with 1.5 mL methanol/chloroform (2:1, *v:v*)[80]. The extraction solvent contained d_7-sphingosine (d_7-Sph), C17-ceramide, and C16-d_{31}-sphingomyelin (all from Avanti Polar Lipids) as internal standards. Sample analysis was carried out by liquid chromatography tandem mass spectrometry (LC-MS/MS) using either a TQ 6490 mass spectrometer (for Sph) or a QTOF 6530 mass spectrometer (for ceramides and sphingomyelins) (both from Agilent Technologies, Waldbronn, Germany) operating in the positive electrospray ionization mode (ESI+). The following selected reaction monitoring (SRM) transitions were used for quantitation: *m/z* 300.3 → 282.3 for Sph and *m/z* 307.3 → 289.3 for d_7-Sph. The precursor ions of ceramide or sphingomyelin species (differing in the lengths of their fatty acid chains) were cleaved into the fragment ions *m/z* 264.270 (for ceramide) or *m/z* 184.074 (for sphingomyelin), respectively[81]. Quantification was performed with Mass Hunter Software (Agilent Technologies).

Electron microscopy: The samples were fixed with glutaraldehyde (2.5% in 100 mM phosphate buffer). Cells were then contrasted with 1% osmium tetroxide, 1% thiocarbohydrazide, 1.5% potassium ferrocyanide, and 0.5% uranyl acetate in water and were then dehydrated in an ascending ethanol row (50%, 70%, 96%, and 3×100%, 10 min each) and stepwise (EPON/EtOH 1:1 and 2:1

each for 2 h, EPON overnight) flat-embedded in EPON resin. Subsequently, EPON-embedded samples were polymerized for 24 h at 60°C. After removal of the glass slide with 40% aqueous hydrofluoric acid, the EPON disk, containing the cells of interest, was removed from the dish, mounted on EPON resin blocks, and processed for ultramicrotomy. Serial sections were cut with a Leica EM UC7 ultramicrotome (Leica Microsystems) set to a thickness of 55 nm. A final post staining of the ultrathin sections was perfomed for 6 minutes on a drop of 1% uranylacetate followed by 1% lead citrate for 3 minutes in aqueous solution.

Transmission electron microscopy (TEM) was conducted on a Jeol 1400FPlus (Tokyo, Japan) instrument at 120 kV with magnifications as indicated. Digital images were acquired with a 4096×4096-pixel complementary metal-oxide semiconductor (CMOS) camera (TemCam-F416, TVIPS; Gauting, Germany). Postprocessing of the resulting 16-bit TIFF image files was performed with Fiji software version 1.52e (Image J). Pixel noise was averaged by a gaussian blur algorithm. A background resulting from inhomogeneous illumination was removed by implementing the "rolling ball" procedure, and the contrast was adjusted with histogram normalization.

Statistical analysis: If not mentioned otherwise, data are expressed as arithmetic mean ± SEM. Student's *t*-test (two-tailed, if not indicated otherwise) in case of normal distribution or in case of multiple comparisons Anova, were used to detect statistically significant differences. *P* values of 0.05 or less were considered statistically significant. Statistical analyses and graphical presentations were computed with Graph Pad Prism software version 5 (Graph Pad, La Jolla, USA).

Data Availability

The data that support the findings of this study are available from the corresponding author [KSL] upon reasonable request.

Author Contributions

Conceptualization, JL, EG, KSL; Investigation JL, ARN, VD, SKF, HB, FC, PB, JF, MB, DO, KAB, JFK, EG, KSL; Formal analysis JL, EG, KSL; Investigation and formal analysis electron microscopy, JL, HJ, BW; Investigation and formal analysis mass spectrometry FS, BK; Investigation and formal analysis click chemistry JL, JF, JS; Investigation and formal analysis microarray JL, PB, KK; Writing – original draft JL, KSL; Writing – review & editing JL, MJE, PAL, EG, BS, JS, UFG, KSL, CH, AK, EBB, JRG,

BK, FS; Resources KSL, PAL, EG, EBB, UFG, BS, JF, AK, BK, MH, AB, HCP; Supervision KSL, EG, UFG;

Declaration of Interests

The authors declare no competing interests.

Acknowledgments

We thank Alexandra Brenzel and Sylvia Voortmann from the Imaging Center Essen (IMCES) for their technical support. We further thank Daniel Herrmann for technical assistance with the mass spectrometric analyses and Michael Möllmann for help with cell sorting. Images shown in this publication were acquired on IMCES instruments. This study was funded by the German Research Council (DFG - Deutsche Forschungsgemeinschaft; GRK2098, SFB974, GRK1949, GU 335/35-1, LA1419/7-1, LA1419/10-1 and SFB1292/TP13) and the EU 7th framework, Marie-Curie Actions ITN-EDGE (https://ec.europa.eu/research/mariecurieactions/about/innovative-training-networks to BS).

References

1. Murray, P.J. & Wynn, T.A. Protective and pathogenic functions of macrophage subsets. *Nat Rev Immunol* **11**, 723-737 (2011).

2. Honke, N.*, et al.* Enforced viral replication activates adaptive immunity and is essential for the control of a cytopathic virus. *Nat Immunol* **13**, 51-57 (2011).

3. Cervantes-Barragan, L.*, et al.* Type I IFN-mediated protection of macrophages and dendritic cells secures control of murine coronavirus infection. *J Immunol* **182**, 1099-1106 (2009).

4. Lang, P.A.*, et al.* Tissue macrophages suppress viral replication and prevent severe immunopathology in an interferon-I-dependent manner in mice. *Hepatology* **52**, 25-32 (2010).

5. Jenne, C.N. & Kubes, P. Immune surveillance by the liver. *Nat Immunol* **14**, 996-1006 (2013).

6. Wardle, E.N. Kupffer cells and their function. *Liver* **7**, 63-75 (1987).

7. Karasneh, G.A. & Shukla, D. Herpes simplex virus infects most cell types in vitro: clues to its success. *Virol J* **8**, 481 (2011).

8. Nicola, A.V. Herpesvirus Entry into Host Cells Mediated by Endosomal Low pH. *Traffic* **17**, 965-975 (2016).

9. Agelidis, A.M. & Shukla, D. Cell entry mechanisms of HSV: what we have learned in recent years. *Future Virol* **10**, 1145-1154 (2015).

10. Gianni, T., Campadelli-Fiume, G. & Menotti, L. Entry of herpes simplex virus mediated by chimeric forms of nectin1 retargeted to endosomes or to lipid rafts occurs through acidic endosomes. *J Virol* **78**, 12268-12276 (2004).

11. Weed, D.J. & Nicola, A.V. Herpes simplex virus Membrane Fusion. *Adv Anat Embryol Cell Biol* **223**, 29-47 (2017).

12. Sodeik, B., Ebersold, M.W. & Helenius, A. Microtubule-mediated transport of incoming herpes simplex virus 1 capsids to the nucleus. *J Cell Biol* **136**, 1007-1021 (1997).

13. Mabit, H.*, et al.* Intact microtubules support adenovirus and herpes simplex virus infections. *J Virol* **76**, 9962-9971 (2002).

14. Ojala, P.M., Sodeik, B., Ebersold, M.W., Kutay, U. & Helenius, A. Herpes simplex virus type 1 entry into host cells: reconstitution of capsid binding and uncoating at the nuclear pore complex in vitro. *Mol Cell Biol* **20**, 4922-4931 (2000).

15. Crameri, M.*, et al.* MxB is an interferon-induced restriction factor of human herpesviruses. *Nat Commun* **9**, 1980 (2018).

16. Flatt, J.W. & Greber, U.F. Viral mechanisms for docking and delivering at nuclear pore complexes. *Semin Cell Dev Biol* **68**, 59-71 (2017).

17. Yamauchi, Y. & Greber, U.F. Principles of Virus Uncoating: Cues and the Snooker Ball. *Traffic* **17**, 569-592 (2016).

18. Virgin, H.W. The virome in mammalian physiology and disease. *Cell* **157**, 142-150 (2014).

19. Bigalke, J.M. & Heldwein, E.E. Nuclear Exodus: Herpesviruses Lead the Way. *Annu Rev Virol* **3**, 387-409 (2016).

20. Mettenleiter, T.C. Herpesvirus assembly and egress. *J Virol* **76**, 1537-1547 (2002).

21. Yamauchi, Y., Kiriyama, K., Kimura, H. & Nishiyama, Y. Herpes simplex virus induces extensive modification and dynamic relocalisation of the nuclear mitotic apparatus (NuMA) protein in interphase cells. *J Cell Sci* **121**, 2087-2096 (2008).

22. Kodukula, P., Liu, T., Rooijen, N.V., Jager, M.J. & Hendricks, R.L. Macrophage control of herpes simplex virus type 1 replication in the peripheral nervous system. *J Immunol* **162**, 2895-2905 (1999).

23. Lee, D.H. & Ghiasi, H. Roles of M1 and M2 Macrophages in Herpes Simplex Virus 1 Infectivity. *J Virol* **91**(2017).

24. Rasmussen, S.B.*, et al.* Type I interferon production during herpes simplex virus infection is controlled by cell-type-specific viral recognition through Toll-like receptor 9, the mitochondrial antiviral signaling protein pathway, and novel recognition systems. *J Virol* **81**, 13315-13324 (2007).

25. Leib, D.A.*, et al.* Interferons regulate the phenotype of wild-type and mutant herpes simplex viruses in vivo. *J Exp Med* **189**, 663-672 (1999).

26. Piper, R.C. & Katzmann, D.J. Biogenesis and function of multivesicular bodies. *Annu Rev Cell Dev Biol* **23**, 519-547 (2007).

27. Babst, M. MVB vesicle formation: ESCRT-dependent, ESCRT-independent and everything in between. *Curr Opin Cell Biol* **23**, 452-457 (2011).

28. Trajkovic, K.*, et al.* Ceramide triggers budding of exosome vesicles into multivesicular endosomes. *Science* **319**, 1244-1247 (2008).

29. Ohanian, J. & Ohanian, V. Sphingolipids in mammalian cell signalling. *Cell Mol Life Sci* **58**, 2053-2068 (2001).

30. Spiegel, S. & Merrill, A.H., Jr. Sphingolipid metabolism and cell growth regulation. *FASEB J* **10**, 1388-1397 (1996).

31. Tirodkar, T.S. & Voelkel-Johnson, C. Sphingolipids in apoptosis. *Exp Oncol* **34**, 231-242 (2012).

32. Puri, A.*, et al.* An inhibitor of glycosphingolipid metabolism blocks HIV-1 infection of primary T-cells. *AIDS* **18**, 849-858 (2004).

33. Dreschers, S.*, et al.* Infections with human rhinovirus induce the formation of distinct functional membrane domains. *Cell Physiol Biochem* **20**, 241-254 (2007).

34. Utermohlen, O., Herz, J., Schramm, M. & Kronke, M. Fusogenicity of membranes: the impact of acid sphingomyelinase on innate immune responses. *Immunobiology* **213**, 307-314 (2008).

35. Jimenez-Rojo, N., Garcia-Arribas, A.B., Sot, J., Alonso, A. & Goni, F.M. Lipid bilayers containing sphingomyelins and ceramides of varying N-acyl lengths: a glimpse into sphingolipid complexity. *Biochim Biophys Acta* **1838**, 456-464 (2014).

36. Li, C.M.*, et al.* The human acid ceramidase gene (ASAH): structure, chromosomal location, mutation analysis, and expression. *Genomics* **62**, 223-231 (1999).

37. Zupancic, E., Carreira, A.C., de Almeida, R.F. & Silva, L.C. Biophysical implications of sphingosine accumulation in membrane properties at neutral and acidic pH. *J Phys Chem B* **118**, 4858-4866 (2014).

38. Nicola, A.V. & Straus, S.E. Cellular and viral requirements for rapid endocytic entry of herpes simplex virus. *J Virol* **78**, 7508-7517 (2004).

39. Dohner, K.*, et al.* Importin alpha1 is required for nuclear import of herpes simplex virus proteins and capsid assembly in fibroblasts and neurons. *PLoS Pathog* **14**, e1006823 (2018).

40. Mikloska, Z. & Cunningham, A.L. Alpha and gamma interferons inhibit herpes simplex virus type 1 infection and spread in epidermal cells after axonal transmission. *J Virol* **75**, 11821-11826 (2001).

41. Kim, E.T., White, T.E., Brandariz-Nunez, A., Diaz-Griffero, F. & Weitzman, M.D. SAMHD1 restricts herpes simplex virus 1 in macrophages by limiting DNA replication. *J Virol* **87**, 12949-12956 (2013).

42. Gebai, A., Gorelik, A., Li, Z., Illes, K. & Nagar, B. Structural basis for the activation of acid ceramidase. *Nat Commun* **9**, 1621 (2018).

43. Coant, N., Sakamoto, W., Mao, C. & Hannun, Y.A. Ceramidases, roles in sphingolipid metabolism and in health and disease. *Adv Biol Regul* **63**, 122-131 (2017).

44. Goni, F.M. & Alonso, A. Biophysics of sphingolipids I. Membrane properties of sphingosine, ceramides and other simple sphingolipids. *Biochim Biophys Acta* **1758**, 1902-1921 (2006).

45. Nicola, A.V., McEvoy, A.M. & Straus, S.E. Roles for endocytosis and low pH in herpes simplex virus entry into HeLa and Chinese hamster ovary cells. *J Virol* **77**, 5324-5332 (2003).

46. Cohen, G.H.*, et al.* Structural analysis of the capsid polypeptides of herpes simplex virus types 1 and 2. *J Virol* **34**, 521-531 (1980).

47. Fink, J. & Seibel, J. Click reactions with functional sphingolipids. *Biol Chem* **399**, 1157-1168 (2018).

48. Langlais, D., Barreiro, L.B. & Gros, P. The macrophage IRF8/IRF1 regulome is required for protection against infections and is associated with chronic inflammation. *J Exp Med* **213**, 585-603 (2016).

49. Qi, C.F.*, et al.* Differential expression of IRF8 in subsets of macrophages and dendritic cells and effects of IRF8 deficiency on splenic B cell and macrophage compartments. *Immunol Res* **45**, 62-74 (2009).

50. Hu, X.*, et al.* IRF8 regulates acid ceramidase expression to mediate apoptosis and suppresses myelogeneous leukemia. *Cancer Res* **71**, 2882-2891 (2011).

51. Yona, S.*, et al.* Fate mapping reveals origins and dynamics of monocytes and tissue macrophages under homeostasis. *Immunity* **38**, 79-91 (2013).

52. Stohlman, S.A., Woodward, J.G. & Frelinger, J.A. Macrophage antiviral activity: extrinsic versus intrinsic activity. *Infect Immun* **36**, 672-677 (1982).

53. Xu, Z., Tian, J., Smith, J.S. & Byrnes, A.P. Clearance of adenovirus by Kupffer cells is mediated by scavenger receptors, natural antibodies, and complement. *J Virol* **82**, 11705-11713 (2008).

54. Maler, M.D.*, et al.* Key Role of the Scavenger Receptor MARCO in Mediating Adenovirus Infection and Subsequent Innate Responses of Macrophages. *MBio* **8**(2017).

55. Stichling, N.*, et al.* Lung macrophage scavenger receptor SR-A6 (MARCO) is an adenovirus type-specific virus entry receptor. *PLoS Pathog* **14**, e1006914 (2018).

56. Le Blanc, I.*, et al.* Endosome-to-cytosol transport of viral nucleocapsids. *Nat Cell Biol* **7**, 653-664 (2005).

57. Nour, A.M., Li, Y., Wolenski, J. & Modis, Y. Viral membrane fusion and nucleocapsid delivery into the cytoplasm are distinct events in some flaviviruses. *PLoS Pathog* **9**, e1003585 (2013).

58. Michen, B. & Graule, T. Isoelectric points of viruses. *J Appl Microbiol* **109**, 388-397 (2010).

59. Olofsson, S. Isoelectric focusing of herpes simplex virus. *Arch Virol* **49**, 93-98 (1975).

60. Jimenez-Rojo, N.*, et al.* Membrane permeabilization induced by sphingosine: effect of negatively charged lipids. *Biophys J* **106**, 2577-2584 (2014).

61. Hafez, I.M., Ansell, S. & Cullis, P.R. Tunable pH-sensitive liposomes composed of mixtures of cationic and anionic lipids. *Biophys J* **79**, 1438-1446 (2000).

62. Hollenbaugh, J.A.*, et al.* Host factor SAMHD1 restricts DNA viruses in non-dividing myeloid cells. *PLoS Pathog* **9**, e1003481 (2013).

63. Chow, A.Y. & Mellman, I. Old lysosomes, new tricks: MHC II dynamics in DCs. *Trends Immunol* **26**, 72-78 (2005).

64. Geiger, T.*, et al.* Initial quantitative proteomic map of 28 mouse tissues using the SILAC mouse. *Mol Cell Proteomics* **12**, 1709-1722 (2013).

65. Ehlert, K.*, et al.* Farber disease: clinical presentation, pathogenesis and a new approach to treatment. *Pediatr Rheumatol Online J* **5**, 15 (2007).

66. Dropulic, L.K. & Cohen, J.I. Severe viral infections and primary immunodeficiencies. *Clin Infect Dis* **53**, 897-909 (2011).

67. Rehwinkel, J.*, et al.* SAMHD1-dependent retroviral control and escape in mice. *EMBO J* **32**, 2454-2462 (2013).

68. Sandbaumhuter, M., *et al.* Cytosolic herpes simplex virus capsids not only require binding inner tegument protein pUL36 but also pUL37 for active transport prior to secondary envelopment. *Cell Microbiol* **15**, 248-269 (2013).

69. Yamauchi, Y., *et al.* The UL14 tegument protein of herpes simplex virus type 1 is required for efficient nuclear transport of the alpha transinducing factor VP16 and viral capsids. *J Virol* **82**, 1094-1106 (2008).

70. Krawczyk, A., *et al.* Overcoming drug-resistant herpes simplex virus (HSV) infection by a humanized antibody. *Proc Natl Acad Sci U S A* **110**, 6760-6765 (2013).

71. Henry, B.D., *et al.* Engineered liposomes sequester bacterial exotoxins and protect from severe invasive infections in mice. *Nat Biotechnol* **33**, 81-88 (2015).

72. Subramanian, A., *et al.* Gene set enrichment analysis: a knowledge-based approach for interpreting genome-wide expression profiles. *Proc Natl Acad Sci U S A* **102**, 15545-15550 (2005).

73. Mootha, V.K., *et al.* PGC-1alpha-responsive genes involved in oxidative phosphorylation are coordinately downregulated in human diabetes. *Nat Genet* **34**, 267-273 (2003).

74. Ashburner, M., *et al.* Gene ontology: tool for the unification of biology. The Gene Ontology Consortium. *Nat Genet* **25**, 25-29 (2000).

75. The Gene Ontology, C. The Gene Ontology Resource: 20 years and still GOing strong. *Nucleic Acids Res* **47**, D330-D338 (2019).

76. Merico, D., Isserlin, R., Stueker, O., Emili, A. & Bader, G.D. Enrichment map: a network-based method for gene-set enrichment visualization and interpretation. *PLoS One* **5**, e13984 (2010).

77. Shannon, P., *et al.* Cytoscape: a software environment for integrated models of biomolecular interaction networks. *Genome Res* **13**, 2498-2504 (2003).

78. Kucera, M., Isserlin, R., Arkhangorodsky, A. & Bader, G.D. AutoAnnotate: A Cytoscape app for summarizing networks with semantic annotations. *F1000Res* **5**, 1717 (2016).

79. Carpenter, A.E., *et al.* CellProfiler: image analysis software for identifying and quantifying cell phenotypes. *Genome Biol* **7**, R100 (2006).

80. Gulbins, A., *et al.* Antidepressants act by inducing autophagy controlled by sphingomyelin-ceramide. *Mol Psychiatry* (2018).

81. Kachler, K., *et al.* Enhanced Acid Sphingomyelinase Activity Drives Immune Evasion and Tumor Growth in Non-Small Cell Lung Carcinoma. *Cancer Res* **77**, 5963-5976 (2017).

Figure Legends

Figure 1: Macrophages control herpes simplex virus type 1 (HSV-1) infection

a: Immunofluorescence of livers from wild-type (WT) mice that were not or were infected with 8×10^7 tissue culture infection dose 50 ($TCID_{50}$) HSV-1 and analyzed after 1 h (n = 3, blue represents Hoechst staining, scale bar 100 µm). **b-d**: Immunofluorescence of livers (b, n = 8, scale bar 200 µm), real-time polymerase chain reaction (RT-PCR) of lymph nodes (LN), spleens and livers (c, n = 12-14) and $TCID_{50}$ of spleens and livers (d, n = 8) from WT mice that were pretreated with control-liposomes and WT mice that were pretreated with clodronate-liposomes (day -3), infected with 6×10^6 $TCID_{50}$ HSV-1 and analyzed after 24 h. **e&f**: Alanine transaminase (ALT) and aspartate transaminase (AST) activity (e; n = 10) and survival of mice (f) that were treated with clodronate-liposomes or control liposomes (n = 10; day -3) and then infected with 6×10^5 $TCID_{50}$ HSV-1 or left uninfected (n = 5; p = 0.0006). **g&h**: RT-PCR of vagina (g) and $TCID_{50}$ of vagina and vaginal fluid (h) of mice that were treated with clodronate-liposomes or control-liposomes (day -3) and then infected with 2×10^7 $TCID_{50}$ HSV-1 intravaginally, analyzed after 24h (n = 6). **i**: Survival of mice that were treated with clodronate-liposomes or control-liposomes (day -3) and then infected with 2×10^7 $TCID_{50}$ HSV-1 intravaginally (n = 9), or left uninfected (n = 5; p = 0.0372). All data are shown as mean +/- SEM. * equals $p \leq 0.05$, ** equals $p \leq 0.01$, # equals $p \leq 0.001$, ## equals $p \leq 0.0001$.

Figure 2: Virus trapping in multivesicular bodies correlates with expression of acid ceramidase

a&b: Immunofluorescence (a) and tissue culture infection dose 50 ($TCID_{50}$) from supernatants (b) of fibroblasts or bone marrow derived macrophages (BMDMs) that were infected with herpes simplex virus type 1 (HSV-1) at a multiplicity of infection (MOI) of 0.01 or MOI 1 (n = 8; scale bar 50 µm). **c**: Gene set enrichment analysis (GSEA) of microarrays showing gene sets enriched in macrophages (red) vs. gene sets enriched in fibroblasts (blue). See Supplementary Table 1a and b for gene sets, ranking and grouping. NES: normalized enrichment score. ER: endoplasmic reticulum. **d&e:** Representative electron microscopic images (d) and quantification (e) of wild-type (WT) BMDMs and/or fibroblasts infected with HSV-1 (MOI 250) analyzed after 30 minutes (BMDMs: n = 77 images from three independent experiments, scale bar 5 µm; Fibroblasts: n = 106 images from three independent experiments, scale bar 5 µm). Overview of one macrophage and one fibroblast is shown. Details show specific compartments containing HSV-1. MVB: multivesicular bodies. **f**: Expression of

membrane-modulating proteins analyzed from microarrays of fibroblasts and macrophages with or without interferon-α4 (IFN-α4) treatment. **g**: Real-time polymerase chain reaction (RT-PCR) for *Asah1* mRNA expression of fibroblasts and macrophages from WT mice (n = 6). **h**: Western Blot for aCDase protein expression of fibroblasts and macrophages from WT mice (1 of 2 is shown). All data are shown as mean +/- SEM. * equals p ≤ 0.05, ** equals p ≤ 0.01, # equals p ≤ 0.001, ## equals p ≤ 0.0001.

Figure 3: Acid Ceramidase protects macrophages from herpes simplex virus type 1 (HSV-1) infection and prevents severe disease

a&b: Representative images (a) and quantification (b) of immunofluorescence from wild-type (WT) and *Asah1*$^{-/-}$ bone marrow derived macrophages (BMDMs) infected with HSV-1 for 6 h (multiplicity of infection [MOI] 10, n = 5, scale bar 50µm). N.D.: not done. **c**: Immunofluorescence of livers from WT and *Asah1*$^{-/-}$ mice that were infected with 7×10^7 plaque forming units (PFU) HSV-1 and analyzed after 12 h (n = 6-9, scale bar 100 µm). **d&e**: Real-time polymerase chain reaction (RT-PCR) of lymph nodes (LN), spleens and livers (d, n = 7-10) and tissue culture infection dose 50 ($TCID_{50}$, e, n = 4-6) of spleens and livers from WT mice and *Asah1*$^{-/-}$ mice that were infected with 2×10^6 $TCID_{50}$ HSV-1 and analyzed on day 3. **f**: $TCID_{50}$ of spleens and livers from WT (n = 9), *Samhd1*$^{-/-}$ (n = 4), *Ifnar1*$^{-/-}$ (n = 4), and *MyD88*$^{-/-}$ *x Trif*$^{-/-}$ *x Cardif*$^{-/-}$ (n = 3) mice that were infected with 2×10^6 $TCID_{50}$ HSV-1 and analyzed on day 3. **g**: RT-PCR of spleens and livers from bone marrow chimera mice receiving Cre$^-$ *Asah1*$^{fl/fl}$ or Cre$^+$ *Asah1*$^{fl/fl}$ bone marrow that were tamoxifen-treated, infected with 6×10^6 $TCID_{50}$ HSV-1 and analyzed on day 3 (n = 5). **h**: Survival of tamoxifen-treated Cre$^-$ *Asah1*$^{fl/fl}$ and Cre$^+$ *Asah1*$^{fl/fl}$ mice which were infected intravaginally with 2×10^7 $TCID_{50}$ HSV-1 (n = 11-12, p = 0.0004). **i**: Survival of tamoxifen-treated Cre$^-$ *Asah1*$^{fl/fl}$ and Cre$^+$ *Asah1*$^{fl/fl}$ mice which were infected intravenously with 5×10^5 $TCID_{50}$ HSV-1 (n = 11-13, p = 0.0004) or left uninfected (Cre$^+$ *Asah1*$^{fl/fl}$, naïve; n = 5). All data are shown as mean +/- SEM. * equals p ≤ 0.05, ** equals p ≤ 0.01, # equals p ≤ 0.001, ## equals p ≤ 0.0001.

Figure 4: Sphingosine protects against herpes simplex virus type 1 (HSV-1) infection

a: Immunofluorescence of wild-type (WT) macrophages, which were infected with HSV-1 (multiplicity of infection [MOI] 10) and stained for acid ceramidase (aCDase) and HSV-1 (n = 5, blue represents Hoechst staining, scale bar 10 µm) after 30 minutes. **b**: Schematic representation showing the metabolism of sphingomyelin (SM) to sphingosine-1-phosphate (S1P). **c&d:** Representative image (c)

and quantification (d) of immunofluorescence from bone marrow derived macrophages (BMDMs) that have been incubated for 30 minutes with β-D-galactosyl ceramide (Cer; 100 µM), D-erythro-sphingosine (Sph; 100 µM), sphingosine kinase inhibitor (SKI-II; 100 µM), ceramidase (CDase; 250 U/L) or sphingomyelinase (SMase; 6.5 U/ml) and subsequently infected with HSV-1 at a multiplicity of infection (MOI) of 100 (n = 5, scale bar 50 µm), fixed and stained after 6h. N.D.: not done. **e**: Tissue culture infection dose 50 ($TCID_{50}$) of BMDMs that have been incubated for 30 minutes with D-erythro-sphingosine (Sph; 40 µM), sphingosine kinase inhibitor (SKI-II; 200µM), or sphingomyelinase (SMase; 6.5 U/ml), subsequently infected with HSV-1 at a MOI of 1 and analyzed after 24h (n = 3-4, one-tailed Student's *t*-test). **f**: $TCID_{50}$ of THP-1 cells that have been incubated for 30 minutes with D-erythro-sphingosine (Sph; 400 µM) and subsequently infected with HSV-1 at a MOI of 0.01, analyzed after 6h (n = 3). **g:** $TCID_{50}$ of Hela cells that have been incubated for 30 minutes with D-erythro-sphingosine (Sph; 100 µM), and sphingosine kinase inhibitor (SKI-II; 100 µM), and subsequently infected with HSV-1 at a MOI of 0.001 analyzed after 24h (n = 3). **h**: $TCID_{50}$ of Vero cells that have been incubated for 30 minutes with D-erythro-sphingosine (Sph; 100 µM), and sphingosine kinase inhibitor (SKI-II; 100 µM), and subsequently infected with HSV-1 at a MOI of 0.01 analyzed after 24h (n = 3). All data are shown as mean +/- SEM. * equals $p \leq 0.05$, ** equals $p \leq 0.01$, # equals $p \leq 0.001$, ## equals $p \leq 0.0001$.

Figure 5: Sphingosine-rich intraluminal vesicles trap herpes simplex virus type 1 (HSV-1)

a&b: Representative images (a) and quantification (b) of immunofluorescence from wild-type (WT) and *Asah1*$^{-/-}$ bone marrow derived macrophages (BMDMs) incubated with HSV-1-VP16-GFP (multiplicity of infection [MOI] 30) for 30 minutes. Intact viral particles are visible through GFP-tagged tegument protein VP16 (green). Exposed capsids were stained with anti-VP5 (red, n = 17 images, one of two experiments is shown, scale bar 10 µm). **c&d**: Representative electron microscopy images (c) and quantification (d) of WT and *Asah1*$^{-/-}$ BMDMs infected with HSV-1 (MOI 250) analyzed after 30 minutes (n = 68 WT images and n = 63 *Asah1*$^{-/-}$ images from three independent experiments; upper scale bar 400 nm, lower scale bar 200 nm). **e**: Immunofluorescence of WT BMDMs, which were loaded with clickable *ω*-azido-sphingosine for 3 hours, infected with HSV-1 (MOI 10) for 30 minutes and then stained for sphingosine, the intraluminal vesicle (ILV) marker CD9, HSV-1 anti-capsid and Hoechst (blue, n = 5, scale bar 20 µm). **f&g**: Representative dot plots (f) and quantification (g) of control liposomes, ceramide-loaded liposomes and sphingosine-loaded liposomes that were incubated

with fluorescently labeled HSV-1 for 10 minutes and then analyzed for HSV-1 binding in flow cytometry (n = 6). All data are shown as mean +/- SEM. * equals $p \leq 0.05$, ** equals $p \leq 0.01$, # equals $p \leq 0.001$, ## equals $p \leq 0.0001$.

Figure 6: Acid ceramidase expression in myeloid cells depends on interferon regulatory factor 8

a: Real-time polymerase chain reaction (RT-PCR) for wild-type (WT) and *Asah1*$^{-/-}$ bone marrow derived macrophages (BMDMs) that were left untreated, infected with herpes simplex virus type 1 (HSV-1) at a multiplicity of infection (MOI) of 1 for 24 h or infected and treated with 100 units interferon-α4 (IFN-α4; n = 10). **b**: RT-PCR for WT and *Asah1*$^{-/-}$ BMDMs that were left untreated or infected with HSV-1 at an MOI of 1 for 24h (n = 10). **c&d:** RT-PCR for *Asah1* (c, n = 5) and Western Blot for aCDase (d, n = 3) of spleen tissues from WT and interferon regulatory factor 8 deficient (*Irf8*$^{-/-}$) mice that were left untreated. **e:** RT-PCR (e) of lymph nodes (LN), spleens and livers and tissue culture infection dose 50 ($TCID_{50}$, f) of spleens and livers from WT and *Irf8*$^{-/-}$ mice that were infected with 2×10^6 $TCID_{50}$ HSV-1 and analyzed on day 3. All data are shown as mean +/- SEM. * equals $p \leq 0.05$, ** equals $p \leq 0.01$, # equals $p \leq 0.001$, ## equals $p \leq 0.0001$.

Suppl. Figure 1: Efficiency of macrophage depletion by clodronate

a&**b**: Immunofluorescence of livers (a) and spleens (b) from wild-type (WT) mice that were pretreated with control-liposomes and WT mice that were pretreated with clodronate-liposomes (day -3), infected with 6×10^6 tissue culture infection dose 50 ($TCID_{50}$) HSV-1 and analyzed after 24 h (n = 3, blue represents Hoechst staining, scale bar 100 µm). **c**: Immunofluorescence of livers from WT mice that were pretreated with clodronate-liposomes (day -3), infected with 8×10^7 $TCID_{50}$ HSV-1 and analyzed after 1 h (n = 3, blue represents Hoechst staining scale bar 100 µm).

Suppl. Figure 2: Herpes simplex virus type 1 (HSV-1) infection of primary fibroblasts

Representative electron microscopy images of wild-type (WT) fibroblasts infected with HSV-1 (MOI 250) analyzed after 30 minutes (n = 106 images from three independent experiments, scale bar 5 µm). Detail shows HSV-1 close to the nucleus.

Suppl. Figure 3: Real-time polymerase chain reaction (RT-PCR) for herpes simplex virus type 1 (HSV-1) in mice with different innate immune deficiencies

RT-PCR of lymph nodes (LN), spleens and livers from wild-type (WT; n = 9), *Samhd1*$^{-/-}$ (n = 4), *Ifnar1*$^{-/-}$ (n = 4), and *MyD88*$^{-/-}$ *x Trif*$^{-/-}$ *x Cardif*$^{-/-}$ (n = 3) mice that were infected with 2×10^6 tissue culture infection dose 50 ($TCID_{50}$) HSV-1 and analyzed on day 3. All data are shown as mean +/- SEM. * equals $p \leq 0.05$, ** equals $p \leq 0.01$, # equals $p \leq 0.001$, ## equals $p \leq 0.0001$.

Suppl. Figure 4: Mass spectrometric analysis of sphingolipids after treatments in different cell lines

a: Mass spectrometric analysis of sphingolipids in Raw264.7 cells and bone marrow derived macrophages (BMDMs) that were incubated for 30 minutes with 250 µM D-erythro-sphingosine (Sph), 100 µM of sphingosine kinase inhibitor (SKI), 250 U/L ceramidase (CDase) or 6.5 U/ml sphingomyelinase (SMase) (n = 6) and analyzed after 24 h (Raw264.7 cells) or 6h (BMDMs). (**b**) BMDMs were treated for 30 minutes with 0,3 µg ceramidase, 90 minutes with 1,56 U / 250µL sphingomyelinase or left untreated (n = 3). All data are shown as mean +/- SD. * equals $p \leq 0.05$, ** equals $p \leq 0.01$, # equals $p \leq 0.001$, ## equals $p \leq 0.0001$.

Suppl. Figure 5: Expression of *Asah1* in macrophages during development is dependent on IRF8

a: Real-time polymerase chain reaction (RT-PCR) results for *Asah1* mRNA expression of monocytes, granulocytes and precursor cells from the myeloid lineage (n = 5-8; one-tailed Student's *t*-test). **b**: Gating strategy for cell sorting. All data are shown as mean +/- SEM. * equals $p \leq 0.05$, ** equals $p \leq 0.01$, # equals $p \leq 0.001$, ## equals $p \leq 0.0001$.

Suppl. Figure 6: Asah1 expression in different tissues

Real-time polymerase chain reaction (RT-PCR) for *Asah1* of the indicated organs derived from naïve C57BL/6 mice (n = 4-5). All data are shown as mean +/- SEM. * equals $p \leq 0.05$, ** equals $p \leq 0.01$, # equals $p \leq 0.001$, ## equals $p \leq 0.0001$.

Suppl. Table 1: Gene set enrichment analysis (GSEA)

a: GSEA report of the most enriched Gene Ontology CC gene sets (FDR < 0.05) in macrophages, ranked by their normalized enrichment score and grouped by function/compartment. **b**: GSEA report of the most enriched Gene Ontology CC gene sets (FDR < 0.05) in fibroblasts, ranked by their normalized enrichment score and grouped by function/compartment.

Suppl. Table 2: Membrane-modulating proteins in macrophages vs fibroblasts

Membrane-modulating proteins from the families of sphingolipids (including gangliosides), cholesterol and phosphatidylcholine which were considered for simplified comparison of macrophages and fibroblasts.

Figure 1

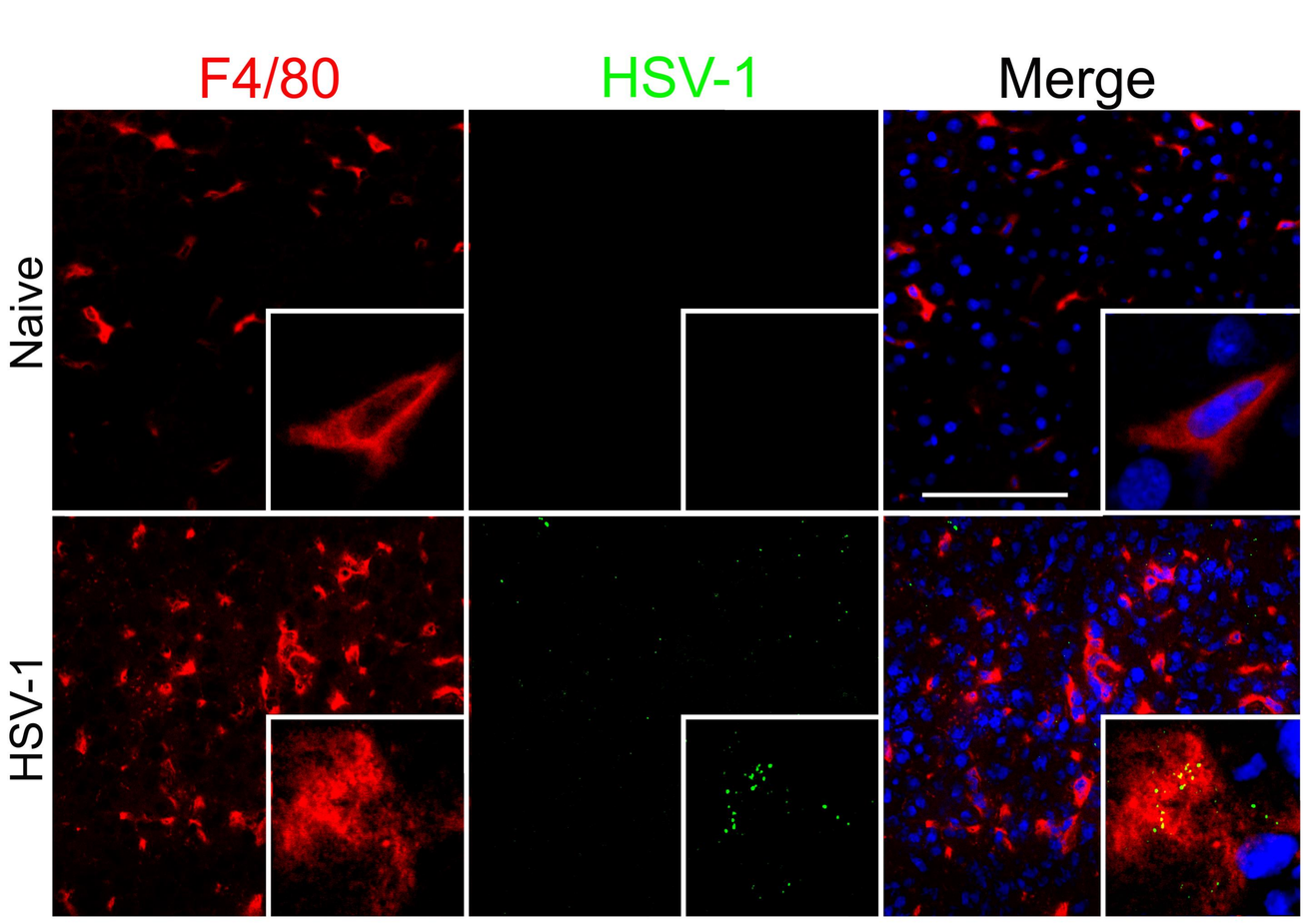
a
F4/80
HSV-1
Merge
Naive
HSV-1

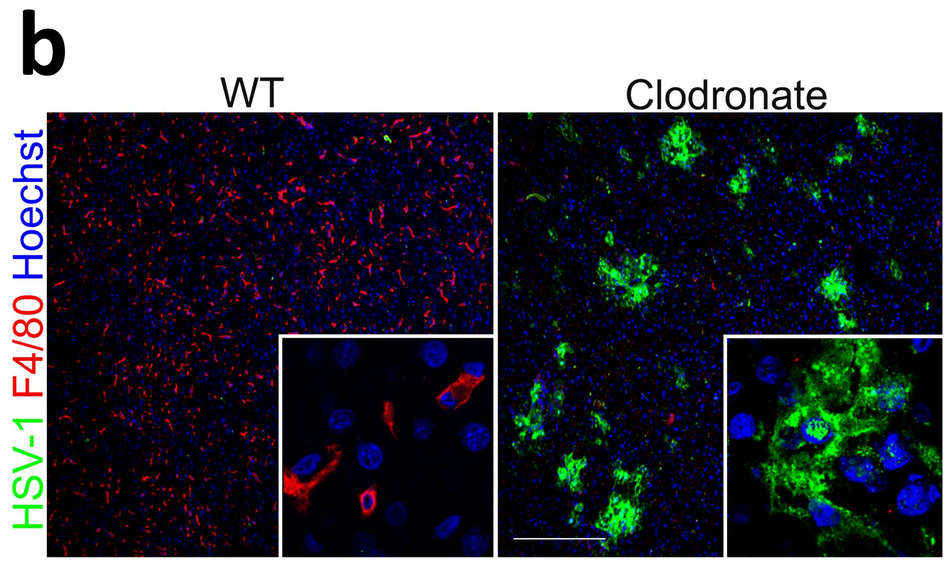
b
WT
Clodronate
HSV-1 F4/80 Hoechst

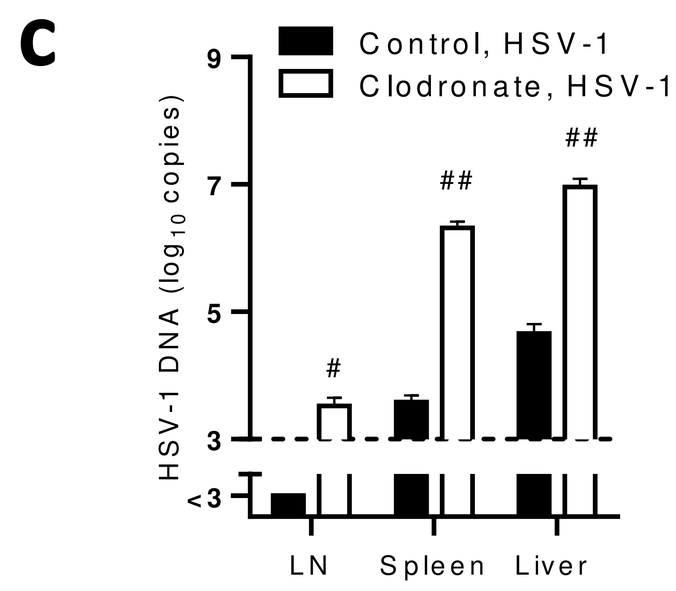
c
Control, HSV-1
Clodronate, HSV-1
HSV-1 DNA (log10 copies)
LN
Spleen
Liver

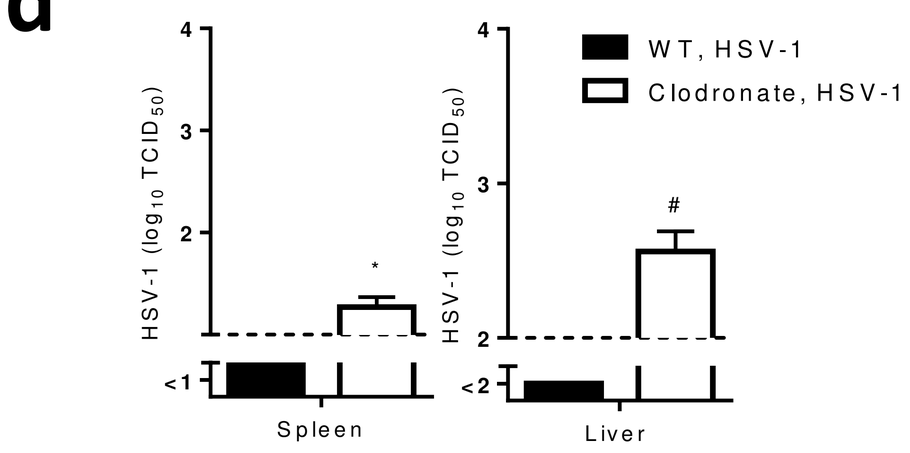
d
WT, HSV-1
Clodronate, HSV-1
HSV-1 (log10 TCID50)
Spleen
Liver

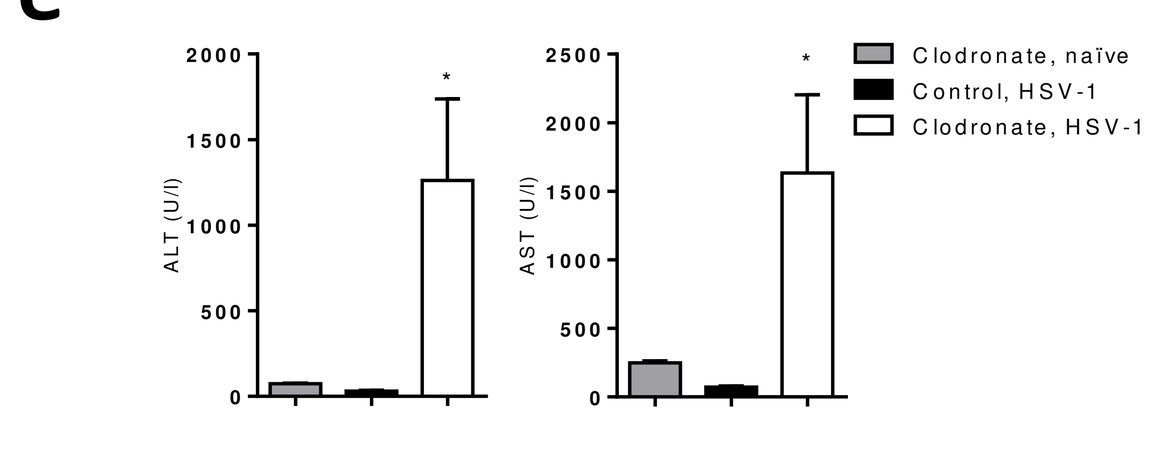
e
Clodronate, naïve
Control, HSV-1
Clodronate, HSV-1
ALT (U/l)
AST (U/l)

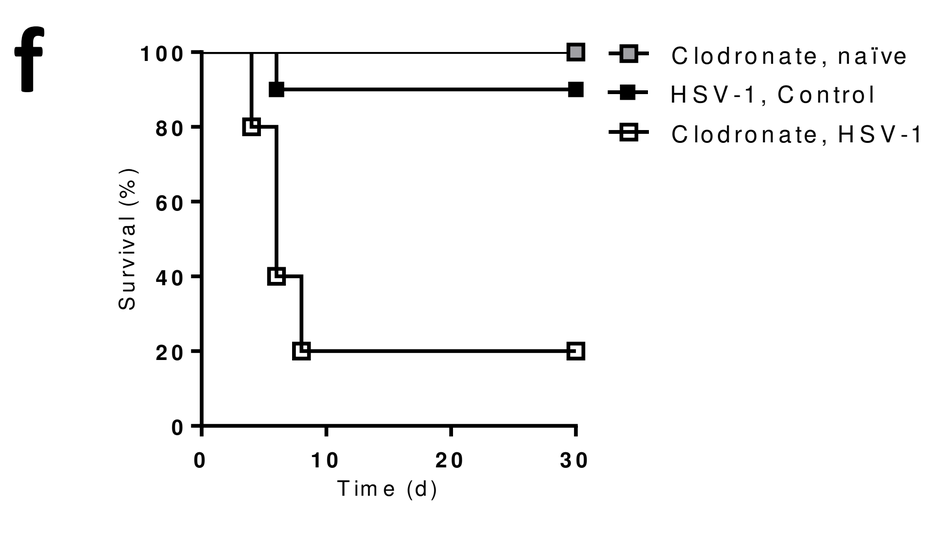
f
Clodronate, naïve
HSV-1, Control
Clodronate, HSV-1
Survival (%)
Time (d)

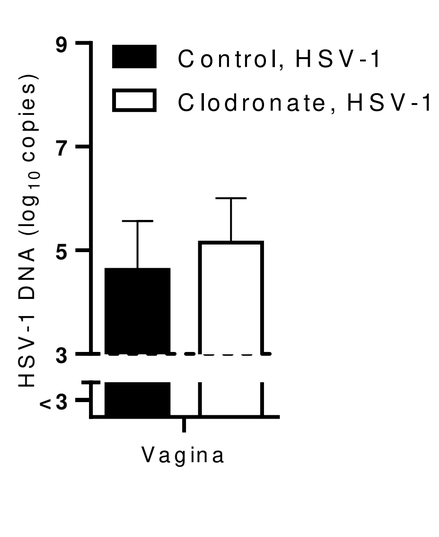
g
Control, HSV-1
Clodronate, HSV-1
HSV-1 DNA (log10 copies)
Vagina

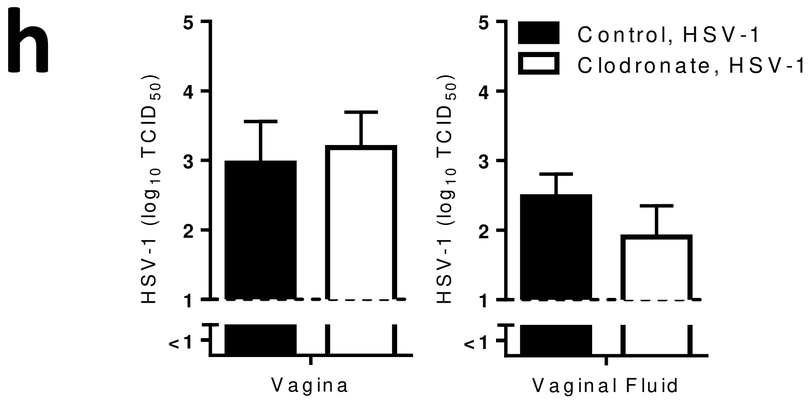
h
Control, HSV-1
Clodronate, HSV-1
HSV-1 (log10 TCID50)
Vagina
Vaginal Fluid

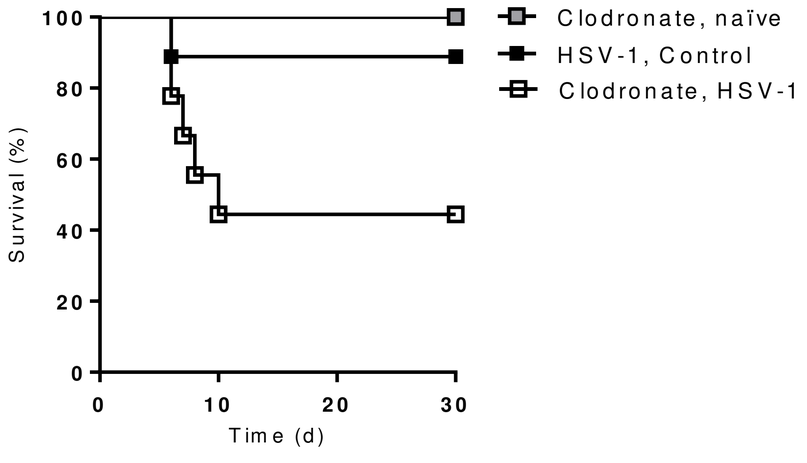
i
Clodronate, naïve
HSV-1, Control
Clodronate, HSV-1
Survival (%)
Time (d)

Figure 2

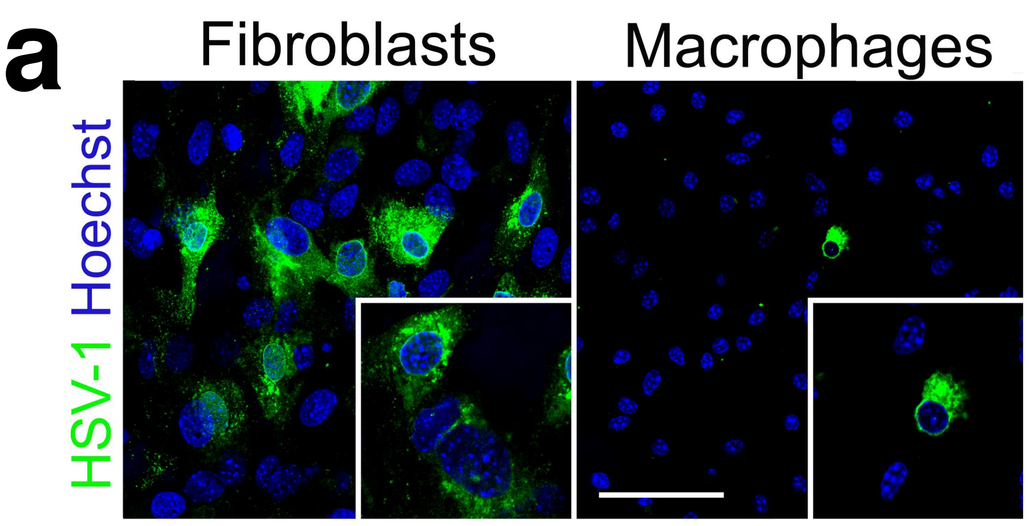
a
Fibroblasts
Macrophages
HSV-1 Hoechst

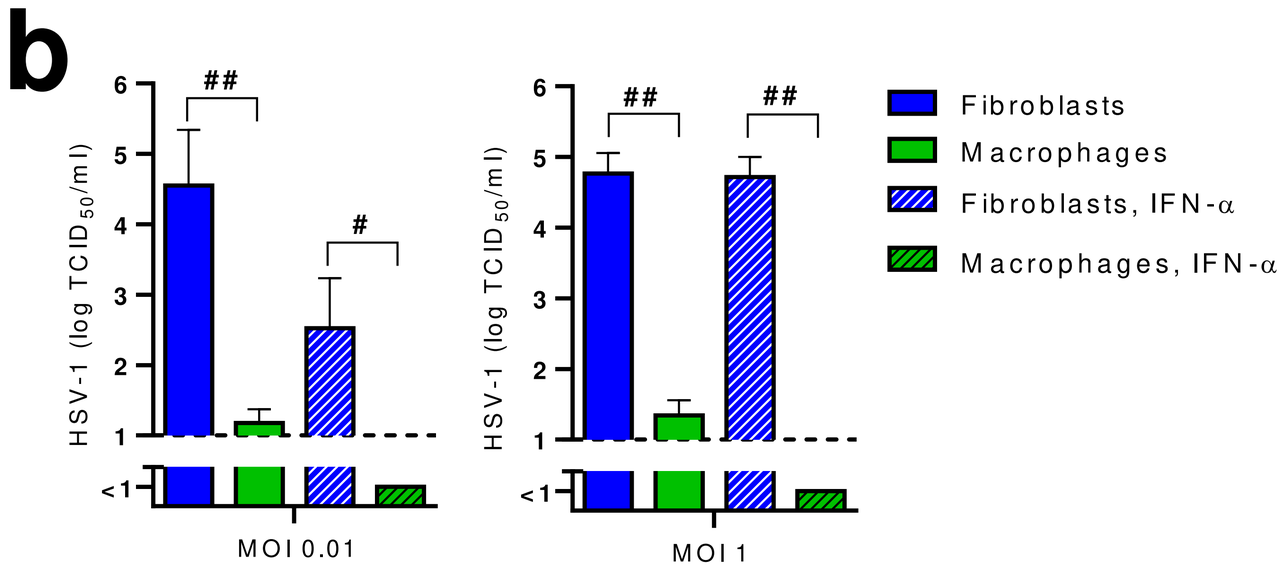
b
HSV-1 (log TCID50/ml)
##
#
MOI 0.01
MOI 1
Fibroblasts
Macrophages
Fibroblasts, IFN-α
Macrophages, IFN-α

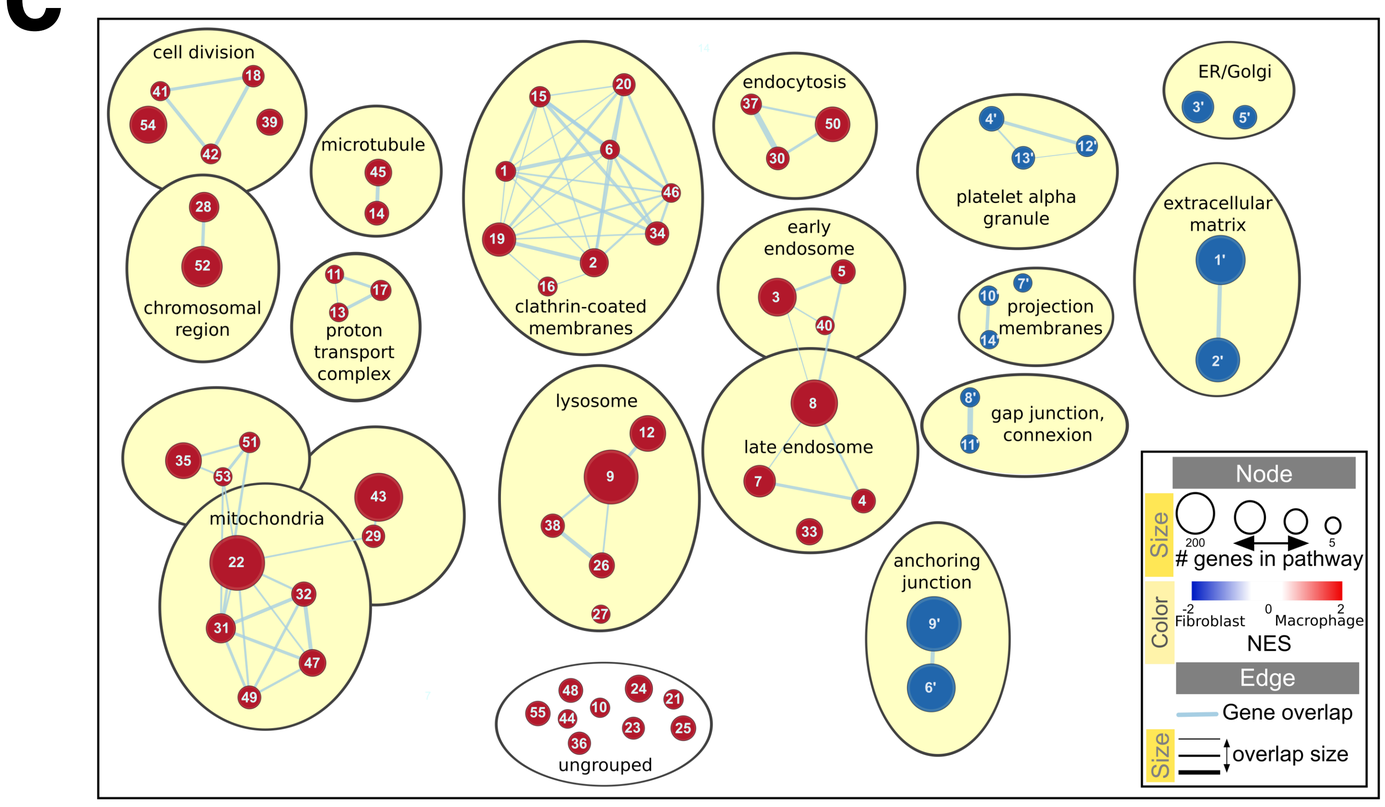
c
cell division
microtubule
endocytosis
ER/Golgi
chromosomal region
proton transport complex
clathrin-coated membranes
early endosome
platelet alpha granule
extracellular matrix
projection membranes
gap junction, connexion
lysosome
late endosome
mitochondria
anchoring junction
ungrouped
Node
Size
genes in pathway
Color
Fibroblast
Macrophage
NES
Edge
Gene overlap
overlap size

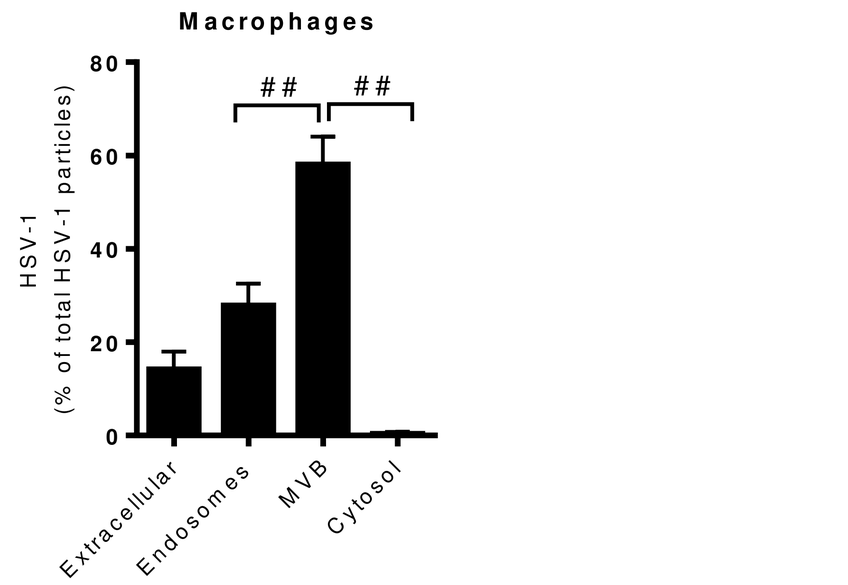
e
Macrophages
HSV-1 (% of total HSV-1 particles)
##
##
Extracellular
Endosomes
MVB
Cytosol

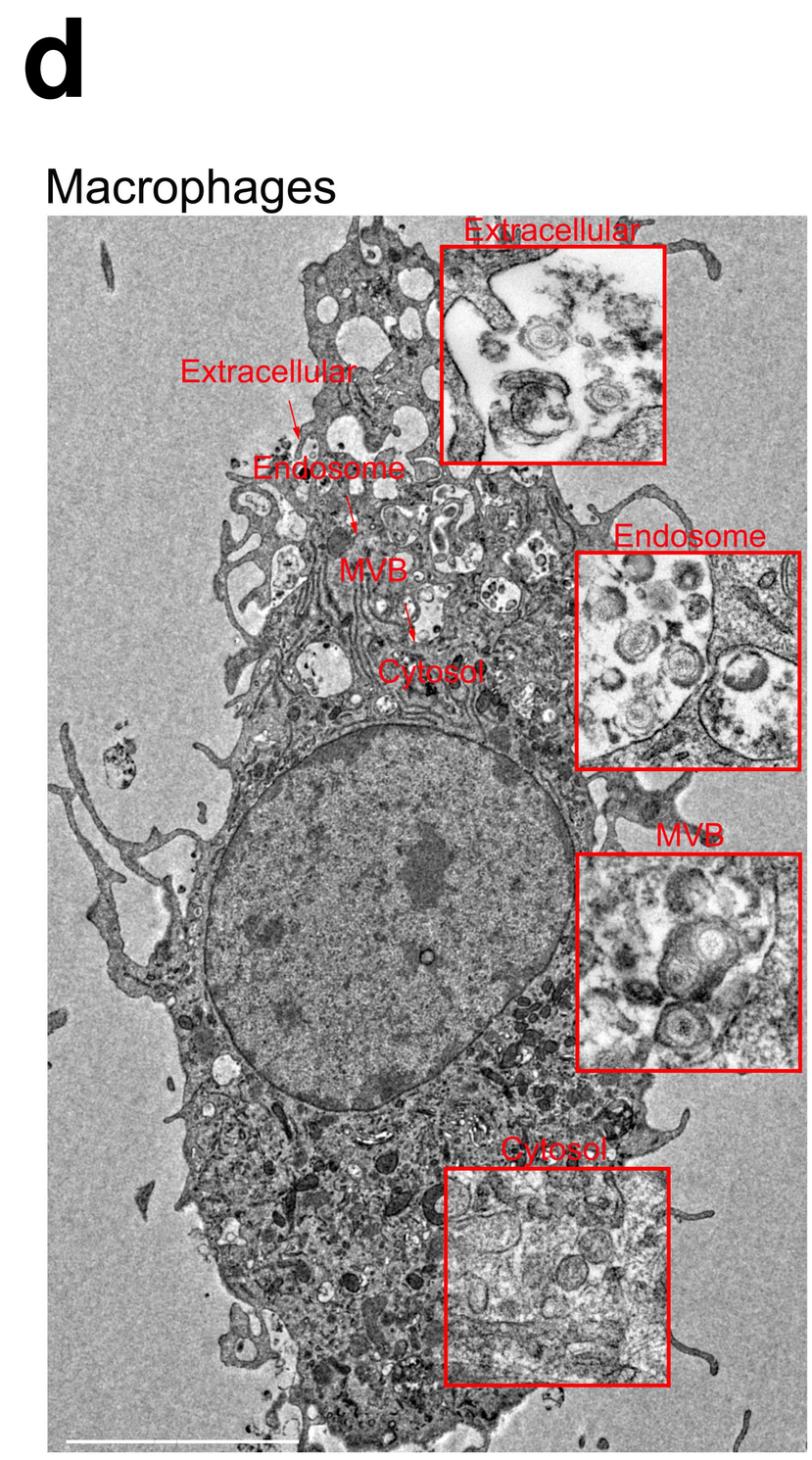
Macrophages
Extracellular
Endosome
MVB
Cytosol

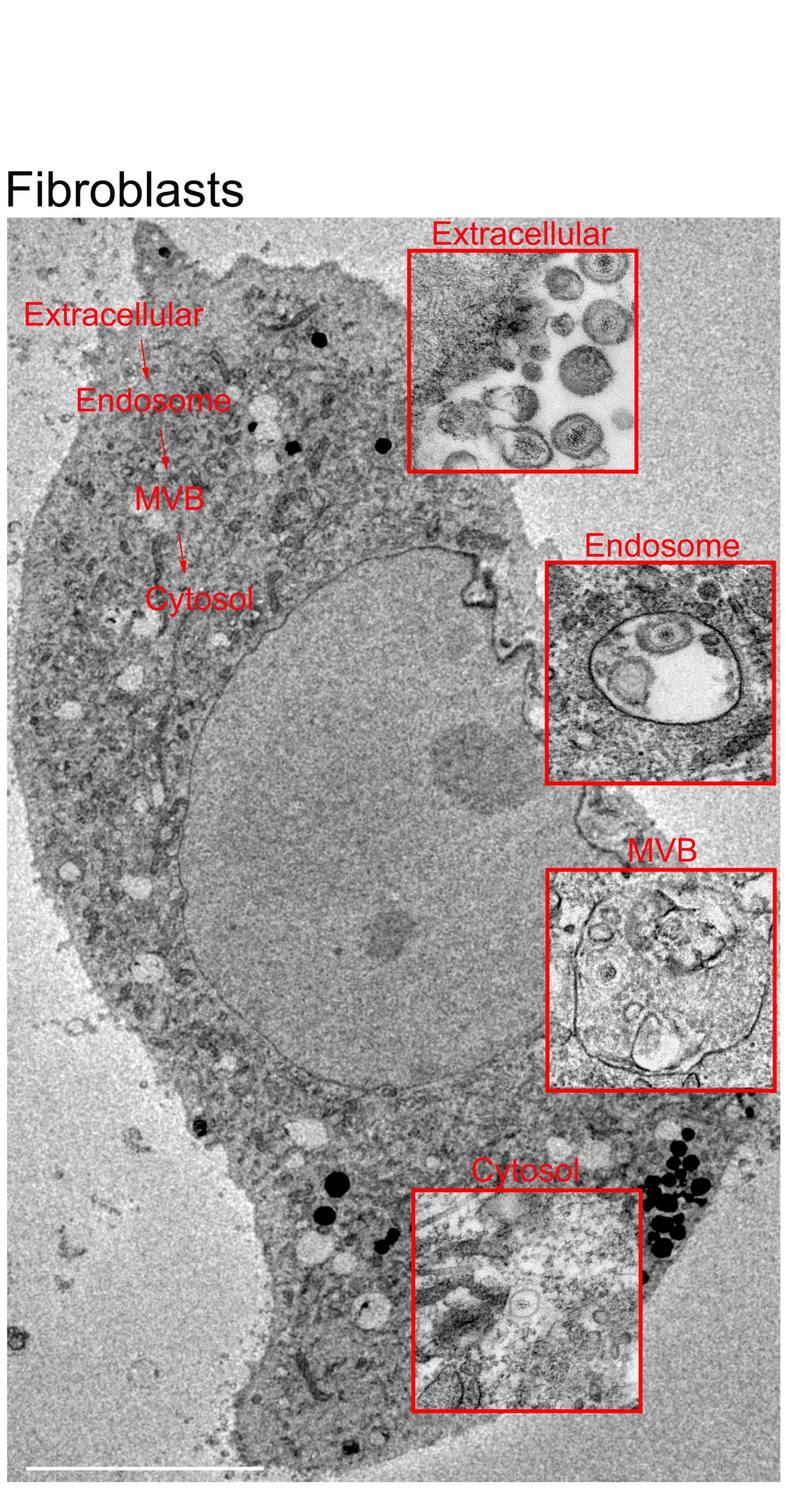
Fibroblasts
Extracellular
Endosome
MVB
Cytosol

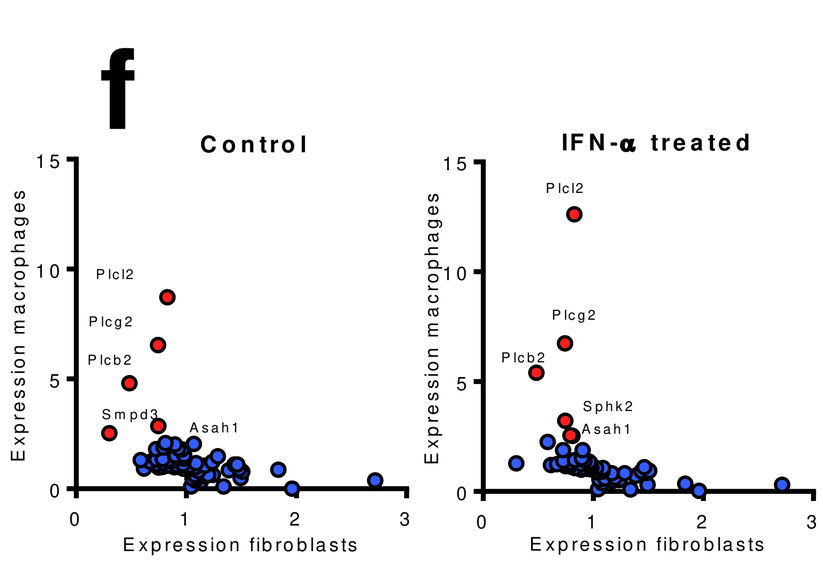
f
Control
IFN-α treated
Expression macrophages
Expression fibroblasts
Plcl2
Plcg2
Plcb2
Smpd3
Asah1
Sphk2

g
Asah1 (relative expression)
#
Fibroblasts
Macrophages

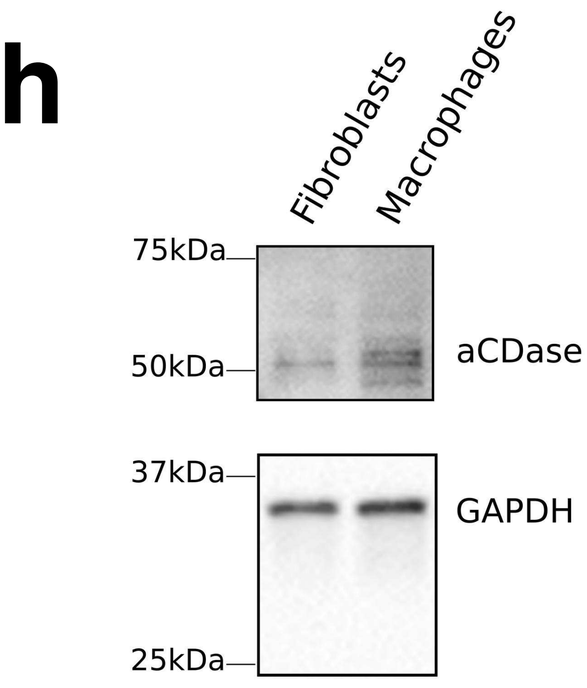
h
Fibroblasts
Macrophages
75kDa
50kDa
aCDase
37kDa
GAPDH
25kDa

Figure 3

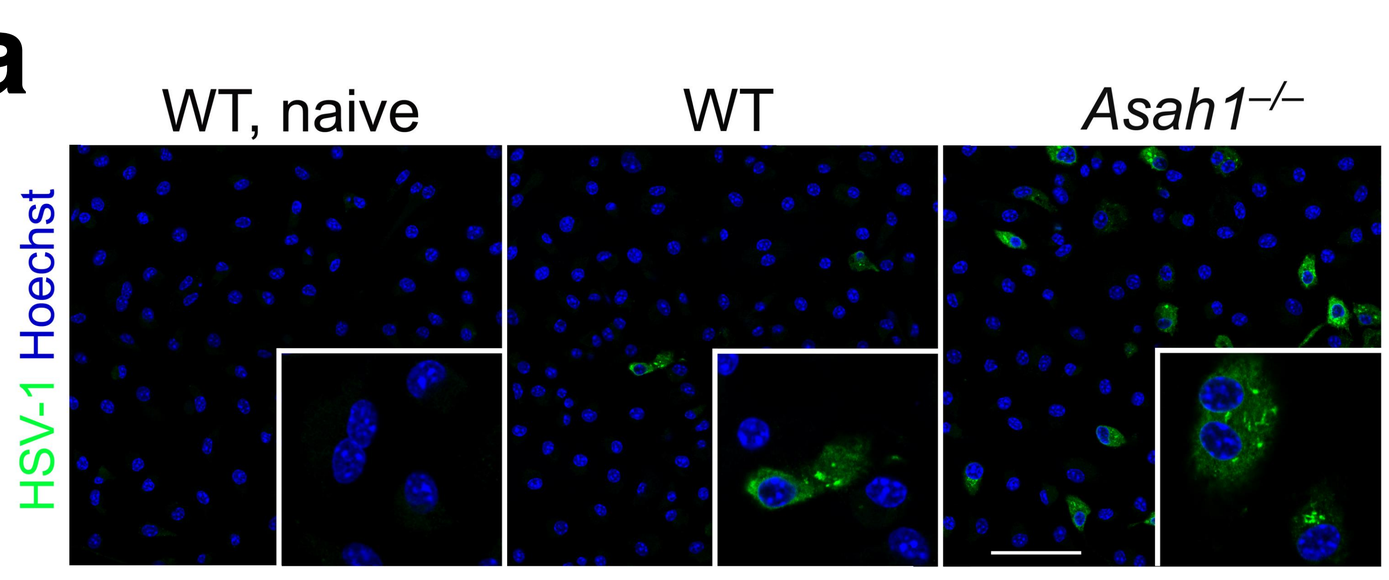
a
WT, naive
WT
Asah1−/−
HSV-1 Hoechst

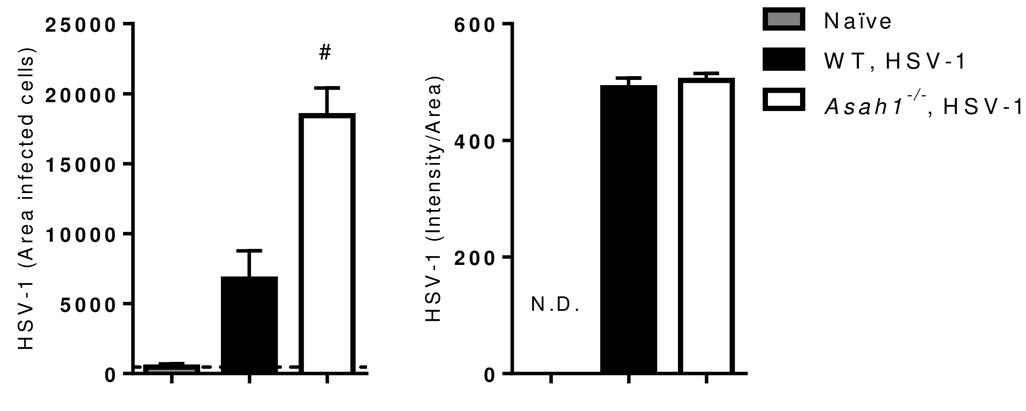
b
HSV-1 (Area infected cells)
25000
20000
15000
10000
5000
0
#
HSV-1 (Intensity/Area)
600
400
200
0
N.D.
Naïve
WT, HSV-1
Asah1-/-, HSV-1

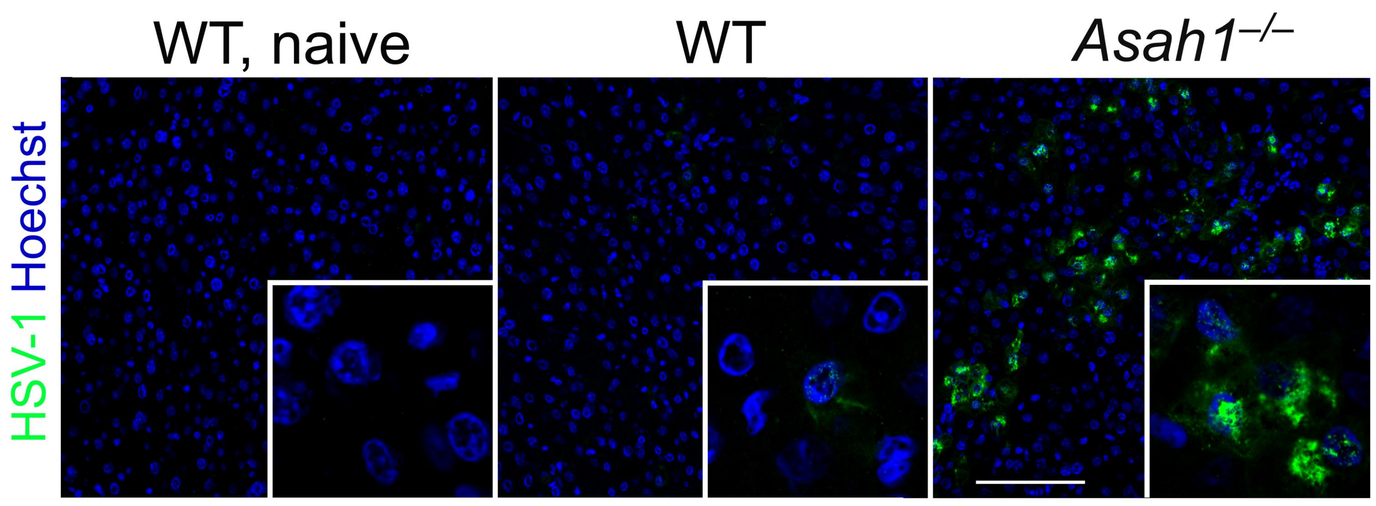
c
WT, naive
WT
Asah1−/−
HSV-1 Hoechst

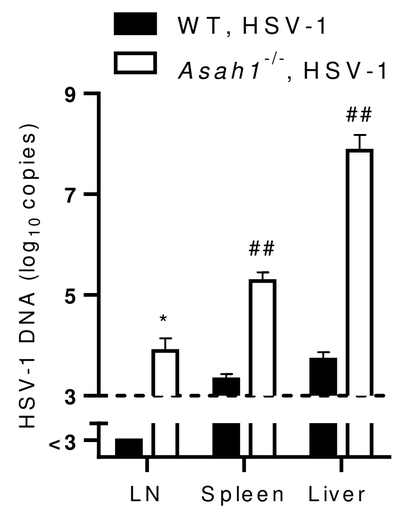
d
WT, HSV-1
Asah1-/-, HSV-1
HSV-1 DNA (log10 copies)
9
7
5
3
<3
*
##
##
LN
Spleen
Liver

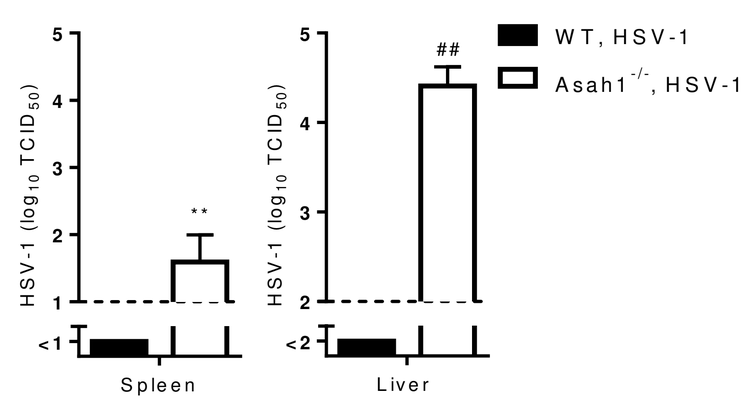
e
HSV-1 (log10 TCID50)
5
4
3
2
1
<1
**
Spleen
<2
##
Liver
WT, HSV-1
Asah1-/-, HSV-1

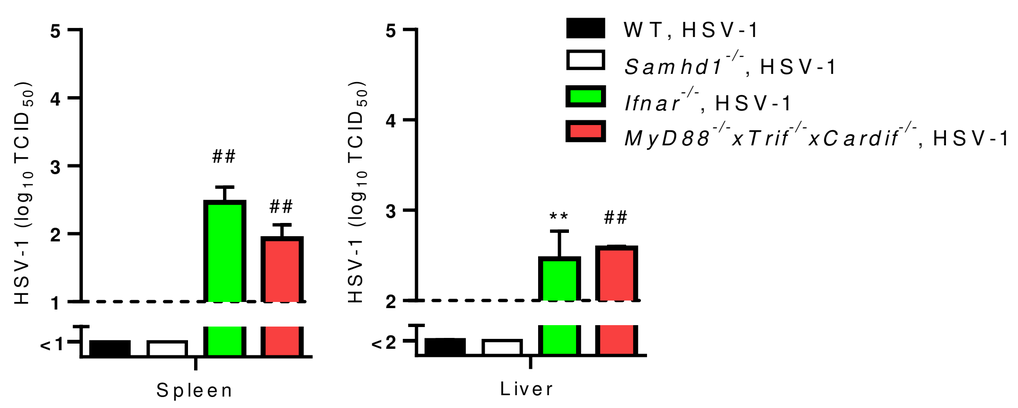
f
HSV-1 (log10 TCID50)
5
4
3
2
1
<1
##
##
Spleen
<2
**
##
Liver
WT, HSV-1
Samhd1-/-, HSV-1
Ifnar-/-, HSV-1
MyD88-/-xTrif-/-xCardif-/-, HSV-1

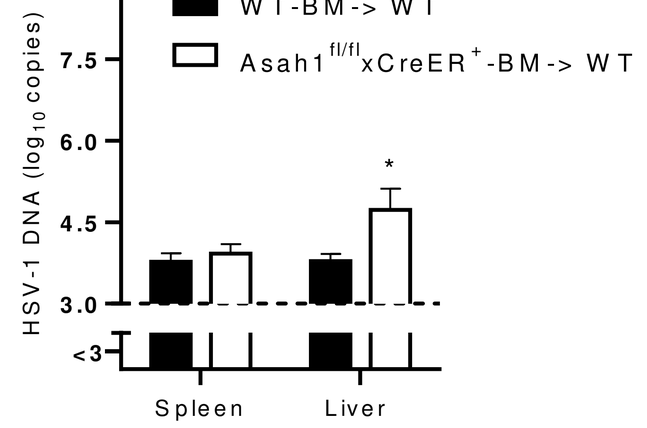
g
HSV-1 DNA (log10 copies)
9.0
7.5
6.0
4.5
3.0
<3
*
Spleen
Liver
WT-BM-> WT
Asah1fl/flxCreER+-BM-> WT

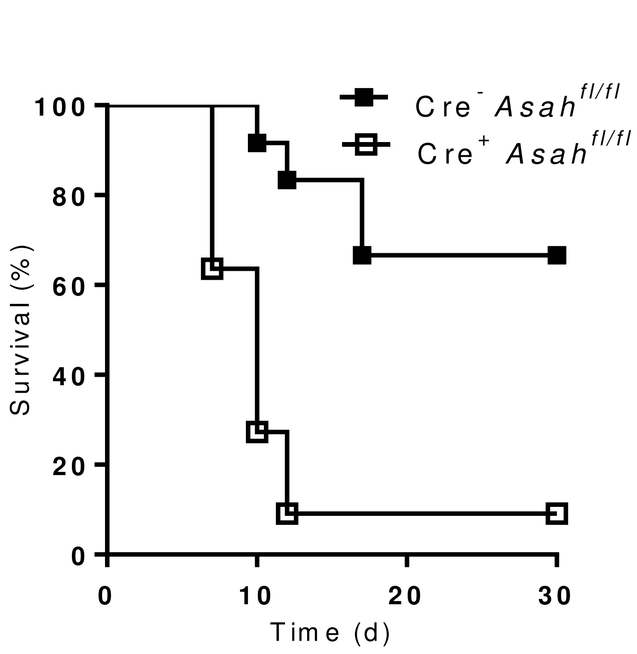
h
Survival (%)
100
80
60
40
20
0
0
10
20
30
Time (d)
Cre- Asahfl/fl
Cre+ Asahfl/fl

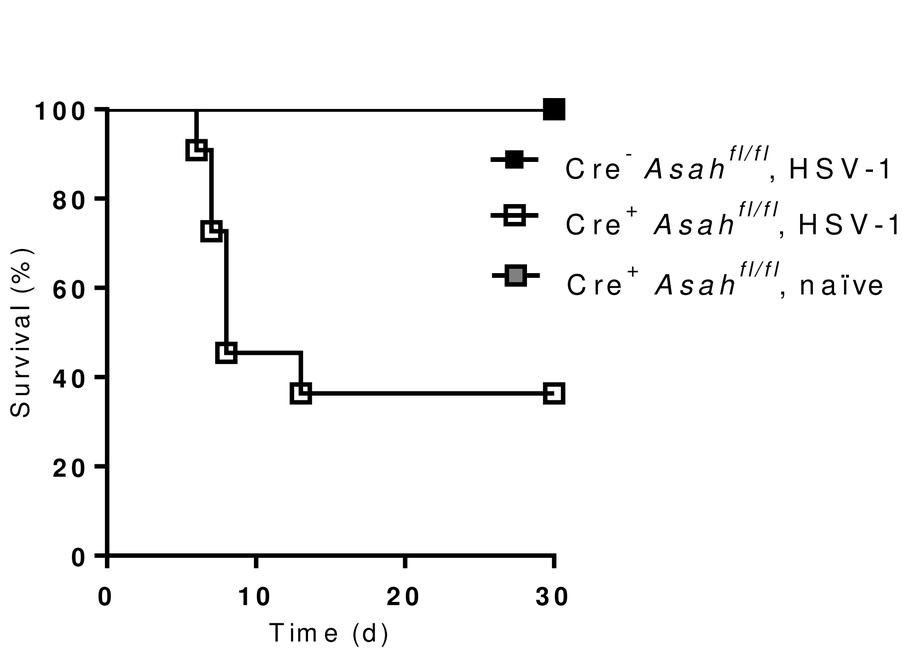
i
Survival (%)
100
80
60
40
20
0
0
10
20
30
Time (d)
Cre- Asahfl/fl, HSV-1
Cre+ Asahfl/fl, HSV-1
Cre+ Asahfl/fl, naïve

Figure 4

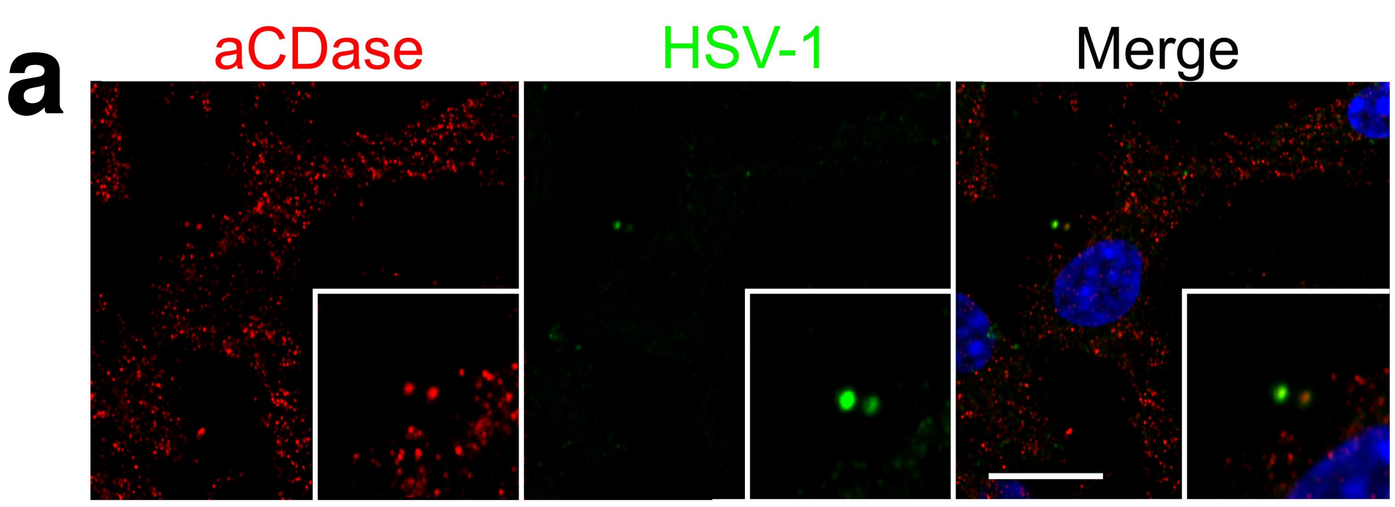
a
aCDase
HSV-1
Merge

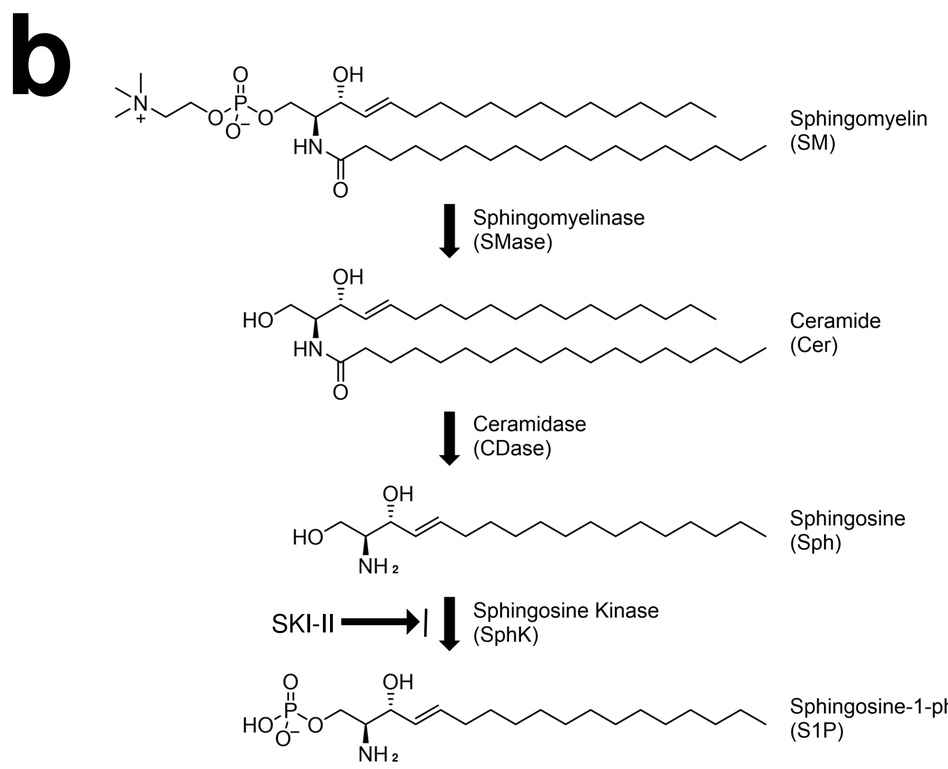
b
Sphingomyelin
(SM)
Sphingomyelinase
(SMase)
Ceramide
(Cer)
Ceramidase
(CDase)
Sphingosine
(Sph)
SKI-II
Sphingosine Kinase
(SphK)
Sphingosine-1-phosphate
(S1P)

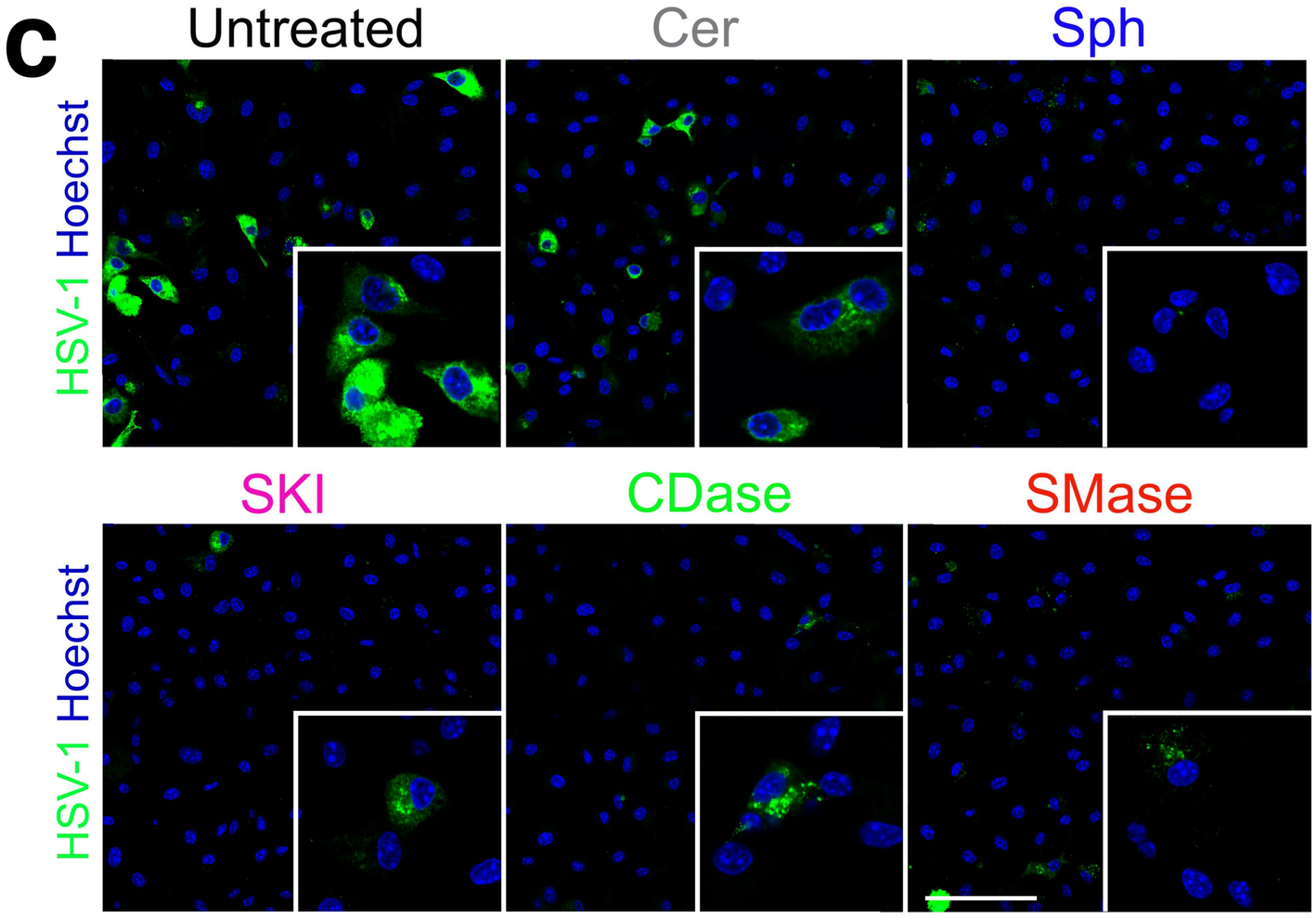
c
Untreated
Cer
Sph
HSV-1 Hoechst
SKI
CDase
SMase
HSV-1 Hoechst

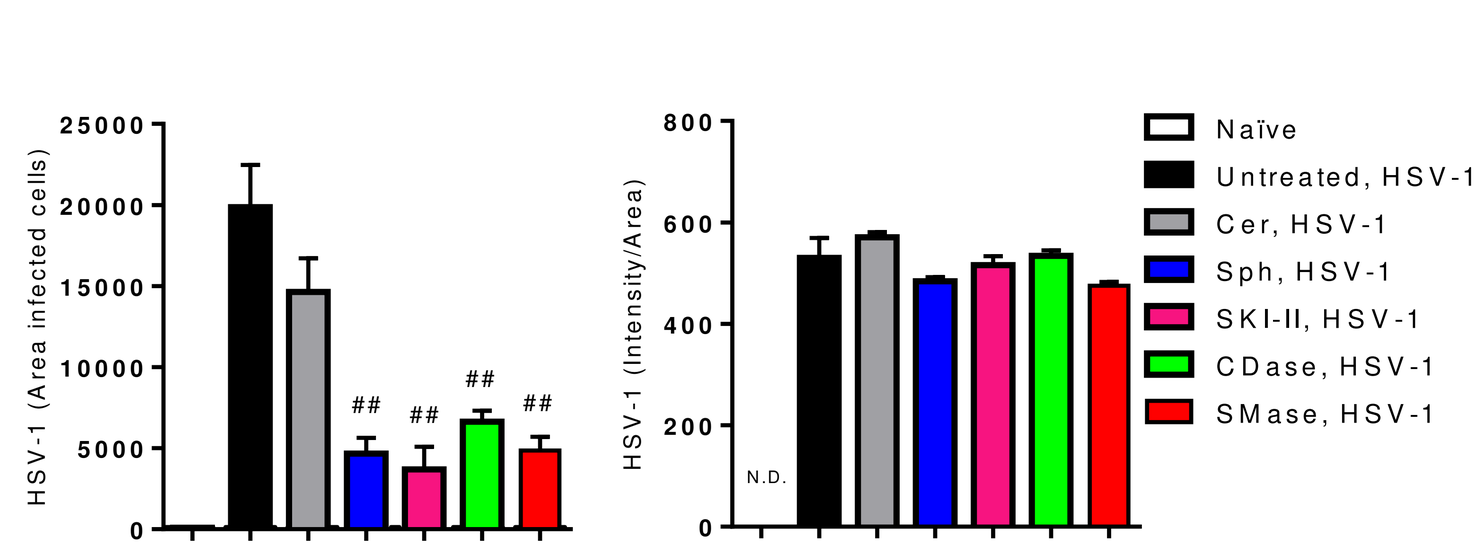
d
HSV-1 (Area infected cells)
25000
20000
15000
10000
5000
0
##
##
##
##
HSV-1 (Intensity/Area)
800
600
400
200
0
N.D.
Naïve
Untreated, HSV-1
Cer, HSV-1
Sph, HSV-1
SKI-II, HSV-1
CDase, HSV-1
SMase, HSV-1

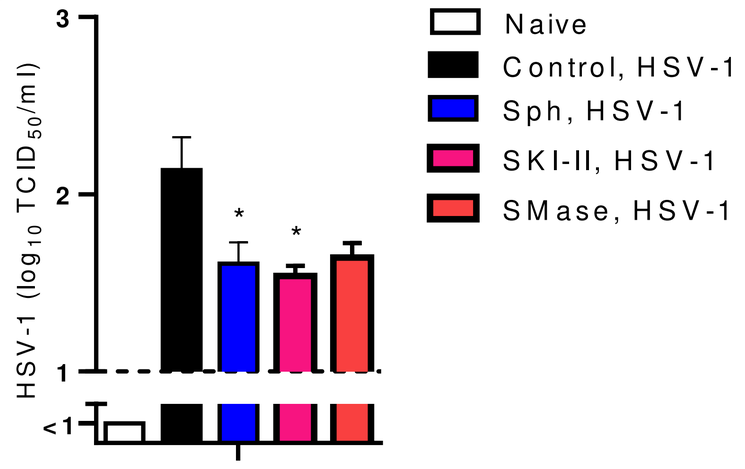
e
HSV-1 (log10 TCID50/ml)
3
2
1
<1
*
*
Naive
Control, HSV-1
Sph, HSV-1
SKI-II, HSV-1
SMase, HSV-1

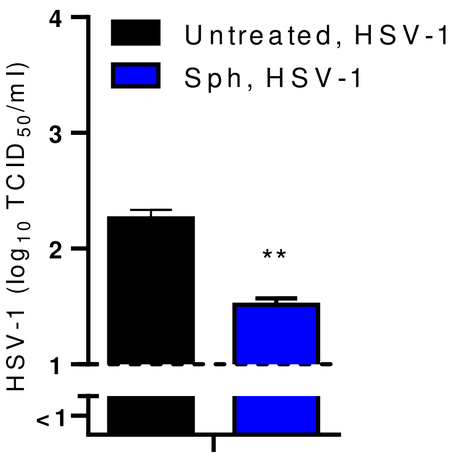
f
THP-1
HSV-1 (log10 TCID50/ml)
4
3
2
1
<1
**
Untreated, HSV-1
Sph, HSV-1

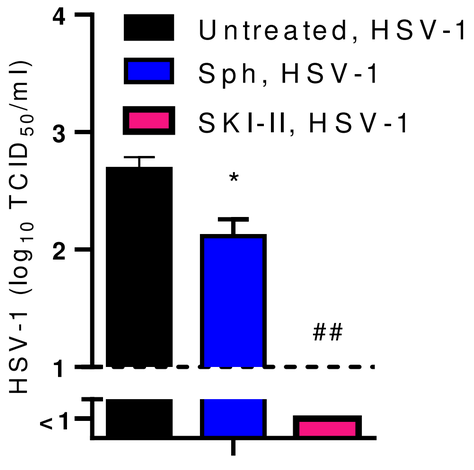
g
Hela
HSV-1 (log10 TCID50/ml)
4
3
2
1
<1
*
##
Untreated, HSV-1
Sph, HSV-1
SKI-II, HSV-1

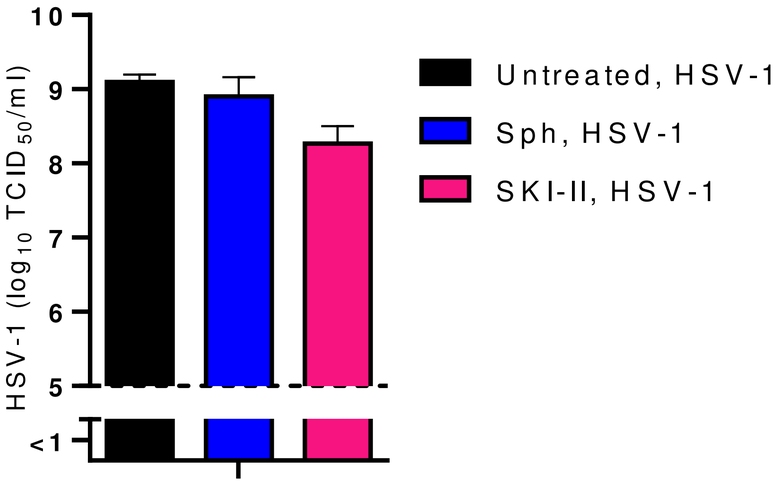
h
Vero
HSV-1 (log10 TCID50/ml)
10
9
8
7
6
5
<1
Untreated, HSV-1
Sph, HSV-1
SKI-II, HSV-1

Figure 5

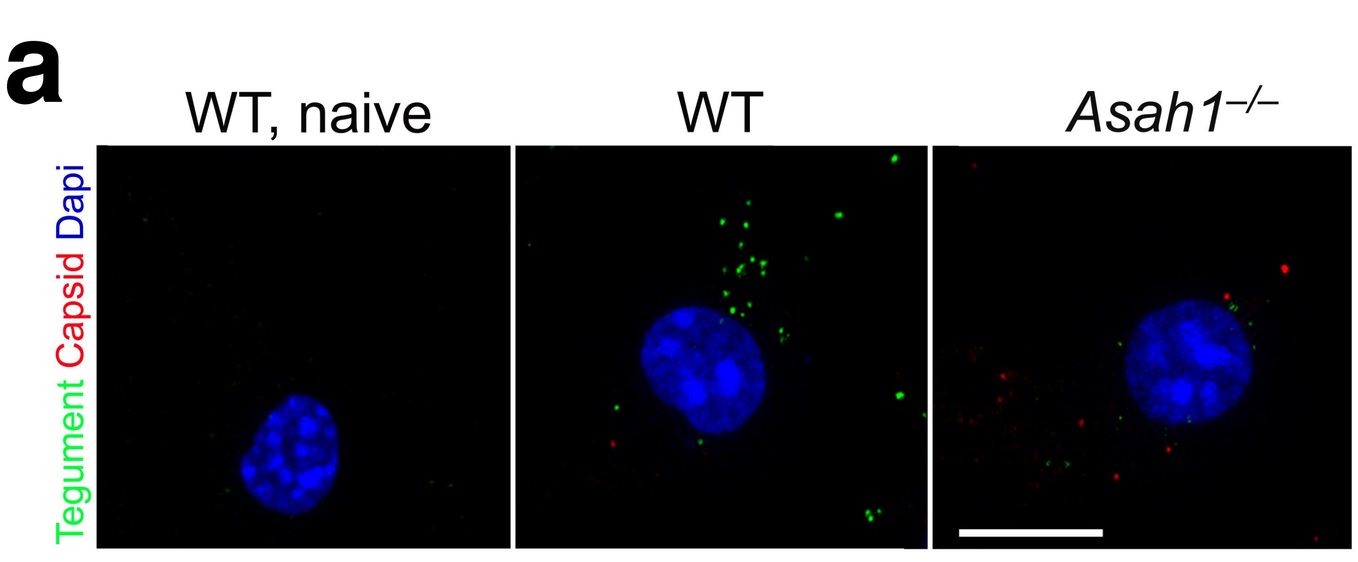
a
WT, naive
WT
Asah1−/−
Tegument Capsid Dapi

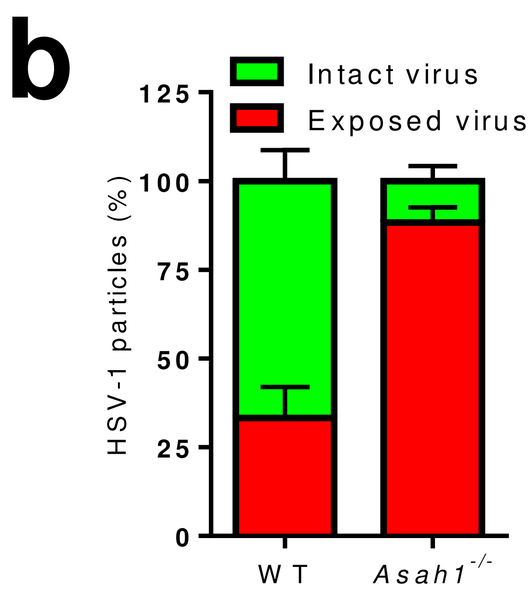
b
Intact virus
Exposed virus
HSV-1 particles (%)
125
100
75
50
25
0
WT
Asah1-/-

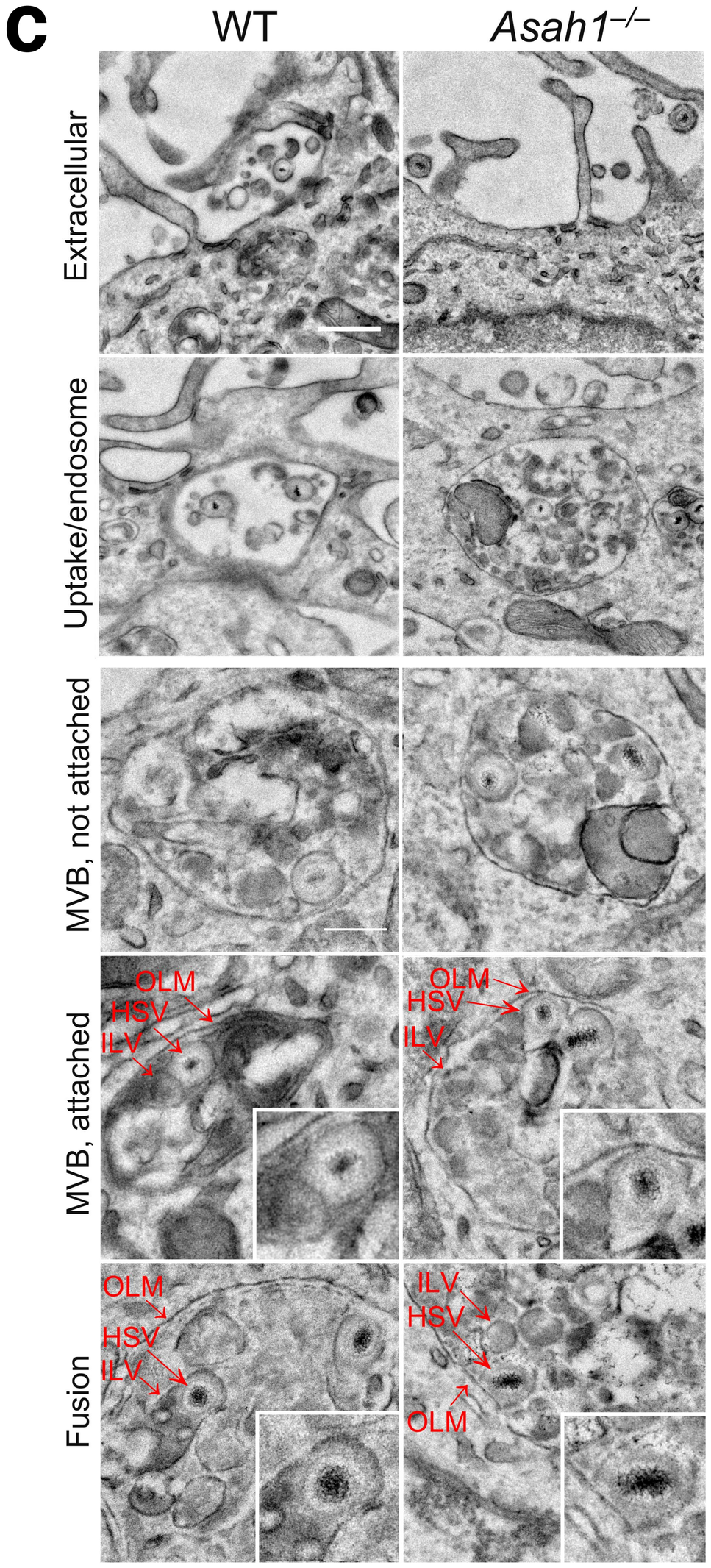
c
WT
Asah1−/−
Extracellular
Uptake/endosome
MVB, not attached
MVB, attached
Fusion
OLM
HSV
ILV

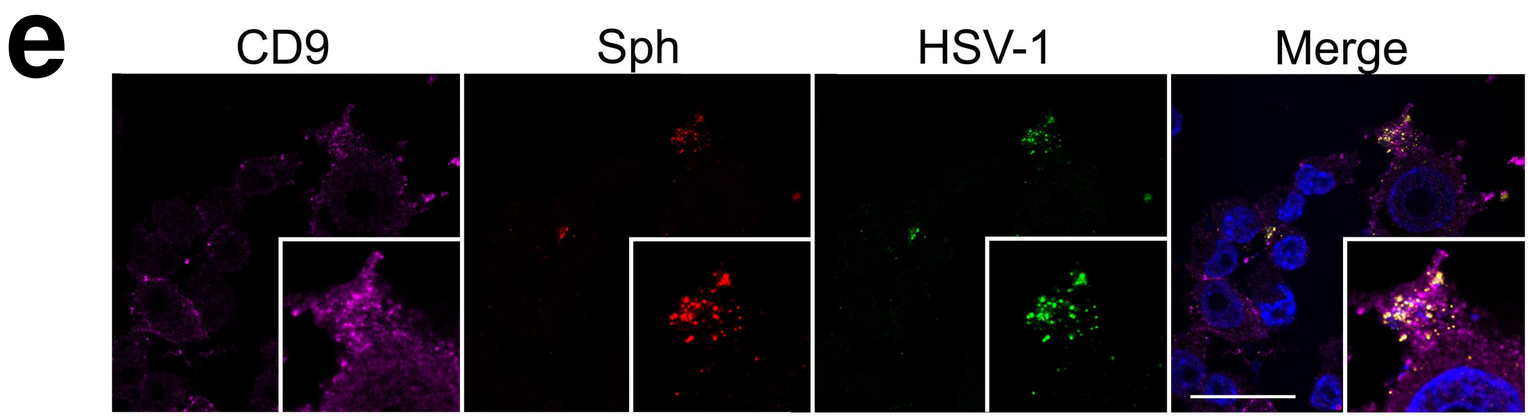
e
CD9
Sph
HSV-1
Merge

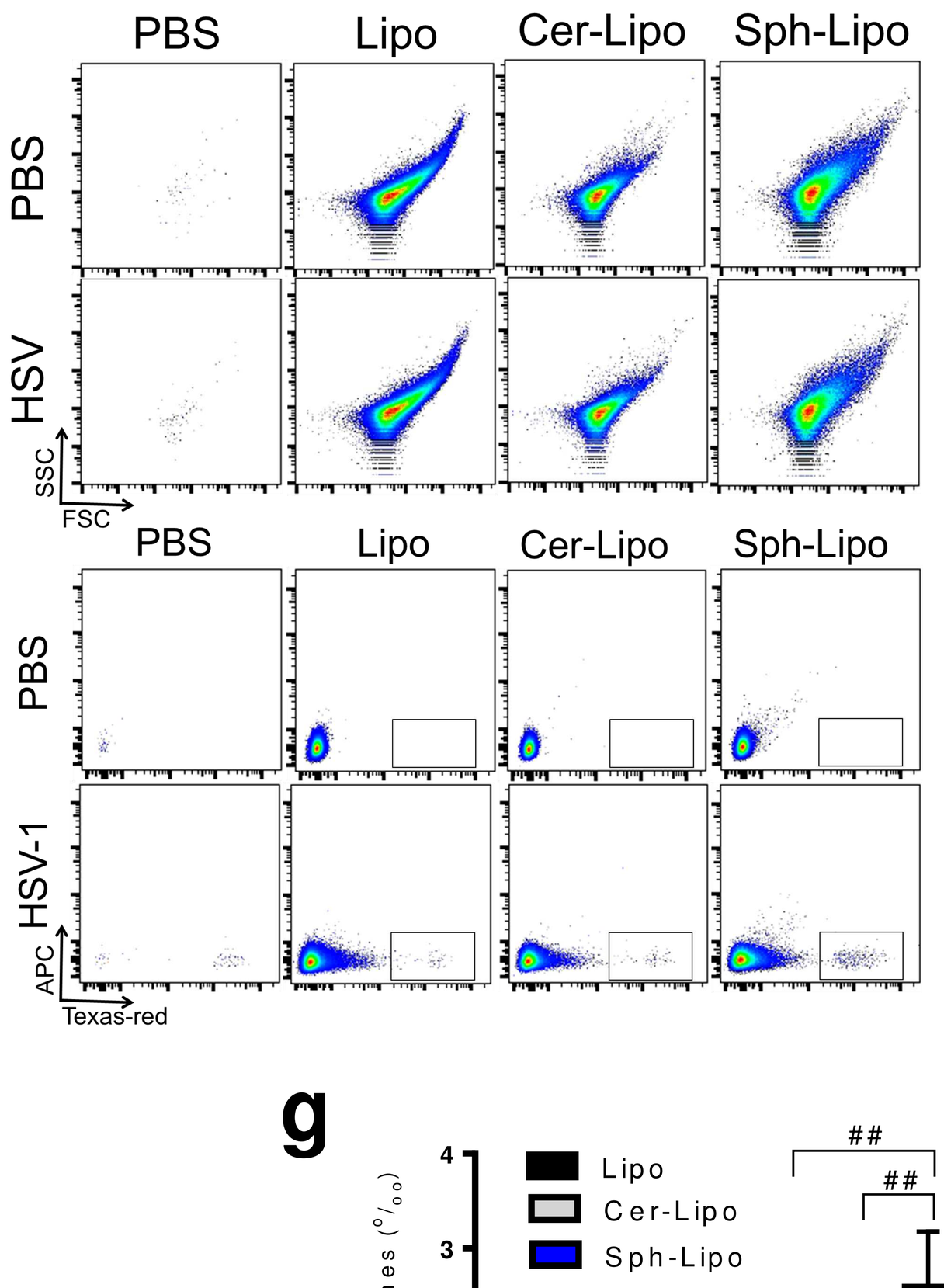
f
PBS
Lipo
Cer-Lipo
Sph-Lipo
HSV
SSC
FSC
HSV-1
APC
Texas-red

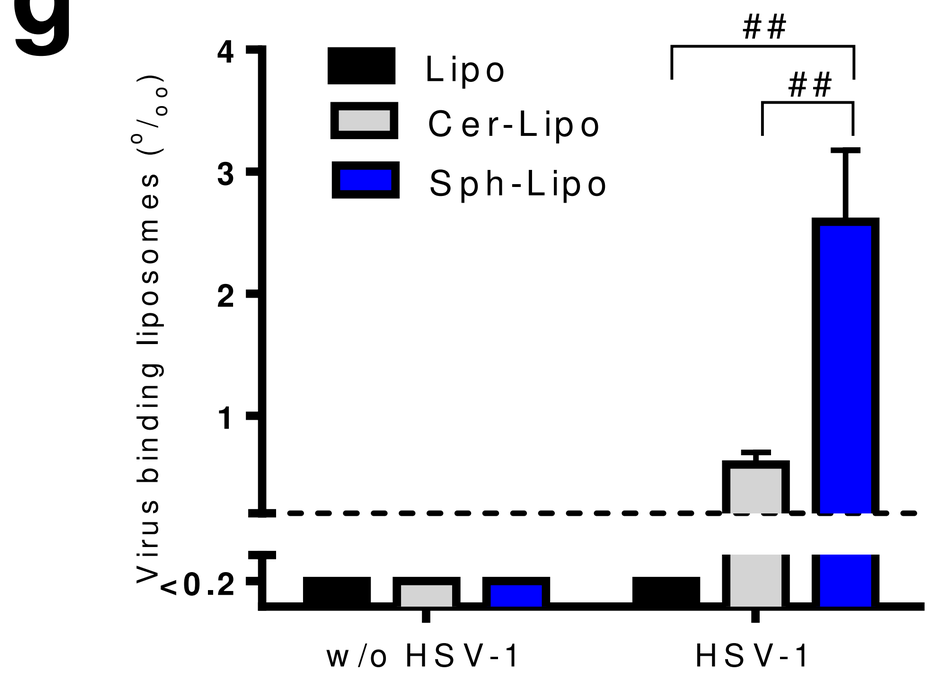
g
Lipo
Cer-Lipo
Sph-Lipo
Virus binding liposomes (‰)
4
3
2
1
<0.2
##
##
w/o HSV-1
HSV-1

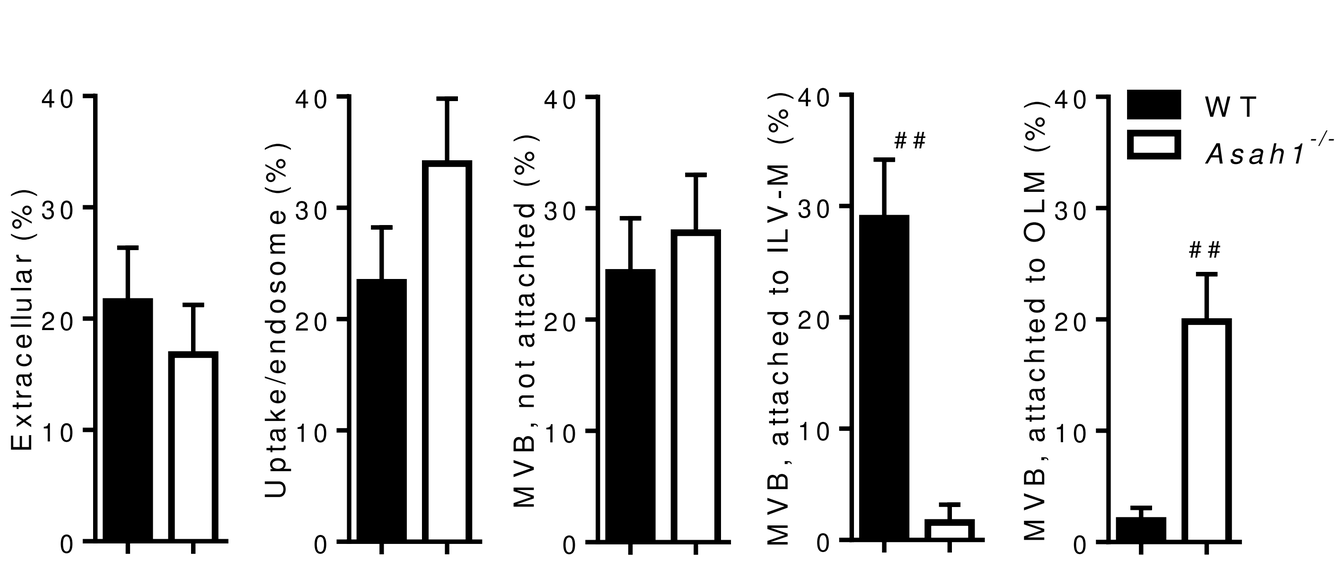
d
Extracellular (%)
Uptake/endosome (%)
MVB, not attachted (%)
MVB, attached to ILV-M (%)
MVB, attached to OLM (%)
40
30
20
10
0
##
##
WT
Asah1-/-

Figure 6

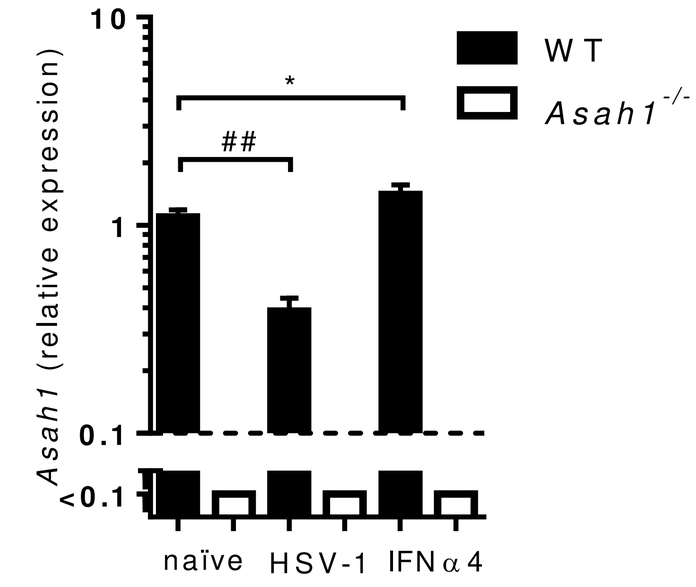
a
10
1
0.1
<0.1
Asah1 (relative expression)
WT
Asah1 -/-
*
##
naïve
HSV-1
IFNα4

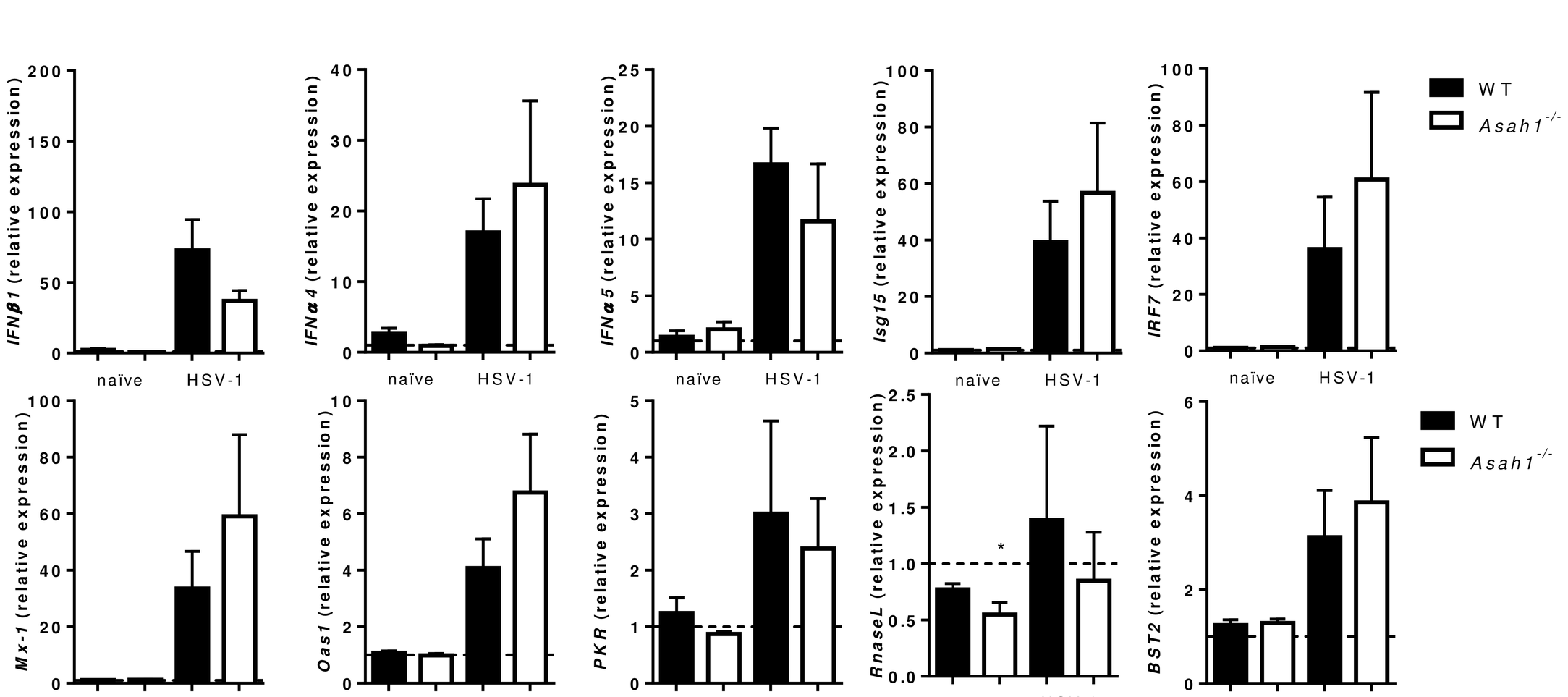
b
IFNβ1 (relative expression)
IFNα4 (relative expression)
IFNα5 (relative expression)
Isg15 (relative expression)
IRF7 (relative expression)
Mx-1 (relative expression)
Oas1 (relative expression)
PKR (relative expression)
RnaseL (relative expression)
BST2 (relative expression)
naïve
HSV-1
WT
Asah1 -/-
*

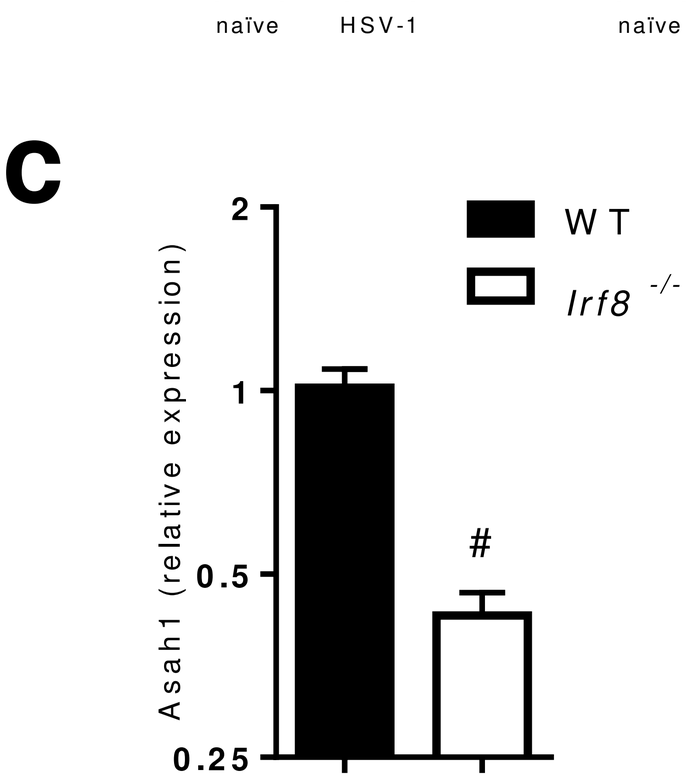
c
Asah1 (relative expression)
WT
Irf8 -/-
#

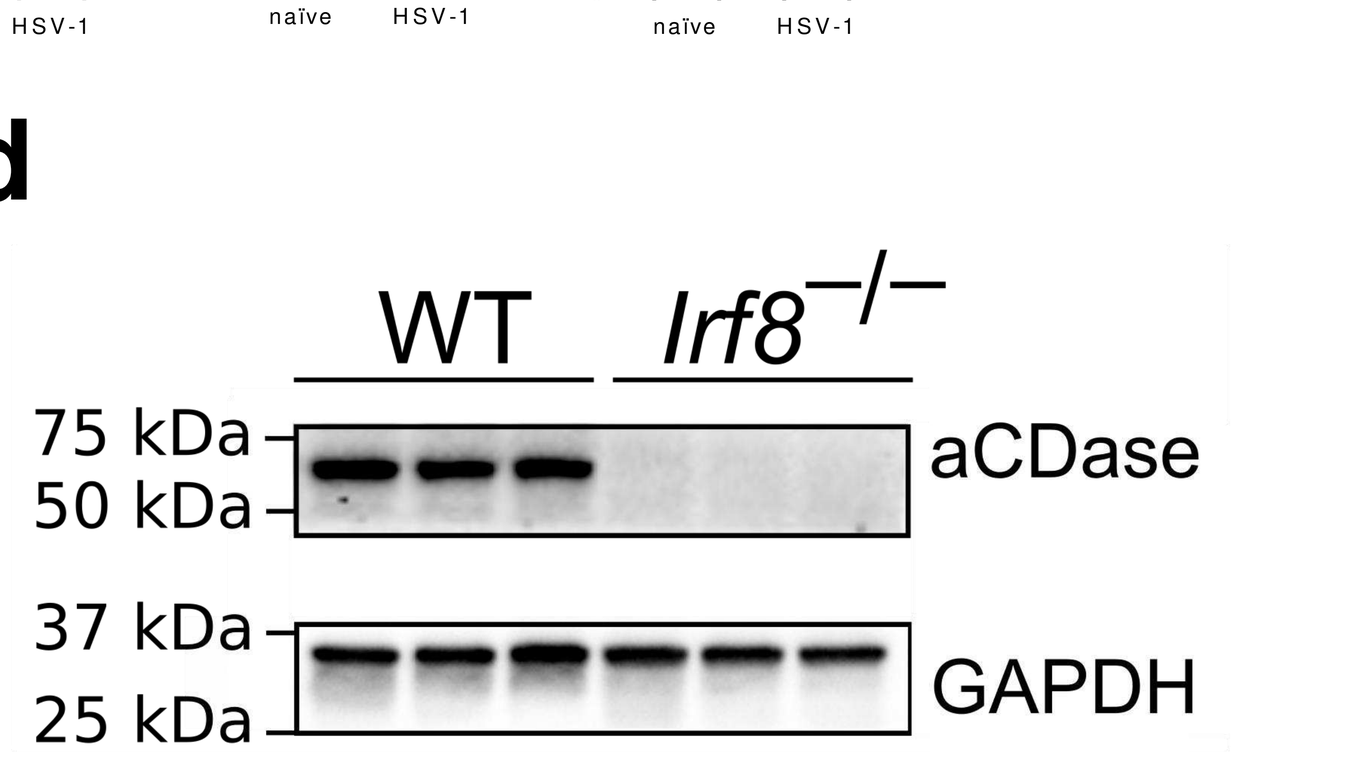
d
WT
Irf8−/−
75 kDa
50 kDa
37 kDa
25 kDa
aCDase
GAPDH

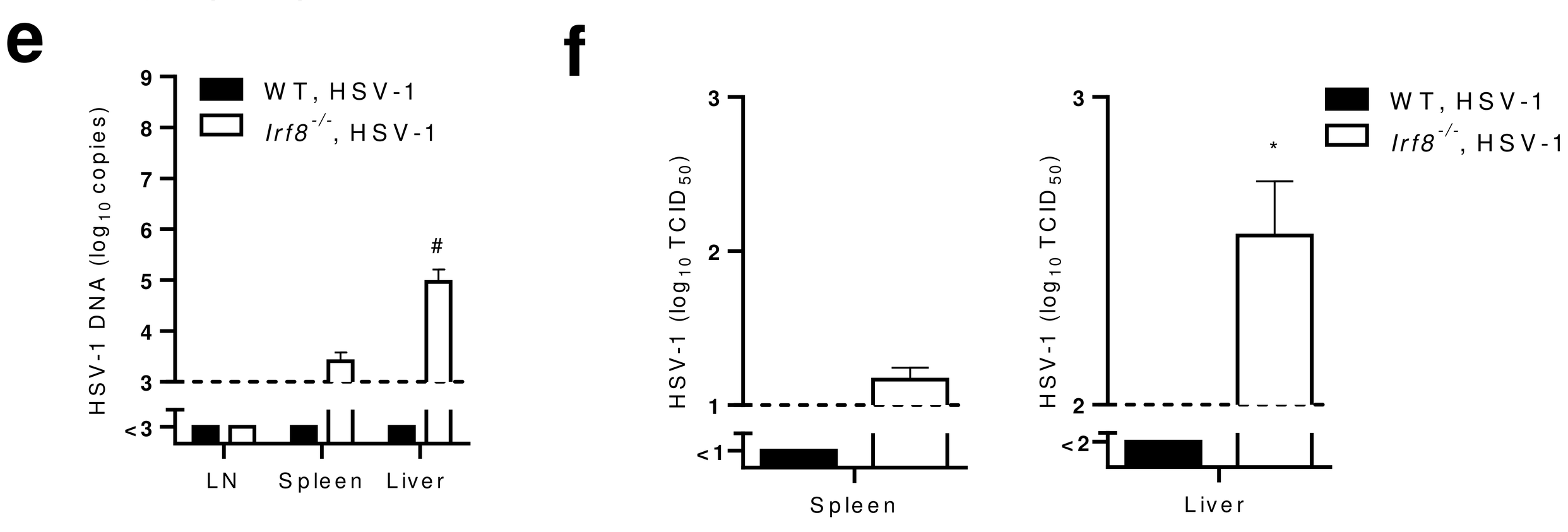
e
HSV-1 DNA (log10 copies)
WT, HSV-1
Irf8-/-, HSV-1
#
LN
Spleen
Liver
f
HSV-1 (log10 TCID50)
WT, HSV-1
Irf8-/-, HSV-1
*
Spleen
Liver

Suppl. Figure 1

a

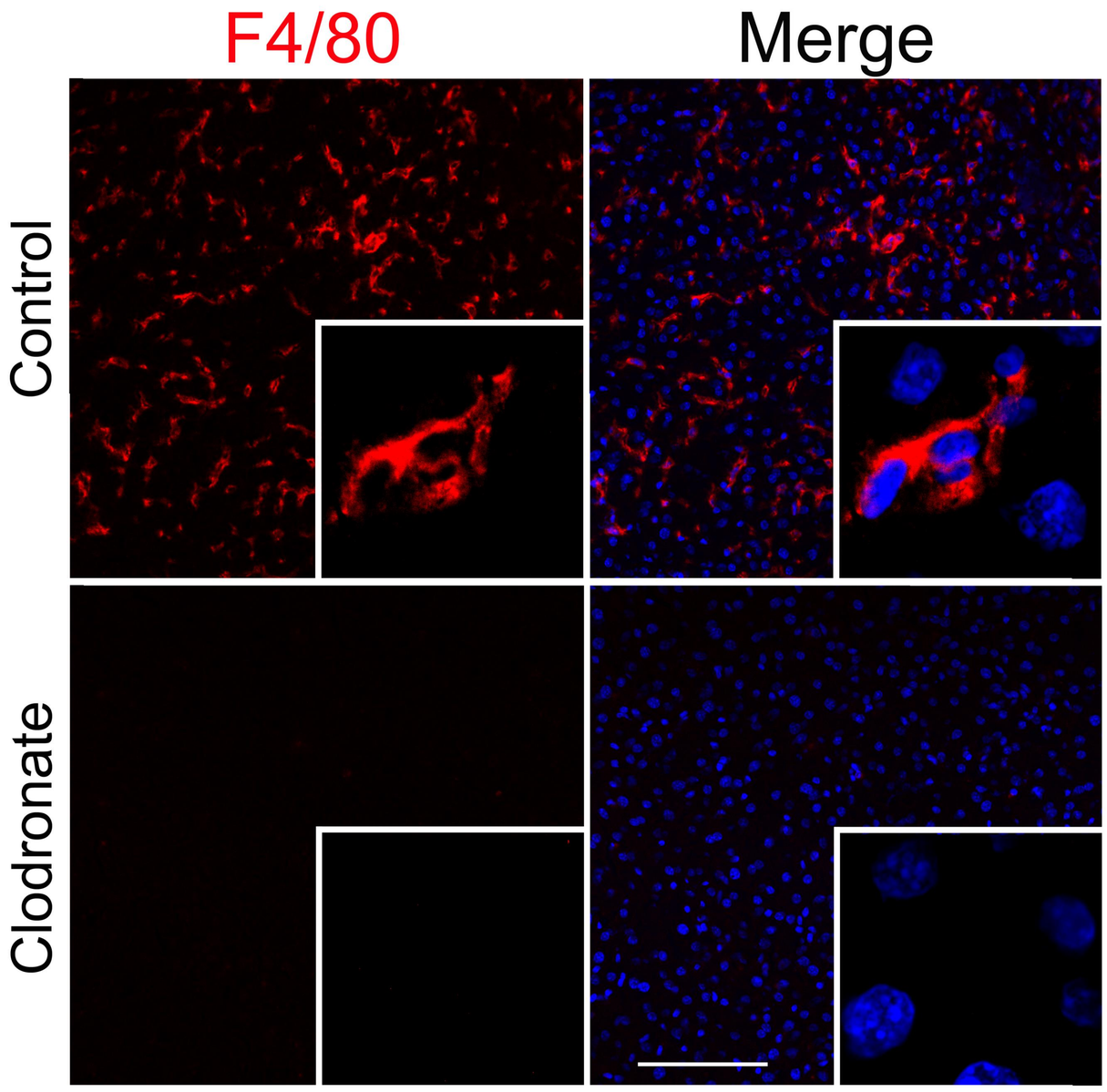

b

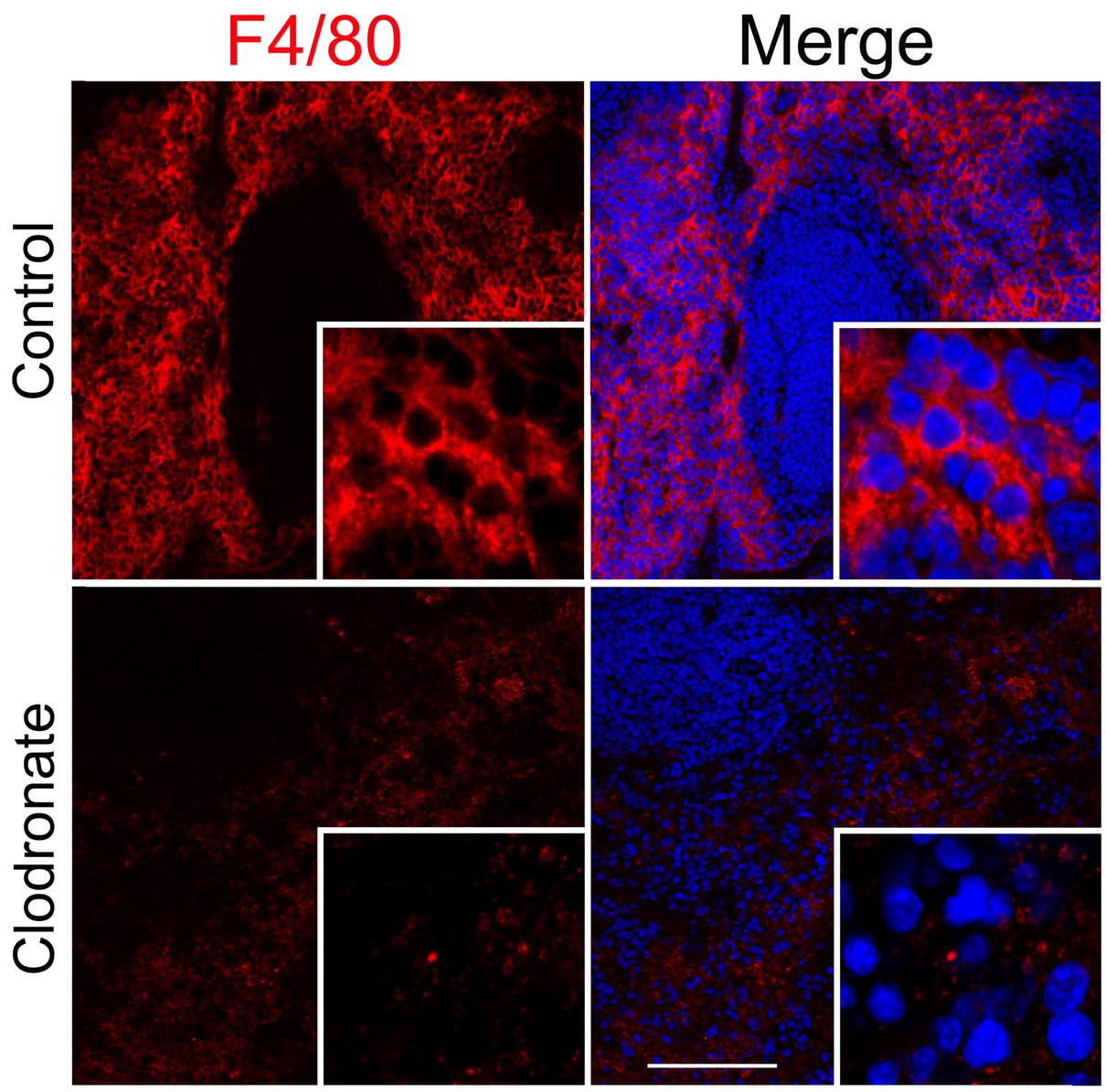

c

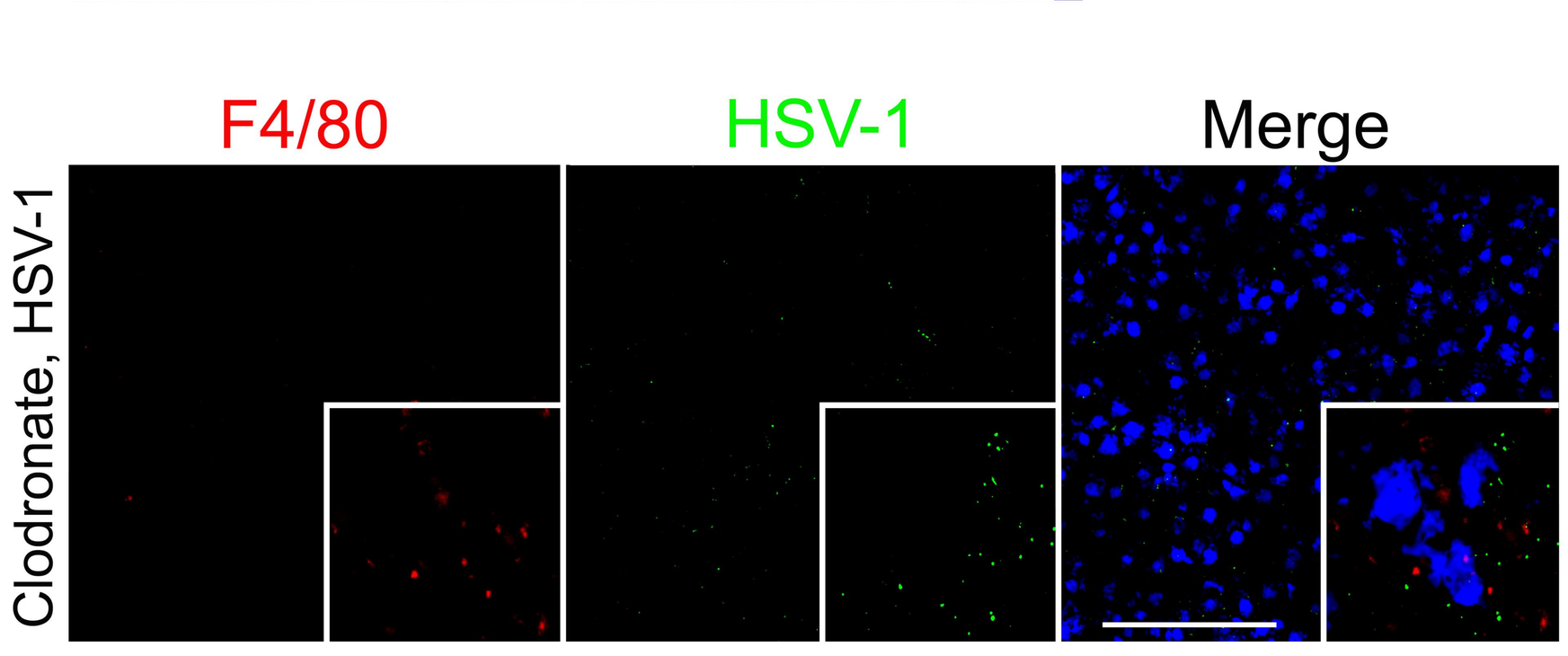

Suppl. Figure 2

Suppl. Figure 3

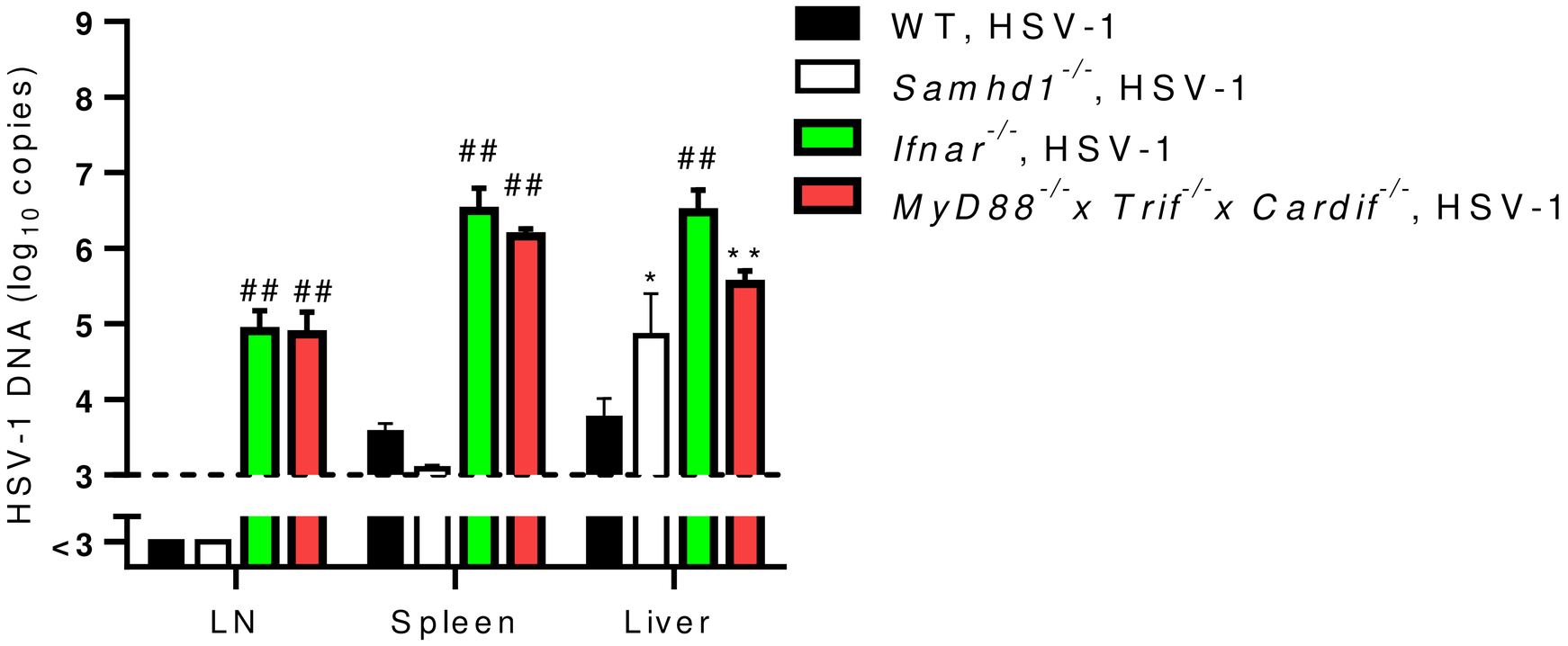

Suppl. Figure 4

a

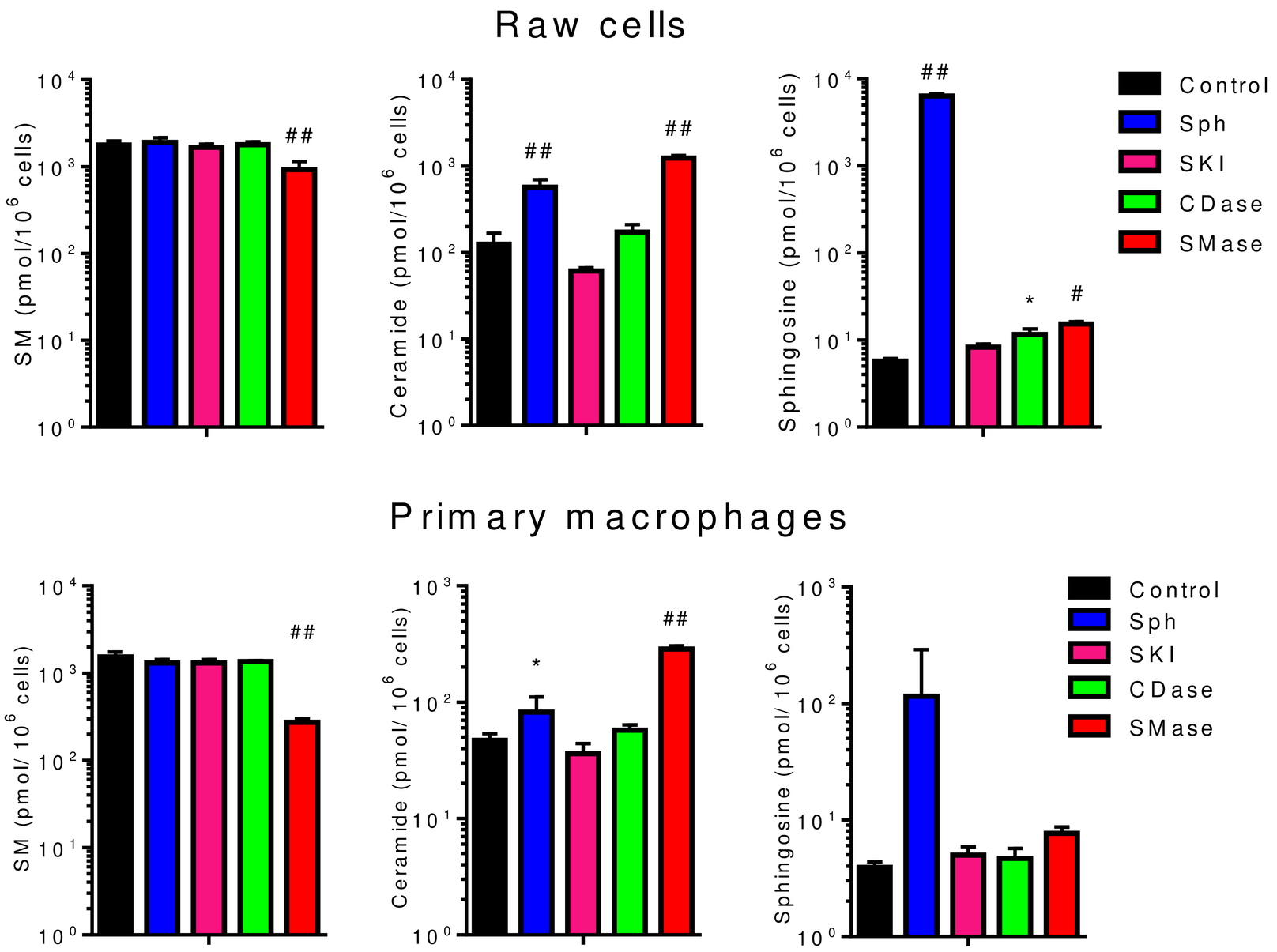

b

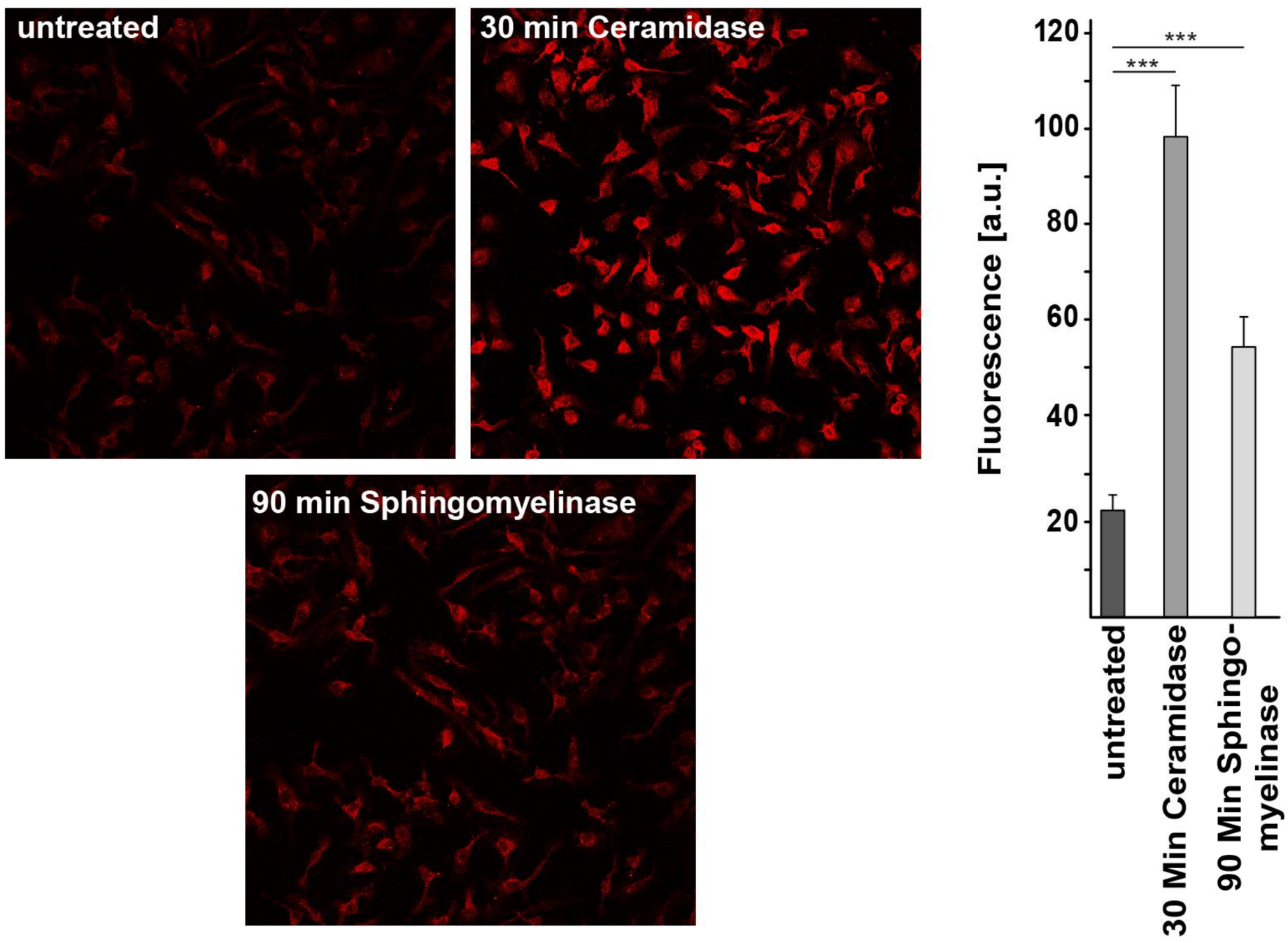

Suppl. Figure 5

a

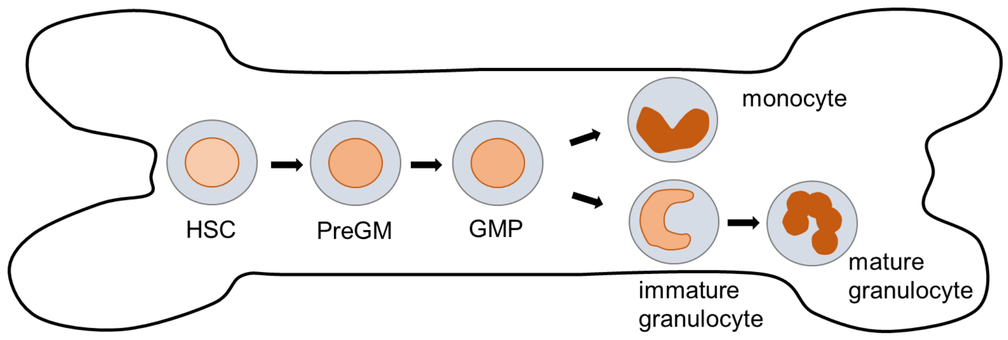

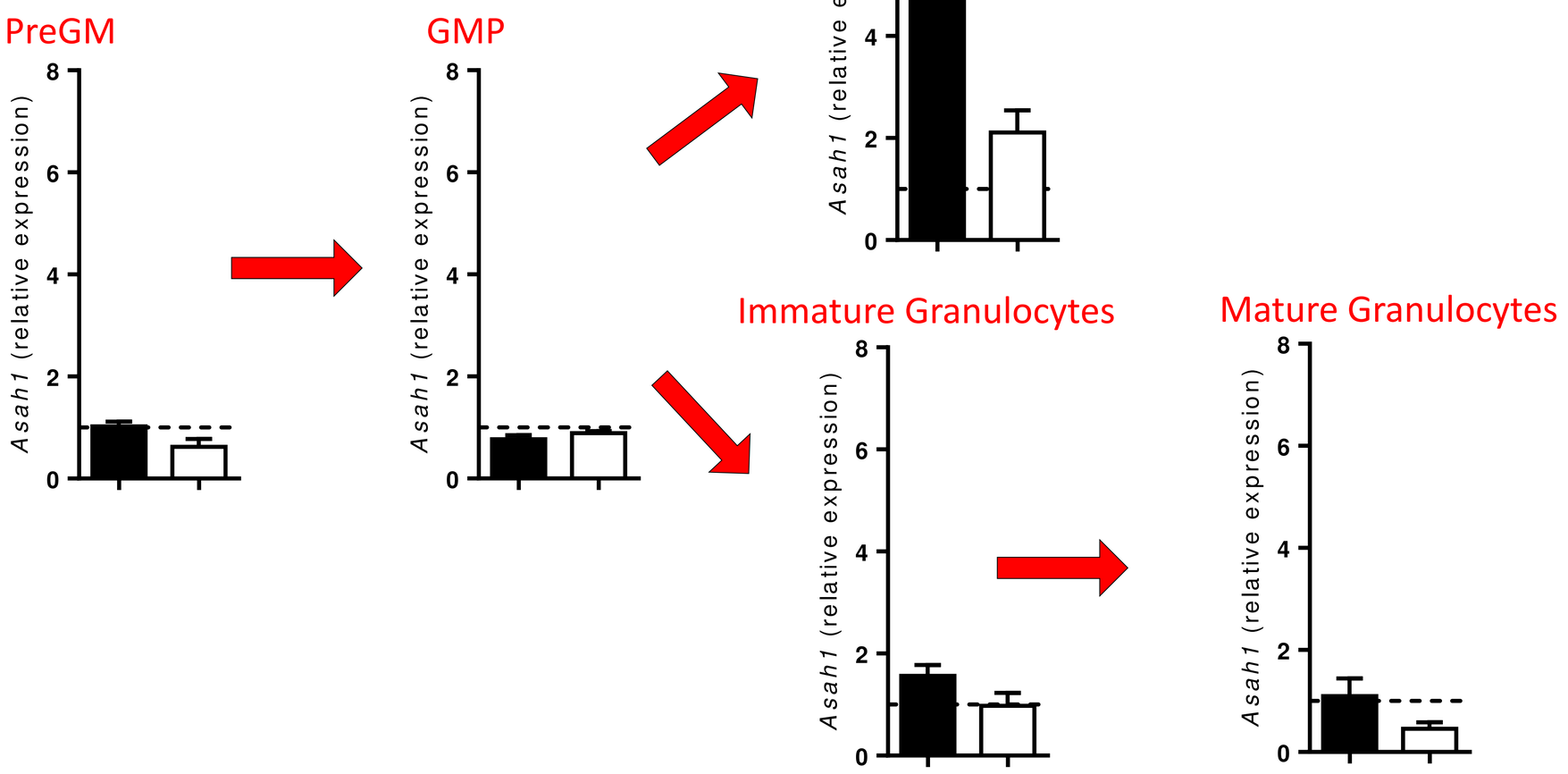

b

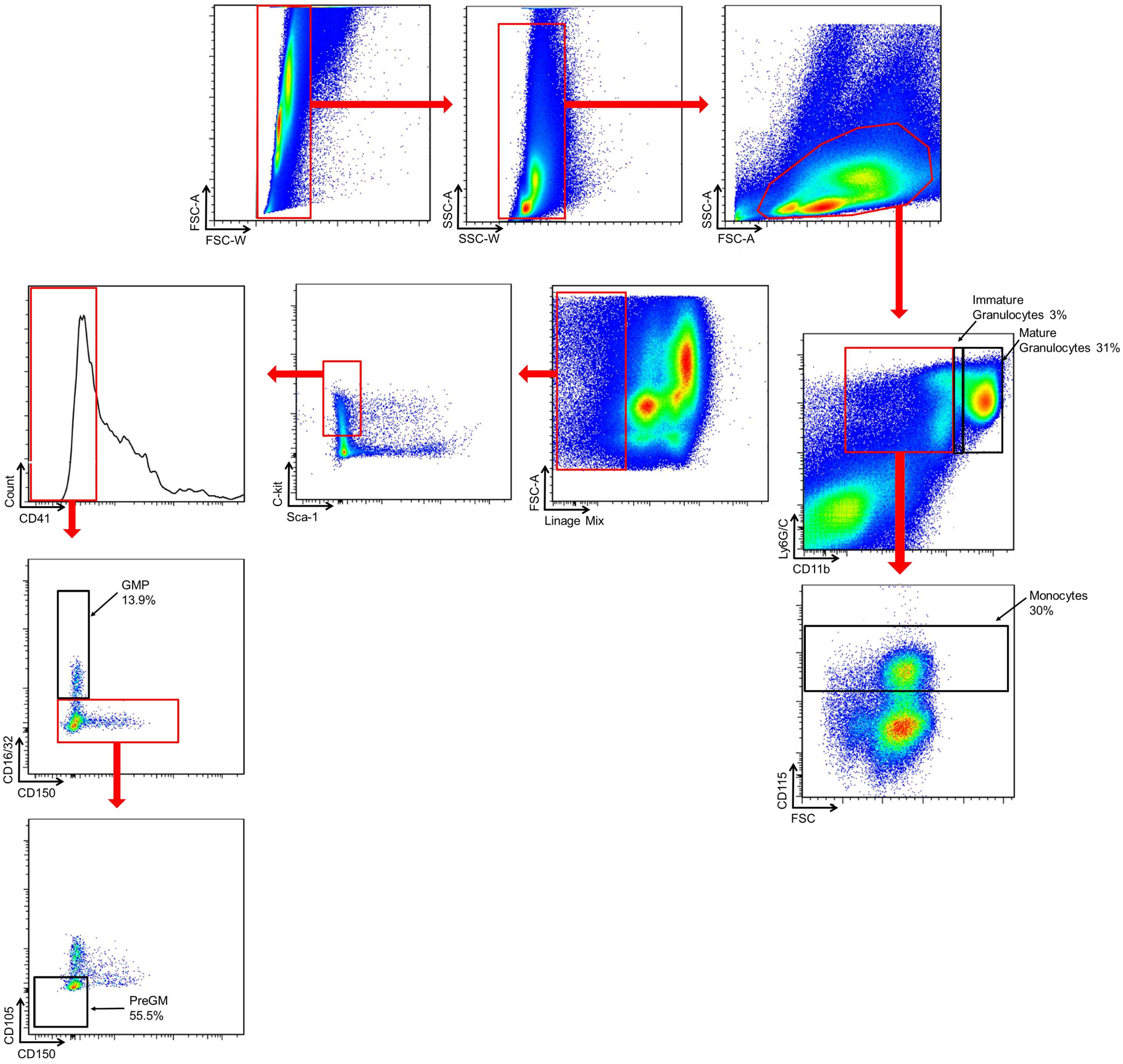

Suppl. Figure 6

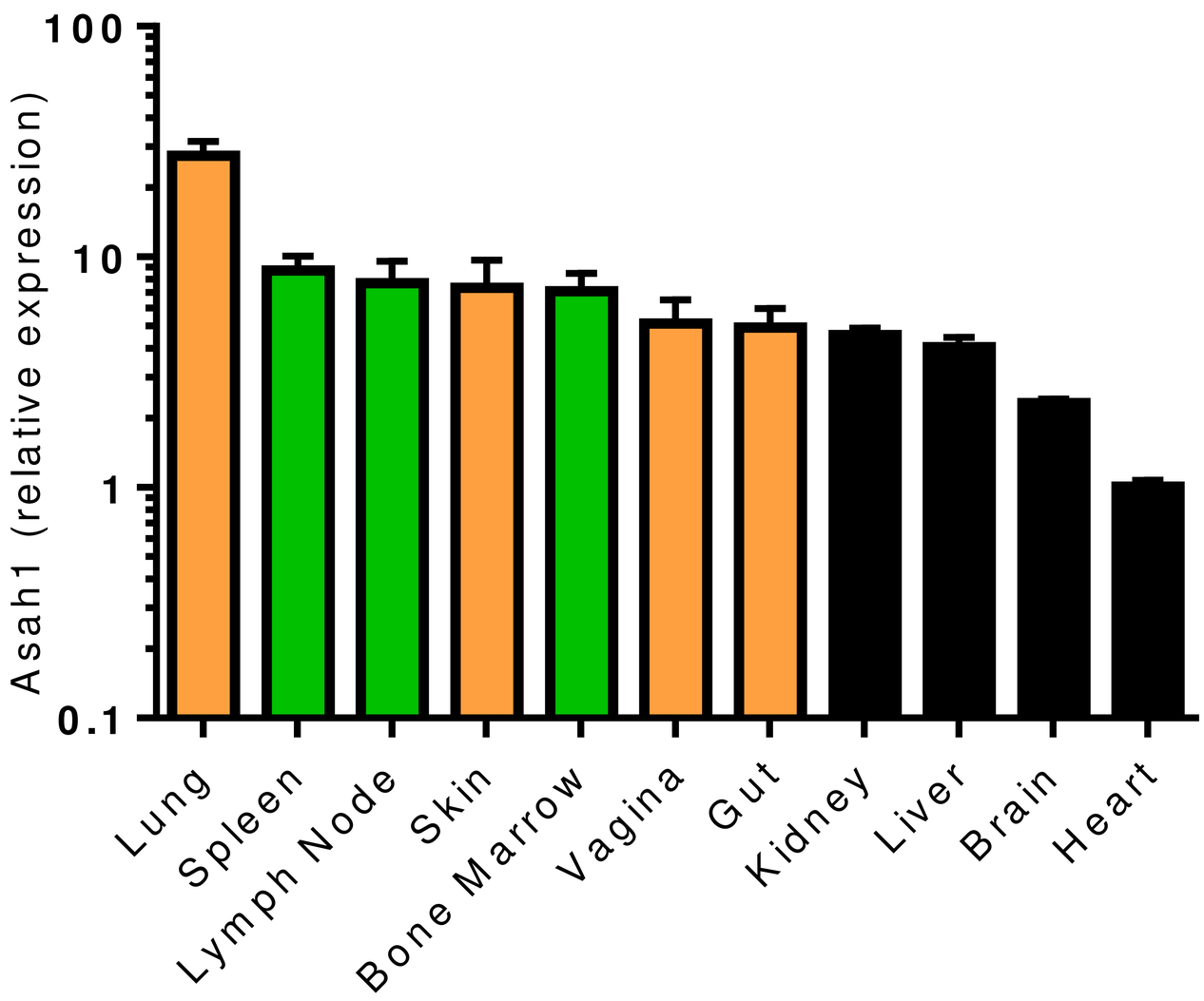

Suppl. Table 1

a

GROUP	RANK (NES)	NAME	SIZE	ES	NES	FDR q-val	FWER p-val	RANK AT MAX	LEADING EDGE
clathrin-coated membranes	1	GO_AP_TYPE_MEMBRANE_COAT_ADAPTOR_COMPLEX	37	0,6817025	2,139373	0,009	0	4769	tags=73%, list=20%, signal=91%
	2	GO_CLATHRIN_COATED_VESICLE	140	0,4177536	2,1109693	0,009	0,009	3360	tags=36%, list=14%, signal=42%
	6	GO_CLATHRIN_ADAPTOR_COMPLEX	27	0,6502399	2,0203426	0,018837286	0,063	4769	tags=70%, list=20%, signal=87%
	15	GO_CLATHRIN_COAT	45	0,6242246	1,87694	0,025962245	0,153	4769	tags=67%, list=20%, signal=83%
	16	GO_TRANS_GOLGI_NETWORK_TRANSPORT_VESICLE	26	0,50127023	1,8702269	0,025858812	0,17	3360	tags=42%, list=14%, signal=49%
	19	GO_COATED_VESICLE	205	0,33293936	1,8079635	0,03574674	0,243	3360	tags=29%, list=14%, signal=33%
	20	GO_CLATHRIN_COATED_VESICLE_MEMBRANE	66	0,42314196	1,8042084	0,03488713	0,243	3124	tags=36%, list=13%, signal=42%
	34	GO_COATED_MEMBRANE	81	0,5143869	1,724187	0,0398519	0,381	4845	tags=51%, list=20%, signal=63%
	46	GO_CLATHRIN_VESICLE_COAT	22	0,56756634	1,6978397	0,035762247	0,429	3019	tags=55%, list=12%, signal=62%
endocytosis	30	GO_PHAGOCYTIC_VESICLE	73	0,52179927	1,7359599	0,03921569	0,35	4086	tags=51%, list=17%, signal=61%
	37	GO_PHAGOCYTIC_VESICLE_MEMBRANE	46	0,53581667	1,7175857	0,03818942	0,388	4086	tags=50%, list=17%, signal=60%
	50	GO_ENDOCYTIC_VESICLE	223	0,34582347	1,6779151	0,041357946	0,499	3881	tags=33%, list=16%, signal=39%
early endosome	3	GO_EARLY_ENDOSOME	262	0,4225165	2,0901139	0,009000001	0,009	4259	tags=40%, list=18%, signal=48%
	5	GO_EARLY_ENDOSOME_MEMBRANE	90	0,45907736	2,0442317	0,017993936	0,048	4368	tags=44%, list=18%, signal=54%
	40	GO_RETROMER_COMPLEX	19	0,70777726	1,7091843	0,037392348	0,419	4075	tags=68%, list=17%, signal=82%
late endosome	4	GO_LATE_ENDOSOME_MEMBRANE	87	0,49950457	2,0850801	0,009	0,009	4528	tags=52%, list=19%, signal=63%
	7	GO_LATE_ENDOSOME	184	0,44429532	2,0017903	0,020909633	0,085	4704	tags=44%, list=19%, signal=54%
	8	GO_ENDOSOMAL_PART	370	0,42579743	1,9757125	0,023100177	0,085	4576	tags=44%, list=19%, signal=53%
	33	GO_RECYCLING_ENDOSOME	118	0,40409502	1,7256137	0,0396777	0,381	4368	tags=41%, list=18%, signal=49%
lysosome	9	GO_LYTIC_VACUOLE	463	0,4277387	1,9631885	0,021533486	0,085	4530	tags=44%, list=19%, signal=53%
	12	GO_LYTIC_VACUOLE_MEMBRANE	235	0,48414743	1,9161127	0,025993459	0,14	4362	tags=49%, list=18%, signal=59%
	26	GO_VACUOLAR_LUMEN	104	0,3773395	1,7634717	0,0366276	0,319	3524	tags=38%, list=15%, signal=45%
	27	GO_BLOC_COMPLEX	17	0,6160383	1,7550533	0,03736286	0,319	3791	tags=59%, list=16%, signal=70%
	38	GO_LYSOSOMAL_LUMEN	81	0,38517004	1,7134563	0,037687793	0,401	3471	tags=41%, list=14%, signal=47%
cell division	18	GO_REPLICATION_FORK	58	0,5975565	1,8338519	0,031645566	0,223	6436	tags=71%, list=26%, signal=96%
	39	GO_MIDBODY	116	0,35698095	1,7105753	0,03786879	0,419	5584	tags=46%, list=23%, signal=59%
	41	GO_REPLISOME	28	0,6371837	1,7077754	0,036902785	0,419	6765	tags=75%, list=28%, signal=104%
	42	GO_NUCLEAR_REPLICATION_FORK	38	0,57244664	1,7048541	0,03673616	0,429	6436	tags=68%, list=26%, signal=93%
	54	GO_SPINDLE	252	0,3613654	1,653535	0,048039164	0,579	5675	tags=42%, list=23%, signal=54%
chromosomal region	28	GO_CHROMOSOME_CENTROMERIC_REGION	158	0,44841677	1,7494394	0,03919173	0,35	5584	tags=46%, list=23%, signal=59%
	52	GO_CHROMOSOMAL_REGION	295	0,39017215	1,6661352	0,04389605	0,553	6047	tags=44%, list=25%, signal=58%
microtubule	14	GO_CENTRIOLE	86	0,45790482	1,8774872	0,027173832	0,153	4879	tags=43%, list=20%, signal=54%
	45	GO_MICROTUBULE_ORGANIZING_CENTER_PART	123	0,42793038	1,6979736	0,03635697	0,429	5643	tags=46%, list=23%, signal=60%
proton transport complex	11	GO_PROTON_TRANSPORTING_TWO_SECTOR_ATPASE_COMPLEX_CATALYTIC_DOMAIN	16	0,67587835	1,9239477	0,026597569	0,13	4100	tags=56%, list=17%, signal=68%
	13	GO_PROTON_TRANSPORTING_V_TYPE_ATPASE_COMPLEX	22	0,6414163	1,8885471	0,027705144	0,14	4100	tags=64%, list=17%, signal=76%
	17	GO_PROTON_TRANSPORTING_TWO_SECTOR_ATPASE_COMPLEX	42	0,58050895	1,8385583	0,030986838	0,206	4100	tags=52%, list=17%, signal=63%
mitochondria	22	GO_ORGANELLE_INNER_MEMBRANE	485	0,3901529	1,7873535	0,036679573	0,278	5738	tags=40%, list=24%, signal=51%
	29	GO_ORGANELLAR_RIBOSOME	70	0,48045403	1,7429737	0,038928393	0,35	5017	tags=47%, list=21%, signal=59%
	31	GO_MITOCHONDRIAL_MEMBRANE_PART	154	0,4452351	1,7304742	0,040072706	0,37	6149	tags=45%, list=25%, signal=60%
	32	GO_INNER_MITOCHONDRIAL_MEMBRANE_PROTEIN_COMPLEX	93	0,4993963	1,7265102	0,040178046	0,37	5710	tags=46%, list=24%, signal=60%
	35	GO_INTRINSIC_COMPONENT_OF_ORGANELLE_MEMBRANE	237	0,32457468	1,7241015	0,038970415	0,381	4674	tags=33%, list=19%, signal=41%
	43	GO_MITOCHONDRIAL_MATRIX	389	0,34331876	1,7011355	0,036091138	0,429	5166	tags=36%, list=21%, signal=45%
	47	GO_MITOCHONDRIAL_PROTEIN_COMPLEX	123	0,44945076	1,6955893	0,03665585	0,475	6139	tags=46%, list=25%, signal=61%
	49	GO_RESPIRATORY_CHAIN	75	0,49076676	1,6788516	0,0411818	0,499	5710	tags=43%, list=24%, signal=56%
	51	GO_INTRINSIC_COMPONENT_OF_MITOCHONDRIAL_MEMBRANE	44	0,46190116	1,6689262	0,04424508	0,535	4932	tags=43%, list=20%, signal=54%
	53	GO_INTRINSIC_COMPONENT_OF_MITOCHONDRIAL_INNER_MEMBRANE	17	0,5082864	1,6564015	0,047987744	0,561	2770	tags=41%, list=11%, signal=46%
ungrouped	10	GO_AXON_CYTOPLASM	31	0,50222677	1,9246219	0,028357327	0,13	3791	tags=42%, list=16%, signal=50%
	21	GO_IMMUNOLOGICAL_SYNAPSE	32	0,54109186	1,7903459	0,037997648	0,278	4488	tags=47%, list=18%, signal=57%
	23	GO_TRANS_GOLGI_NETWORK_MEMBRANE	64	0,49522012	1,7766278	0,037670236	0,305	3780	tags=44%, list=16%, signal=52%
	24	GO_MICROBODY	129	0,3392097	1,7741073	0,036906812	0,305	5560	tags=37%, list=23%, signal=48%
	25	GO_PIGMENT_GRANULE	99	0,41682222	1,7652943	0,0377327	0,319	3780	tags=34%, list=16%, signal=41%
	36	GO_AUTOPHAGOSOME	68	0,3550243	1,7179679	0,039000235	0,388	4494	tags=43%, list=19%, signal=52%
	44	GO_EXTRINSIC_COMPONENT_OF_ORGANELLE_MEMBRANE	22	0,46452084	1,6993158	0,035895374	0,429	5634	tags=50%, list=23%, signal=65%
	48	GO_PML_BODY	87	0,46760246	1,6898024	0,037775308	0,483	5943	tags=45%, list=24%, signal=59%
	55	GO_EXTRINSIC_COMPONENT_OF_CYTOPLASMIC_SIDE_OF_PLASMA_MEMBRANE	95	0,33212984	1,6519495	0,04801346	0,579	2920	tags=26%, list=12%, signal=30%

b

Group	RANK (NES)	NAME	SIZE	ES	NES	FDR q-val	FWER p-val	RANK AT MAX	LEADING EDGE
extracellular matrix	1	GO_EXTRACELLULAR_MATRIX	403	-0,6421122	-2,1020749	0,046640944	0,029	3660	tags=48%, list=15%, signal=55%
	2	GO_PROTEINACEOUS_EXTRACELLULAR_MATRIX	336	-0,65685314	-2,0959249	0,027820474	0,038	3660	tags=48%, list=15%, signal=55%
ER/Golgi	3	GO_ENDOPLASMIC_RETICULUM_LUMEN	184	-0,5300437	-1,9498274	0,04489303	0,11	3157	tags=38%, list=13%, signal=43%
	5	GO_GOLGI_LUMEN	82	-0,5789842	-1,8918775	0,046840988	0,181	3386	tags=35%, list=14%, signal=41%
anchoring junctions	6	GO_CELL_SUBSTRATE_JUNCTION	387	-0,38705605	-1,8837918	0,045543816	0,199	3782	tags=36%, list=16%, signal=42%
	9	GO_ANCHORING_JUNCTION	469	-0,39091176	-1,8360764	0,047074653	0,275	4155	tags=37%, list=17%, signal=44%
projection membranes	7	GO_LAMELLIPODIUM_MEMBRANE	18	-0,76415986	-1,88053	0,042221658	0,199	3290	tags=72%, list=14%, signal=83%
	10	GO_NEURON_PROJECTION_MEMBRANE	32	-0,61009735	-1,8091	0,04889716	0,285	3837	tags=50%, list=16%, signal=59%
	14	GO_DENDRITE_MEMBRANE	18	-0,57180417	-1,7932113	0,04320775	0,303	2095	tags=39%, list=9%, signal=43%
platelet alpha granules	4	GO_VESICLE_LUMEN	96	-0,5390744	-1,9249805	0,04230829	0,11	3943	tags=40%, list=16%, signal=47%
	12	GO_PLATELET_ALPHA_GRANULE_LUMEN	53	-0,5812689	-1,8022362	0,047483716	0,303	3943	tags=42%, list=16%, signal=49%
	13	GO_PLATELET_ALPHA_GRANULE	72	-0,4918661	-1,7938668	0,045219976	0,303	3943	tags=39%, list=16%, signal=46%
gap junction, connexion	8	GO_GAP_JUNCTION	28	-0,61969125	-1,8709532	0,041193422	0,222	3631	tags=39%, list=15%, signal=46%
	11	GO_CONNEXON_COMPLEX	18	-0,6039202	-1,8056597	0,046751294	0,285	3631	tags=39%, list=15%, signal=46%

Suppl. Table 2

Gene	Name
Acaa1a	3-ketoacyl-CoA thiolase A, peroxisomal
Acaa1b	3-ketoacyl-CoA thiolase B, peroxisomal
Acaa2	3-ketoacyl-CoA thiolase, mitochondrial
Asah1	Acid ceramidase
Asah2	Neutral ceramidase
Chpt1	Choline Phosphotransferase 1
Degs1	Delta 4-Desaturase, Sphingolipid 1
Degs2	Delta 4-Desaturase, Sphingolipid 2
Far1	Fatty Acyl-CoA Reductase 1
Far2	Fatty Acyl-CoA Reductase 2
Fdft1	Farnesyl-diphosphate farnesyltransferase 1
Fdps	farnesyl diphosphate synthase
Ggps1	Geranylgeranyl Diphosphate Synthase 1
Gk2	Glycerol Kinase 2
Gk5	Glycerol Kinase 5
Gnpat	Glyceronephosphate O-Acyltransferase
Gpd1	Glycerol-3-Phosphate Dehydrogenase 1
Gpd1l	Glycerol-3-Phosphate Dehydrogenase 1 Like
Gpd2	Glycerol-3-Phosphate Dehydrogenase 2
Hmgcr	3-Hydroxy-3-Methylglutaryl-CoA Reductase
Hmgcs1	3-Hydroxy-3-Methylglutaryl-CoA Synthase 1
Hmgcs2	3-Hydroxy-3-Methylglutaryl-CoA Synthase 2
Idi1	Isopentenyl-Diphosphate Delta Isomerase 1
Idi2	Isopentenyl-Diphosphate Delta Isomerase 2
Kdsr	3-Ketodihydrosphingosine Reductase
Lass2	Ceramide Synthase 2
Lass3	Ceramide Synthase 3
Lass4	Ceramide Synthase 4
Lass5	Ceramide Synthase 5
Lass6	Ceramide Synthase 6
Mvk	Mevalonate Kinase
Pcyt1a	Phosphate Cytidylyltransferase 1, Choline, Alpha
Pcyt1b	Phosphate Cytidylyltransferase 1, Choline, Beta
Pcyt2	Ethanolamine-phosphate cytidylyltransferase
Pemt	Phosphatidylethanolamine N-Methyltransferase
Pisd	Phosphatidylserine Decarboxylase
Plcb1	Phospholipase C Beta 1
Plcb2	Phospholipase C Beta 2
Plcb3	Phospholipase C Beta 3
Plcb4	Phospholipase C Beta 4
Plcg1	Phospholipase C Gamma 1
Plcg2	Phospholipase C Gamma 2
Plcl1	Phospholipase C Like 1 (Inactive)
Plcl2	Phospholipase C Like 2
Pmvk	Phosphomevalonate Kinase
Ptdss1	Phosphatidylserine Synthase 1
Ptdss2	Phosphatidylserine Synthase 2
Sgms1	Sphingomyelin Synthase 1
Sgms2	Sphingomyelin Synthase 2
Sgpl1	Sphingosine-1-Phosphate Lyase 1
Sgpp1	Sphingosine-1-Phosphate Phosphatase 1
Sgpp2	Sphingosine-1-Phosphate Phosphatase 2
Smpd1	Sphingomyelin Phosphodiesterase 1
Smpd2	Sphingomyelin Phosphodiesterase 2
Smpd3	Sphingomyelin Phosphodiesterase 3
Smpd4	Sphingomyelin Phosphodiesterase 4
Sphk1	Sphingosine Kinase 1
Sphk2	Sphingosine Kinase 2
Sptlc1	Serine Palmitoyltransferase Long Chain Base Subunit 1
Sptlc2	Serine Palmitoyltransferase Long Chain Base Subunit 2
Sptlc3	Serine Palmitoyltransferase Long Chain Base Subunit 3
Sqle	Squalene Epoxidase
Tpi1	Triosephosphate Isomerase 1